

Excited States of Light Nuclei

Some Measurements on Nuclear Energy Levels Excited
in Reactions Induced by Bombardment with
Low-energy Charged Particles

by

R.D. Smith

Department of Natural Philosophy
University of Glasgow

Presented as a thesis for the degree
of Ph.D., The University of Glasgow

February 1952.

ProQuest Number: 13838525

All rights reserved

INFORMATION TO ALL USERS

The quality of this reproduction is dependent upon the quality of the copy submitted.

In the unlikely event that the author did not send a complete manuscript and there are missing pages, these will be noted. Also, if material had to be removed, a note will indicate the deletion.



ProQuest 13838525

Published by ProQuest LLC (2019). Copyright of the Dissertation is held by the Author.

All rights reserved.

This work is protected against unauthorized copying under Title 17, United States Code
Microform Edition © ProQuest LLC.

ProQuest LLC.
789 East Eisenhower Parkway
P.O. Box 1346
Ann Arbor, MI 48106 – 1346

Preface.

In this thesis I have attempted to describe the construction of a high-voltage proton accelerator and the results of some investigations of the properties of the energy levels of light nuclei carried out with its aid.

Part I contains a brief review of these properties and the applications of the proton accelerator in their investigation. This Section has been based largely on the work of Devons (Excited States of Nuclei) and Fowler, Lauritsen and Lauritsen (Gamma-radiation from Excited States of Light Nuclei).

Part II describes the design and construction of the accelerator tube and associated equipment. The initial work on the accelerator was carried out by Dr. J.B. Warren, who, however, left the department in September 1947. I was not associated with the project until the August of that year, at which time the generator had been erected and tested, and the major part of the vacuum system completed but not yet put into operation. The accelerating tube was being constructed to a design of Messrs. Philips, of Eindhoven, but no work had been started on the equipment for the magnetic beam analysis and general techniques for quantitative measurements on reaction products.

Dr. J.G. Rutherglen was at that time working on the design of the ion source for the accelerator tube. During the completion of this work I erected

the accelerating tube. The ion source was then installed, and since this date Dr. J.G. Rutherglen and I have been working in collaboration; the responsibility for individual items being divided between us as circumstances dictated. In the main Dr. J.G. Rutherglen remained responsible for the ion source and its associated equipment described in Section II.4., and designed the ripple cancellation circuit described at the end of Section II.2.6. and the resolving chamber and magnet. The remainder of the electronic equipment and much of the work on the accelerator tube was my sole concern.

Part III describes some of the experimental results so far obtained with the aid of the accelerator. It has been found that owing to the complexity of the equipment, if full use is to be made of the operating time of the generator it is normally essential for at least two persons to be concerned with each experiment. Where the apparatus pertaining to a particular experiment was itself complex, it was found advantageous for one individual to be concerned primarily with the initial design and construction of that apparatus, that individual later forming a member of the team carrying out that particular experiment.

Thus in the work on gamma-ray high energy measurements (Section III.1.) Dr. E.R. Rae designed and constructed the spectrometer and associated circuits (III.1.4.). I was responsible for the design of the stabiliser for the magnet current,

while the actual measurements were made by Dr. E.R. Rae, Dr. J.G. Rutherglen and myself.

The charged particle measurements were made with the 90° analyser (Section III.3.4.) designed by Dr. J.G. Rutherglen and carried out in collaboration with him.

The proportional counter experiments were carried out solely by myself, with the exception of the investigation of the $Al^{27}(d,p)Al^{28}$ reaction which was carried out with the assistance of Mr. R.A. Anderson.

Some of the results presented in this thesis have been published elsewhere as joint papers or letters^{(51) (59) (94)}. References to these papers are made at the ends of the appropriate Sections.

I wish to thank Professor P.I. Dee for his continuous help and encouragement during the course of this work. My thanks are also due to Dr. S.C. Curran and Mr. A.L. Cockroft, for helpful advice about the design and operation of proportional counters, to Dr. B.F.X. Touschek and Dr. K.M. Guggenheimer for helpful discussion on some theoretical points, to Mr. W. McCall, who was responsible for the constructional work carried out by the department workshops and Mr. T. Pollok, technician attached to the project, who constructed much of the electronic equipment.

Contents.

Part I. Introduction.

I.1. Energy Levels	1.
I.2. Excitation of Levels.	2.
I.3. Types of Reactions	4.
I.4. Description of Levels	8.
I.5. Experimental Data	12.
I.6. Experimental Procedure	16.
1. Excitation Curves	16.
2. Gamma-ray Energy Measurement	22.
3. Particle Energy Measurement	28.

Part II. Accelerating Equipment 33.

II.1. General	33.
1. Site	33.
2. History of Installation	33.
3. Personnel	35.
II. 2. Cascade Generator	36.
1. General	36.
2. Details of Generator	36.
3. Voltage Measurement	37.
4. Voltage Stabilisation	41.
5. Ripple Voltage	44.
6. Smoothing Circuit	48.
7. Operation of Generator	56.
8. Reliability of Generator	57.
9. Servicing of Generator	58.
II.3. Accelerator Tube	61.
1. General	61.
2. Construction of Tube	62.
3. Initial Installation	66.
4. Modified Accelerating Tube	67.
5. Space Charge Effects	70.
6. Initial Alignment of Tube	74.
7. Subsequent Adjustment of Tube	75.
8. Typical Operating Conditions	76.

II.4.	Ion Source	77.
	1. General	77.
	2. First Type Source	78.
	3. Modified Source	78.
	4. Gas Supply	79.
	5. Power Supplies for Ion Source	80.
	6. Performance of Ion Source	80.
II.5.	Vacuum System	84.
	1. General	84.
	2. Pumps	84.
	3. Valves and Interlocks	85.
	4. Resolving Chamber	85.
	5. Leak Detection	89.
II.6.	General Purpose Auxiliary Equipment	91.
	1. General	91.
	2. Layout	91.
	3. Current Integrator	92.
	4. Timing Unit	94.
	5. Resolving Magnet and Power Supply	95.
Part III.	Experimental Results	99.
III.1.	Hard Gamma-radiation	99.
	1. General	99.
	2. Principle of Operation of Spectrometer	99.
	3. Target Arrangement and Experimental Procedure	103.
	4. The Reaction $F^{19}(p,\gamma)Ne^{20}$	105.
	5. The Reaction $Al^{27}(p,\gamma)Si^{28}$	109.
	6. Gamma-radiation Resulting from the Bombardment of Boron by Deuterons	116.
	7. Constructional Details of Spectrometer	127.
III.2.	Soft Gamma-radiation	131.
	1. General	131.
	2. Origin of Soft Gamma-radiation	131.
	3. Radiation by Extra-nuclear Electrons	138.
	4. Characteristic X-radiation	138.
	5. "White" Background Radiation	149.
	6. Low Energy Nuclear Radiation	151.
	7. The Reaction $Al^{27}(d,p)Al^{28}$	152.
	8. The Reaction $P^{31}(d,p)P^{32}$	159.
	9. Apparatus	159.

III.3. Emission of Charged Particles	170.
1. General	170.
2. The Reaction $B^{10}(d,p)B^{11}$	173.
3. The Reaction $Al^{27}(p,\alpha)Mg^{24}$	181.
4. Constructional Details of Spectrometer	198.
III.4. Summary of Experimental Results	203.
Appendix 1.	206.
Appendix 2.	208.
References	213.

Part I. Introduction

I. 1. Energy Levels.

The existence of a system of discrete nuclear energy levels was originally suggested by a study of gamma-ray spectra of the radioactive elements and confirmed by measurements on the fine structure of alpha-rays and the corresponding homogeneous gamma-rays. In artificially produced nuclear reactions these phenomena also occur and in addition strong resonance effects are observed which may also be attributed to the existence of these sharp nuclear energy levels. Such a discrete set of values for the total energy of a nucleus would be expected on quantum mechanical grounds if the nucleus can be considered as an assembly of particles occupying a limited volume in space.

A study of the properties of these levels should provide information on the structure of nuclei and the interaction of nucleons. Although the application of quantum mechanical methods to the nucleus is not straightforward, a certain amount of progress has been made towards a theoretical interpretation of the experimental results so far obtained.

This thesis will be concerned with some reactions produced by bombardment of light nuclei with protons and deuterons having energies up to 800 KeV. The results form a small part of the large amount of information now available on the behaviour of these nuclei. This data for nuclei with $Z \leq 10$ has been summarised by Hornyak et al.⁽¹⁾ and the

positions of levels in nuclei with Z between 10 and 20 has been tabulated by Alburger and Hafner⁽²⁾. The nuclear energy levels are in a general way analogous to the excited levels of atoms, and the emission and absorption of light quanta may be compared with that of gamma-rays and particles by nuclei. There are, however, certain fundamental differences which render the theoretical and experimental study of the nuclear problem more difficult than the corresponding atomic one.

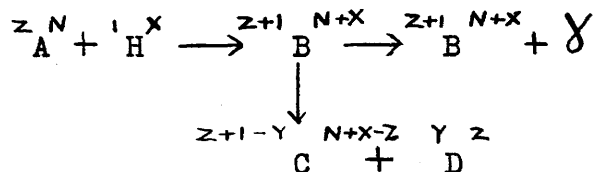
Some of the more obvious of these difficulties are:

- (a) The energies involved in nuclear processes are of the order of a million times as great as those in the corresponding atomic process.
- (b) When a particle suffers a collision with a nucleus it cannot pass through without interacting strongly with the nucleons; whereas particles may easily traverse the electron cloud of an atom.
- (c) The forces between the nucleus and the atomic electrons are of a type well known and understood from macroscopic experiments; the forces between nucleons are of a new type that cannot be studied except in relation to the nucleus itself.

I.2 Excitation of Levels.

As a result of the large energies involved the excitation of nuclear levels is much more difficult than the excitation of atomic levels. This

thesis is concerned with one particular method of excitation; the collision of a proton or a deuteron with a nucleus resulting in a reaction. This process may be written as:



where the index before the symbol representing a nucleus is the nuclear charge and the index after the symbol is the number of nucleons. ${}^{Z+1}_B^{N+X}$ is the compound nucleus which will be formed in an excited state. This state may lose its excess energy by emitting either gamma-radiation or a particle ${}^Y_Z D$. This particle will normally be either a single nucleon or an alpha particle and the energy available will not, in the reactions considered, be sufficient for it to be emitted in an excited state. The residual nucleus ${}^{Z+1-Y}_C^{N+X-Z}$, on the other hand, may be left in an excited state and may, in its turn, emit a gamma ray or, more rarely, a second particle.

If it is energetically impossible for an excited nucleus to emit a particle then the nuclear energy level is a "bound" level, analogous to an excited level in an atom. The compound nucleus ${}^{Z+1}_B^{N+X}$ must be formed with an excitation energy greater than that necessary for the emission of a particle (e.g. the incident particle). Nevertheless the nucleus may still possess "virtual" levels which

are very similar to the bound levels just below the dissociation energy. These levels exist owing to the comparatively long life-time of the compound nucleus. This long life may be attributed to the short-range character of nuclear forces and the consequent rapid sharing of the available energy among all the nucleons. Not until the necessary energy is, by chance, concentrated on one particular particle can the disintegration occur. The life-time of a "bound" level may be many days in the case of an isomeric state, but is more usually of the order of 10^{-16} sec. The typical life-time of a virtual state is of the order of 10^{-19} sec. though this will often be greatly increased by the effect of the coulomb and centrifugal barriers.

I.3. Types of Reactions.

The maximum bombarding energy available with the present apparatus is 800 KeV. This limits the number of reactions that are energetically possible. Even where the threshold is below this value the incident particle has to penetrate the coulomb barrier of the bombarded nucleus. For $Z = 15$ the barrier height for protons is about $4\frac{1}{2}$ MeV and the yield of most proton reactions involving nuclei with $Z > 15$ is rather small.

With these limitations the general characteristics of the possible reactions may be summarised as follows:

(a) (p,n) reactions.

The threshold for this reaction for light nuclei is, with few exceptions (e.g. $C^{14}(p,n)N^{14}$ Threshold 664 KeV.), greater than 800 KeV. and does not lead to highly excited states with the bombarding energy available.

(b) (p,d) reactions.

This reaction is not usually energetically possible. An exception is the reaction $Be^9(p,d)Be^8$ $Q = 0.54$ MeV.

(c) (p α) reactions.

The compound nucleus by the capture of a proton of light nuclei will have an excitation energy which ranges up to about 17 MeV. The (p α) process is usually exothermic and the alpha-particles may be emitted with sufficient energy to take them over the Coulomb potential barrier. In this case no sharp resonances will be observed as the life-time of the alpha-emitting state will be very short and its width will be of the order of 1 MeV.

If the energy of the alpha-particle is insufficient to surmount the barrier the width of the alpha-emitting level is reduced by a factor due to the penetrability of the alpha-particle and this width may become small compared with that for the re-emission of a proton. Sharp resonances may then be observed if there are levels of the compound nucleus

in the excitation range considered. Such resonances occur, for example, in the reaction $\text{Al}^{27} (p\alpha) \text{Mg}^{24}$. (See section III 3.2).

(d) (p γ) reactions.

As the excitation of the compound nucleus is high, the emission of a charged particle will normally be more probable than the emission of a gamma-ray. In some cases, however, the emission of these particles is so reduced by symmetry properties of the nuclear states involved and by the Coulomb barrier that the (p γ) process becomes predominant or at any rate comparable with the particle reaction. The best known example is the 440 keV resonance in the $\text{Li}^7 (p\gamma) \text{Be}^8$ reaction. A second example is the de-excitation of the various levels of Si^{28} formed by the capture of protons by Al^{27} . In this case some levels emit only gamma-radiation while others emit alpha-particles in addition to gamma-rays. This reaction is considered in detail in section III.4.2.

(e) (pp) reactions.

The inelastic scattering of protons may give data on levels whose excitation energies are less than that of the incident protons.

Anomalies in the elastic scattering cross-section have been observed with light nuclei ⁽³⁾, and the positions and widths of resonance levels deduced from these anomalies. Experimental difficulties have,

so far, limited the usefulness of this approach.

(f) (dn) reactions.

The compound nucleus formed by the bombardment of a light element by deuterons is very highly excited so that the energy available for neutron emission is normally greater than 6 MeV. These reactions have a high yield and several groups of neutrons of different energies may be emitted. The residual nucleus may thus be left in an excited state which usually emits a gamma-ray but occasionally a second particle may be emitted. (e.g. $F^{19} (dn\alpha) O^{16}$) (4).

(g) (dp) reactions.

The energy available for this reaction is similar to that for the d-n reaction but the emission of a proton is hindered by the potential barrier. This factor is, however, off set by the 'polarisation' of the incident deuteron so that the neutron may be captured without the proton entering the compound nucleus. This process (the Oppenheimer-Phillips process) (5) results in comparable cross-sections for the d-p and d-n reactions.

(h) (d- α) reactions.

For this reaction there can be no mechanism similar to the Oppenheimer-Phillips process so that the yield of the reaction will be small compared with the d-n and d-p reactions. The compound nucleus will be excited to 5 or 10 MeV. and in some cases it

is energetically possible for another alpha-particle to be emitted (e.g. $B^{10} (d\alpha) (Be^8)$).

(1) (d γ) reactions.

The deuteron capture process has not been observed. The excitation of the compound nucleus would be of the order of 20 MeV so that the gamma-radiation would be of high energy. The width for gamma-ray emission is reduced by interaction with neighbouring levels as the level spacing is small at this excitation energy.

The disintegration of the compound nucleus by the emission of a particle is, of course, much more probable and unless all such processes are forbidden by symmetry properties the emission of gamma-radiation would not be detected.

I.4. Description of levels.

An attempt to obtain a further insight on to nuclear structure by a study of energy levels must be based on the available information on (a) the existence and position of the levels and (b) the detailed properties of the levels manifested by their mode of formation and decay.

The existence and spacing of levels can be predicted on the basis of the various nuclear models proposed (6) (7) (9) and the results of these theories may be compared with experiment. Usually it is easiest to estimate the position of the lowest level

and the level density at high excitation energies. Consequently, a systematic knowledge of these quantities for all the light nuclei would be desirable. Alternatively, complete information on the level system of any one nucleus would be valuable. Unfortunately, neither of these objects has been even approximately attained. Owing to experimental difficulties the present knowledge of the level positions and spacings, though fairly comprehensive for certain ranges of the excitation energy of some nuclei, is very sparse for others, and there is never any certainty that the lowest level actually detected is in fact the lowest level of the nucleus in question.

Each level will be the initial or final product of one or more nuclear reactions. (In this sense inelastic scattering is regarded as a nuclear reaction). Each of these reactions must involve the properties of at least two states, but by combining the results from more than one reaction properties peculiar to individual levels may be deduced. The information most commonly available is the absolute yield and excitation functions of the reactions, the angular correlation of the particles or quanta involved, and the relative yield of competing reactions; though in some cases further data, for example the internal conversion coefficient of a gamma-ray, may be known.

Thus once the position of a nuclear level has been determined, further detailed properties of the level

may be ascertained. The most important of these properties are:

- (a) The level width Γ . If the life-time of the excited state is τ then $\Gamma = \hbar/\tau$. Partial widths may similarly be defined for de-excitation by a particular process, for example by gamma-ray emission, and the total width will then be the sum of these partial widths.
- (b) The angular momentum. Nuclei possess angular momentum as a result of the spins and orbital motions of the constituent nucleons. The expression "nuclear spin (I)" usually refers to this total angular momentum. The spin of the ground state of nuclei can be found in several ways, as for example, from measurements of the hyperfine structure of spectral lines and the band spectra of diatomic molecules. The spin has been determined for nearly all the stable and many of the unstable light nuclei (8). From the observed nuclear reactions spin values may be assigned to some of the excited states.
- (c) The parity. The symmetry of a nuclear energy level as expressed by the parity* of the wave-function

* A wave-function describing a system of particles is said to have even parity if the wave-function is unaltered by reversing the sign of all the co-ordinates of the particles: for a wave function of odd parity this operation will reverse the sign of the wave function.

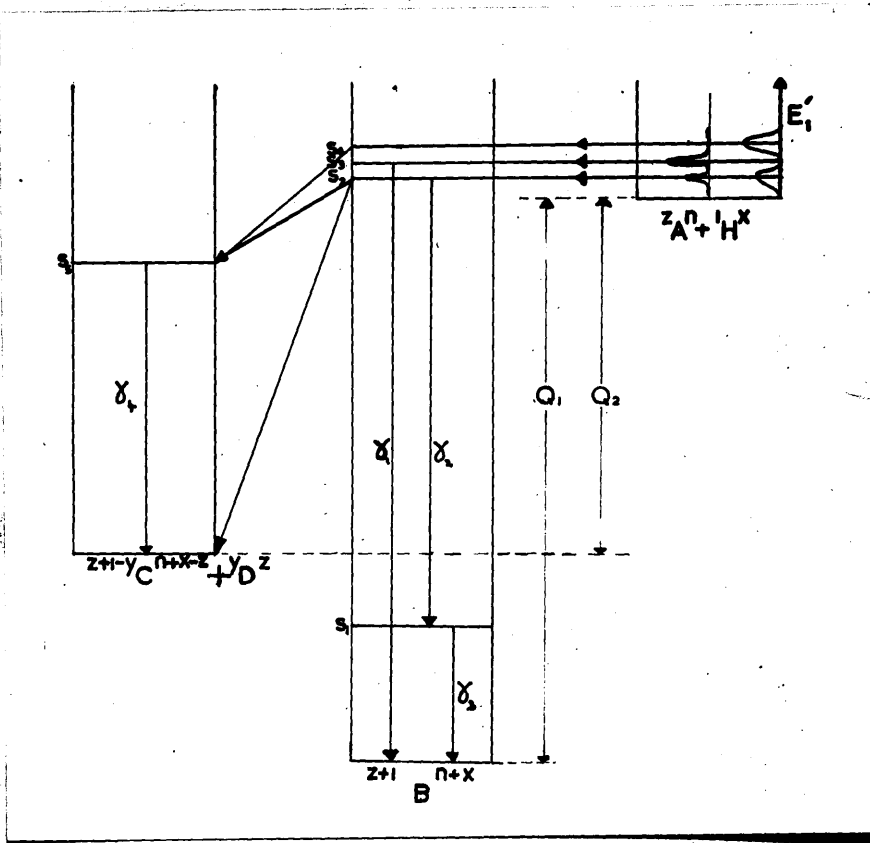


Figure 1. 1. Typical Level Diagram.

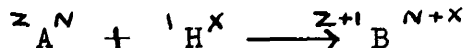
describing it, together with the spin of the level, may forbid certain transitions otherwise energetically possible. These effects give rise to a series of 'selection rules' determining which transitions may occur.

I. 5. Experimental Data.

In section I.3. the various types of reaction that may be performed with the equipment available are considered. This section will show how the study of these reactions can yield the desired information. In order to represent the various levels it is convenient to use a diagram on which the nuclear energy levels are positioned according to their excitation energies on a vertical scale. For example, the reactions considered in section I.2. involving the compound nucleus ${}^{Z+1}_{N+X}B$ may be shown on such a diagram. (fig.1.1.) The diagram is drawn primarily to show the levels of ${}^{Z+1}_{N+X}B$, but the total energy, including the rest mass, of the initial and final components of the reaction will be of the same order of magnitude so that the systems ${}^Z_A + {}^N_H + {}^X_C$ and ${}^{Z+1-Y}_{N+X-Z}C + {}^Y_D$ which contain the same total number of nucleons may also be included in the diagram on the same scale and in the correct positions relative to the compound nucleus. As the particles N_H and Y_D have no excited states in the energy range considered, the excited states of ${}^{Z+1-Y}_{N+X-Z}C$ may be included, arrows may then be drawn to show the transitions that

occur, and the vertical displacement between any two levels will represent directly the energy change that occurs in passing from one to the other. It should be noted that a system containing a different number of nucleons could not be conveniently represented on the same scale, as the energy difference involved is of the order of 100 times as great as any in the diagram.

In fig. I.1. four excited states of the compound nucleus are shown. It will be seen at once that the lowest of these, S_1 , cannot be excited directly by bombarding the nucleus ${}^Z_A N$. In fact, if Q_1 is the energy release ("Q value") of the reaction:



only those levels in the compound nucleus with an excitation energy above Q_1 and lower than $Q_1 + E'$, where E' is the additional energy resulting from the maximum available bombarding energy of the particle (see appendix 1) can be excited directly (In practice the lower limit will be appreciably higher than Q_1 , owing to the small penetration of the Coulomb barrier by bombarding particles of low energy). As the interval between Q_1 and $Q_1 + E'$ occupies only a small part of the level system of the compound nucleus direct excitation can only yield information on a limited number of levels. However, for those levels which are accessible,

the excitation curves, that is to say, the yields of the reactions as a function of the bombarding energy E give detailed information not otherwise available. Typical excitation curves are shown to the right of the diagram, where the total yields of particles ${}^Y D^Z$ and of gamma-rays are plotted against excitation energy in the centre of mass system. Levels S_1, S_3 and S_4 in fig.1.1. can be investigated in this way. The bound level S_1 is excited by a cascade gamma-ray transition from the resonance level S_2 . In competition with the gamma-ray this level also emits particles ${}^Y D^Z$ leaving the nucleus ${}^{Z+1-Y}_{N+X-Z} C$ in an excited state, which in turn emits a gamma-ray. Thus the positions of levels S_1 and S_5 can be determined by measurement of the relevant gamma-ray energies. Confusion between the various gamma-rays may be avoided by observing coincidences between the particles ${}^Y D^Z$ and the gamma-ray γ_4 or between the two gamma-rays γ_1 and γ_3 . The level S_3 excited with bombarding particles of slightly higher energy, de-excites only by the emission of a gamma-ray to the ground state. Measurement of the energy of this gamma-ray γ_1 will give the mass difference between the nuclei ${}^Z A^N$ and ${}^{Z+1} B^{N+X}$ and will assist in the identification of γ_1 and γ_3 . If the cascade gamma-rays and the direct ground state transition are in competition from the same level $\gamma_1 = \gamma_2 + \gamma_3$. In the case shown in the figure γ_1 will be the greater by the amount of the spacing

between the levels S_2 and S_3 .

An alternative method of determining the position of the level S_5 is the measurement of the energy of the particles ${}^Y D^Z$. The difference in energies of the group from the level S_2 which leaves the nucleus ${}^{Z+1-Y} C^{N+X-Z}$ in its ground state and that from the resonance level S_4 which leaves it in the excited state S_5 , together with the energy difference between the levels S_2 and S_4 will give the excitation energy of the state S_5 . In actual practice the system will be more complex than is shown in the diagram as there will be many more excited states, several of which may be involved in more than one reaction.

Nevertheless, the basic methods for the location of levels, i.e. particle energy measurement, gamma-ray energy measurement, and excitation curves, may still be applied and these are considered in more detail in section I.5. The detailed properties of the levels can be determined by measurements of such quantities as the multipole order of gamma-ray transitions, the angular distribution of reaction products, and the relative and absolute cross-sections for the various reactions. A general survey of these methods will not be made here, but those instances relevant to the experiments described in this thesis will be described in section III.

measured; in practice this is often difficult to achieve.

The homogeneity of the incident beam is discussed in section II.2.6. When targets can be prepared by evaporation in vacuo thickness of 10^{-6} cm. or less can readily be achieved. The energy loss of the incident protons or deuterons in traversing such targets will be only a few hundred volts, but the yield from such targets is small and they are also rapidly destroyed by the incident beam. For these reasons thick targets are often to be preferred. Targets of intermediate thickness are less useful, owing to the difficulty of determining the thickness exact.

The cross-section near the resonance for the excitation of a virtual state is given by the Breit-Wigner dispersion formula:

$$\sigma_b = \frac{\lambda^2}{4\pi} g \frac{\Gamma_a \Gamma_b}{(E - E_r)^2 + \Gamma^2/4}$$

- σ_b = partial cross-section for process "b".
- σ_{br} = partial cross-section for process "b" at resonance.
- Γ_b = partial width for process "b".
- Γ_a = partial width for re-emission of incident particle.
- Γ = total width, i.e. sum of the partial widths for all possible modes of decay of the compound nucleus including the re-emission of the incident particle.
- E_r = energy of incident particle at resonance.

E = energy of incident particle of mass m .

λ = De Broglie wavelength of incident particles

$$= \frac{h}{\sqrt{2Em}}$$

g = statistical weight factor.

$$g = \frac{2J+1}{(2i+1)(2j+1)}$$

where J = angular momentum of compound nucleus,

j = total intrinsic angular momentum of
bombarded nucleus,

i = total intrinsic angular momentum of
incident particle,

" g " will be of the order of unity.

If the total width of the resonance is small so that Γ_a and Γ_b do not vary appreciably over the resonance then:

$$\sigma_b = \sigma_{br} \frac{\Gamma^2/4}{(E-E_r)^2 + \Gamma^2/4}$$

The yield Y of the reaction is obtained by integrating the cross-section over a range of bombarding energies corresponding to the energy of the incident particles in the target. Thus:

$$Y = \int_{E-y}^E \frac{\sigma}{\Sigma} dE.$$

Y = loss of energy of incident particle in traversing target,

Σ = stopping cross-section of target material per nucleus ${}^Z_A N$ for the incident particle ${}^1_1 H^x$.

If the target is "thick" it is necessary to integrate over those values of E for which σ_b is appreciable and then the "thick target yield" $Y_{b\infty}$ for process "b"

is given by

$$Y_{b\infty} = \frac{\lambda_g}{2\xi} \frac{\Gamma_a \Gamma_b}{\Gamma} = \frac{h^2}{4E_r m \xi} g \frac{\Gamma_a \Gamma_b}{\Gamma}$$

Now $\Gamma = \Gamma_a + \Gamma_b + \Gamma_c \dots$

and it may happen that one of the partial widths is much larger than all the others. If Γ_a , the width for the re-emission of the incident particle, predominates, then $\Gamma \approx \Gamma_a$, and the thick target yield for the process "b" will be given by:

$$Y_{b\infty} = \frac{h^2 g}{4E_r \xi} \Gamma_b$$

independent of Γ_a .

If, on the other hand, the width Γ_b for the process "b" predominates, then similarly:

$$Y_{b\infty} = \frac{h^2 g}{4E_r \xi} \Gamma_a$$

independent of Γ_b .

Thus by measuring the yield of a particular reaction "b", the smaller of the two widths Γ_a , Γ_b may be determined. The total width Γ may be deduced from the shape of the excitation curve, provided the resolution of the apparatus is sufficient.

In the case of particle emission the observed yield may be lower than the true yield owing to the absorption or "straggling" of particles produced below the surface of target by the target material itself. In the case of gamma-radiation this absorption is usually negligible and the effect of target thickness

on the yield and shape of the resonance curve may readily be calculated. A summary of these results and a comparison with experiment has been published by Fowler et al. (10). They show:

$$Y'/Y'_\infty = \frac{2}{\pi} \tan^{-1} \frac{Y}{\Gamma}$$

where

Y' = maximum yield from target of thickness Y .

Y'_∞ = maximum yield from target of infinite thickness

and

$$\Gamma' = \sqrt{\Gamma^2 + Y^2}$$

where

Γ' = apparent width at half maximum

Γ = true width at half maximum,

and a graph of these two functions which enables corrections for finite targets widths to be made is given in their paper.

The effect of target thickness on the shape of the excitation curve observed in reactions resulting in the emission of charged particles depends to some extent on the type of detector used, as the energy of particles originating beneath the surface of the target is lower than that of those from the surface. Therefore, the spectrum of a resonant particle group will vary as the bombarding energy varies, the energy of the peak of the spectrum decreasing as the bombarding energy is raised. The actual shape of the spectrum can be found by graphical integration and a knowledge of this shape is of importance when measuring the Q-value of the reaction. (11) (12)

For the determination of alpha-particle resonances it is usual to use thin targets and a particle detector of low energy resolution arranged to detect particles of an energy computed from the Q-value of the reaction. (Appendix 1). By using a high resolution analyser set to reject those particles of lower energy originating below the target surface a "thin" target excitation curve could be obtained from a thick target.

The presence of thin films on the target surface may cause errors in the location of resonances (and in the determination of Q-values by measurement of particle energy). These films may originate during the preparation of the target (e.g. oxide films or tungsten films from the heater used in an evaporation process) or may be due to the condensation of pump-oil vapour on the target surface. This oil will be rapidly converted to carbon by the action of the beam and blackens the target surface. This latter effect can be reduced by the use of a liquid air trap near the target and by heating the target to about 200°C before allowing the beam to strike it. These carbon films, though readily visible, normally have a stopping power of less than 500 volts.

In the experiments described in this thesis excitation curves were usually recorded by setting the timing unit to accept a predetermined number of counts from the current integrator. Thus, assuming that

secondary emission effects had been suppressed, the yield of gamma-radiation or particles for a fixed number of incident protons could be recorded for a series of bombarding energies. The gamma resonances of fluorine, lithium and aluminium were used to calibrate the H.T. voltmeter.

I. 6.2. Gamma-ray Energy Measurement.

In section I.5. it was shown that measurement of the energy of the gamma-rays $\gamma_1, \gamma_2, \gamma_3$ and γ_4 in figure 1.1 would give information on the position of levels S_1 and S_5 . The technique of accurate gamma-ray energy measurement is, therefore, important and has advanced rapidly in the last few years.

Prior to 1948 the most important methods of measurement were:

- (a) Measurement of the absorption coefficient.
- (b) Measurement of the Compton electrons and pairs produced in a cloud chamber.
- (c) Coincidence absorption measurements of the absorption of the secondary electrons.
- (d) Spectrometer measurements of the energy of the secondary electrons,

and these methods have been reviewed by Fowler, Lauritsen and Lauritsen⁽¹³⁾

The new methods that have been developed since that date include the measurement of the total energy of electron-positron pairs in a "pair" spectrometer, the photo-disintegration of deuterium and various methods based on the scintillations

produced when gamma-quanta are absorbed by certain crystals and liquids. The pair spectrometer is, so far, the most precise instrument for the measurement of high energy radiation but it has a low efficiency. A special spectrometer of this type was used for measurements of the gamma-radiation of light nuclei by Walker and McDaniel⁽¹⁴⁾. Further measurements using a similar spectrometer are described in Section III.

The photodisintegration method has been developed by Carver and Wilkinson⁽¹⁵⁾. The deuterium, either pure or mixed with argon, is confined at high pressure in an ionisation chamber, and energy of the photo-proton obtained from the pulse size produced. An accuracy comparable with that obtained with a pair spectrometer (of the order of 2% in energy) has been achieved by this method. Its efficiency does not vary with energy as rapidly as does the pair spectrometer but it cannot be used in the presence of a background of fast neutrons.

In the scintillation technique secondary electrons due to the gamma-ray are stopped in a suitable material such as a transparent sodium iodide crystal. Light quanta are produced and detected by a photomultiplier and the size of the pulse produced is closely related to the energy expended by the electron in the crystal. The numerous methods employed may be subdivided roughly according to the origin of the electrons producing the light pulse detected. For soft radiation the

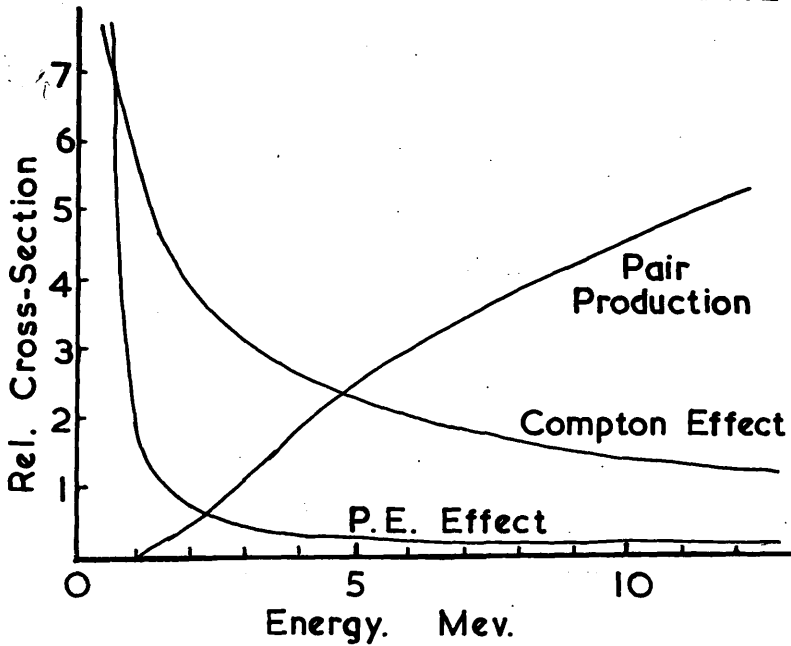


Figure 1.2. Absorption of Gamma-rays in Lead.

photo-electric absorption will be high and by using crystals containing material of high atomic number (e.g. sodium iodide) gamma-rays of energies of about 100 keV down to 10 keV or less can be measured as single peaks in a pulse size distribution⁽¹⁶⁾.

A single gamma-ray of higher energy will give rise to a complicated pulse size distribution. In addition to the photo-electric peak there will be a more or less continuous distribution of pulses with a sharp upper limit due to absorption of Compton electrons without absorption of the scattered quanta. For energies above 1 MeV there will also be a peak due to the absorption of a positron-electron pair without absorption of the annihilation radiation. The peaks due to these various processes will be broadened by such effects as imperfect light collection, escape of electrons from the crystal, and absorption in the crystal of secondaries produced outside it, and unless special precautions are taken the pulse-size distribution due to the simultaneous presence of more than one gamma-ray will be very difficult to interpret. Simplification may be effected by focussing attention on one of the processes mentioned. In the first instance, depending on the nature of the crystal and the energy of the gamma-ray, one process may predominate, as the absorption coefficient for photoelectric absorption, pair production and Compton absorption are proportional to Z^4 , Z^2 , and Z respectively and vary rapidly with gamma-ray energy.

The dependence on energy of these coefficients for lead is indicated in figure 1.2. which is based on curves of Bonner and Evans⁽¹⁷⁾ .

The predominance of the photoelectric peak for low energy gamma-rays has already been mentioned. Organic crystals, consisting chiefly of carbon, oxygen and hydrogen, tend to accentuate the Compton process, while at high energies in materials of high atomic number pair production will predominate.

Sharp peaks may be obtained from the Compton process if a second crystal is used to detect the scattered quanta and only the scintillations due to quanta scattered at a particular angle observed⁽¹⁸⁾ ⁽¹⁹⁾ . Similarly, the pair production peak may be isolated by using counters in coincidence to detect the annihilation radiation⁽²⁰⁾ ⁽²¹⁾ .

Methods of this kind are rapidly being developed and though their accuracy is so far less than that of magnetic spectrometers, their comparatively high sensitivity and short resolving time (especially short for the organic materials where the fluorescence is essentially a molecular and not a crystal structure effect) makes them extremely important. A general survey of the technique, together with data on suitable crystals, has been given by Jordan and Bell⁽²²⁾ , and data on fluorescent liquids by Kallman and Furst⁽²³⁾ .

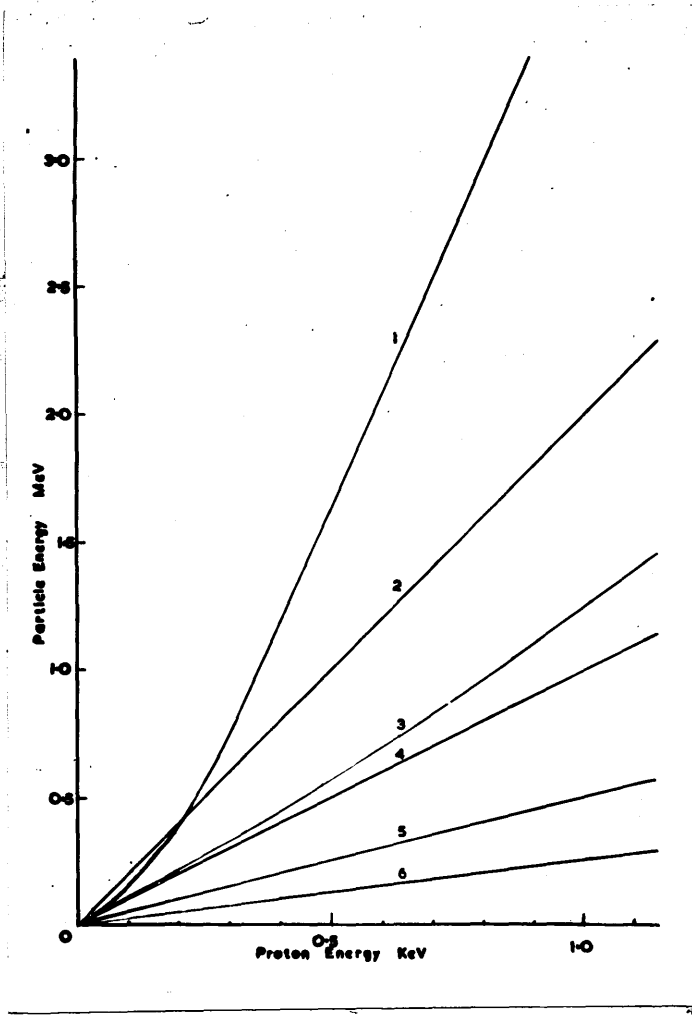


Figure 1.3

Comparison of proton range and deflection with other particles.

1. Alpha-particle with same range.
2. Deuteron with same range.
3. Alpha-particle with same electrostatic deflection.
4. Deuteron with same electrostatic deflection.
- He⁺ ion with same electrostatic deflection.
- Alpha-particle with same electromagnetic deflection.
5. Deuteron with same electromagnetic deflection.
6. He⁺ ion with same electromagnetic deflection.

I. 6.3. Particle energy Measurement.

The third method of locating energy levels involves the measurement of the energy of the particle Y_D^Z (fig.1.1.). This particle will usually be either a neutron, proton, or alpha-particle.

Considering first the neutrons, those from reactions involving light nuclei will have energies up to 18 MeV. ($T^3(d, n)He^4$). These energies are usually measured by measuring the energy of protons or carbon nuclei set in motion by elastic collision with the neutron. As the range of these recoil nuclei depends on the angle of recoil this angle must be known. This may be achieved either by the use of special counters sensitive only to recoils in a particular direction or by observing the tracks of the recoil particles in a cloud chamber or a photographic emulsion. In some special cases use may be made of radioactive threshold detectors, but this method is not generally applicable. The most accurate determinations of the energy of fast neutron groups have an accuracy of about 2%.

The energies of charged particles, on the other hand, can be measured with greater precision. Originally, the particle groups from light nuclei were measured by determining their range in air or thin foils, suitable corrections being made for the straggling of the particles⁽²³⁾. The energies were deduced by comparison with the ranges of alpha-particles from radioactive sources. The energies

of the alpha-particles had been measured accurately by finding the curvature of their path in a magnetic field⁽²⁴⁾. Recently, more accurate determinations of the energies from light nuclear reactions have been made by direct comparison with particles from radioactive sources in magnetic or electrostatic fields. An absolute determination of the energy is more difficult. Owing to the deflection of the incident particles it is not usually possible for the target to lie within the field, and difficulties arise in the exact calculation of fringing field effects. This limitation is most severe in the case of magnetic analysers; though it is possible to avoid it by allowing the beam to enter through a hole in one of the poles, parallel to the magnetic field. With electrostatic analysers, calculation of the fringing fields is possible and such analysers have been used for absolute measurements of the energy of both the bombarding particles and the reaction products⁽²⁵⁾⁽²⁶⁾. With magnetic spectrometers energy measurements have been made with errors of less than 0.1%⁽²⁷⁾.

In addition to increased accuracy the analysers have another advantage over range measurements for short range particles. The bombarding particles will be scattered from the target in great numbers, and if the target is thick or has a thick backing, these scattered particles will prevent range measurements being made on any

particle groups with ranges not greater than the maximum range of the scattered particles. However, if the particles to be detected are heavier than the bombarding particles and a magnetic analyser is used, particles having the same charge and not less than the same momentum but less range than the bombarding particles can now be detected. Electrostatic analysers will detect particles of the same charge only if they have greater energy than the scattered particles.

In order to detect particle groups of lower energy than can be separated by an electromagnetic analyser it is necessary to use thin foil targets. The scattered particles will then form a single group or, if the target contains nuclei of differing masses, a series of groups. Low energy reaction products can then be detected in regions where scattering from thick targets would obscure them. By suitable choice of electrostatic or electromagnetic deflection it is usually possible to avoid the coincidence of a scattered group with the group to be investigated. Graphs showing how groups of differing particles of various energies may be separated are given in figure 1.3.

The Q-value for a particular reaction can be obtained from the particle energy by use of the expressions given in appendix 1, corrections being made for the effects of target thickness and surface films as indicated in section I. 6.1. A full

treatment of these and relativistic corrections has been given by Brown, Snyder, Fowler and Lauritsen⁽²⁸⁾.

In addition to the determination of level position by measurement of the energy of heavy charged particles, the end point of a beta spectrum will locate an energy level in the residual nucleus if the nucleus is left in an excited state. Several levels in light nuclei can be excited in this way, (e.g. levels in Ne^{20} , O^{16} , N^{14} , and Li^7). The excitation of nuclei by the use of high energy electrons or electromagnetic radiation is also possible, but these methods of excitation are outside the scope of this thesis.

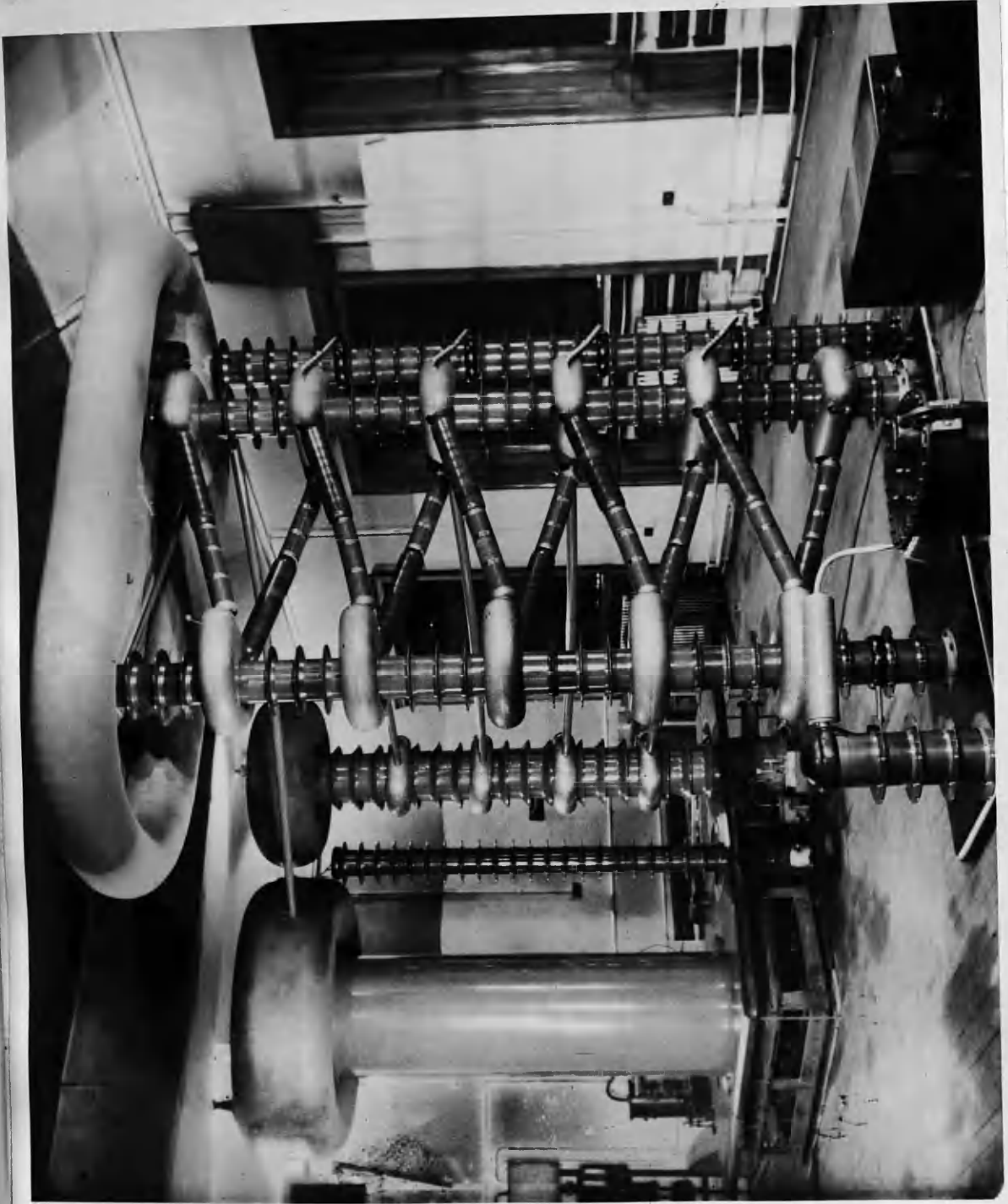


Figure 2.1. General view of accelerating equipment.

Part II. Accelerating Equipment.

II. 1. General.

II. 1.1. Site.

The generator and accelerating tube are housed in a large room previously used as a practical laboratory for the honours class. Sufficient clearance for a voltage of 800Kv was obtained by raising the ceiling. The beam travels through the floor of this room to the floor below, where one room contains the target assembly and the detecting equipment. An adjacent room on the same floor acts as a control room. This arrangement has proved very satisfactory in practice, though the space available in the control room is rather less than would be desirable.

II. 1.2. History of installation.

The generator was initially erected in July 1947. The first ion beam was obtained in April 1948. The first nuclear physics experiments were started in October of that year, though numerous troubles with the ion source prevented much work being done before the second half of 1949. Since then more rapid progress has been made, but various faults in the cascade generator have occurred. The repair of these faults has occupied a great deal of time, especially since spares for the generator have not been easy to obtain.

Table I shows the dates of the important stages in the development of the accelerating equipment.

TABLE I

July 1947	Cascade generator erected and tested.
August 1947	Vapour pumps tested.
October 1947	Erection and optical alignment of tube completed.
November 1947	Voltage applied to tube and outgassing started.
March 1948	Ion source installed on accelerating tube.
April 1948	Beam of 20 μ a at 400 Kv obtained.
June 1948	Beam increased to 150 μ a by alignment.
August 1948	Analysing magnet and resolving chamber fitted. Beam of 60 μ a protons obtained.
October 1948	First nuclear physics experiments started.
January 1949	Breakdowns of generator due to failures of condensers. Short life of ion source causing difficulty.
February 1949	Development of new ion source started.
June 1949	New source installed. Design of first accelerating stage improved. Resolved proton beam of 120 μ a obtained.

II. 1.3. Personnel.

The original work on the accelerator was carried out by Dr. Warren, who, however, left the department in 1947. The author was not associated with the project until August 1947, at which time the cascade generator had been erected and tested, the power stack had been erected and the major part of the pumping system completed but not tested. The accelerating tube was being constructed to a design of Messrs. Philips, but no work had been started on the equipment for the target room.

Dr. J.G. Rutherglen was, at this time, working on the design of the ion source. While this was being done the erection of the accelerator column was completed. Since this was installed Dr. Rutherglen and the author have been working continuously on the equipment; the work on individual items being divided between them as circumstances permitted.

Mr. W. McCall was responsible for the work carried out in the department's workshops and Mr. T. Pollok, technician attached to the project, for much of the electrical equipment necessary.

II. 2. Cascade Generator.

The high voltage generator is a five-stage Cockcroft and Walton generator supplied by Messrs. Philips of Eindhoven. This cascade generator is capable of supplying up to 5 ma of rectified current at 800Kv.

The maximum useful voltage from the generator is fixed by the size of the room in which it is installed. This room was originally 16 feet high, but the centre section of the ceiling was raised to give an overall height of 19 feet 6 inches. This enabled the five-stage generator to be erected with a clearance from the roof of about 8 feet. This is adequate for 800Kv; in fact it is hoped in the future to reach one million volts before corona and spark-over become serious.

In the space available a higher voltage could only be obtained using a pressurised generator. Such generators are, however, more difficult of access for servicing and as it was desired to have a machine operating in the shortest possible time, the simpler type was preferred. Although the generator itself was designed and erected by Messrs. Philips, in order to achieve a proton beam of the degree of homogeneity desired it was necessary to develop the smoothing and stabilising circuits described in the following sections.

II. 2.2. Details of generator.

The circuit of the generator is shown in figure 2.2. and a general view of the installation in figure 2.1. The generator is similar to those in use in several other laboratories which have been described elsewhere^{(29) (30)}. The power supply to the machine is at a frequency of 400 cycles,

supplied at 200 volts by a rotary convertor running from the three phase mains supply. The valves are heated by a 500 kilocycle current fed through the condensers associated with the multiplying circuit. Two bridging condensers (C_{16}, C_{17} fig.2.2.) are necessary to complete the R.F. circuit. These condensers are liable to be charged to an abnormally high voltage if the accelerating tube goes 'soft' and discharges the generator, so they are protected by spark gaps.

II. 2.3. Measurement of H.T. voltage.

The H.T. voltmeter on the generator control desk is a 0-500 micro-ammeter indicating the current through a $1,300 \text{ M}\Omega$ resistance R_3 whose high potential end is connected to the probe of the ion source. After passing through this meter the current traverses two stable wire wound resistors, (R_4, R_5 fig.2.2.), the potential across R_4 providing an input signal for the stabilising circuit (section II. 2.4.) and that across R_5 being fed to a potentiometer unit. This allows the current to be measured with an accuracy of 1 in 10^4 , though the $1,300 \text{ M}\Omega$ resistor cannot be relied upon to remain constant to this accuracy.

This resistance consists of a large number of 1 Watt, $1 \text{ M}\Omega$ spiral film carbon resistors, arranged spirally on a five-sided perspex former, and enclosed in a vertical tube built up of moulded bakelite sections. The tube is filled with

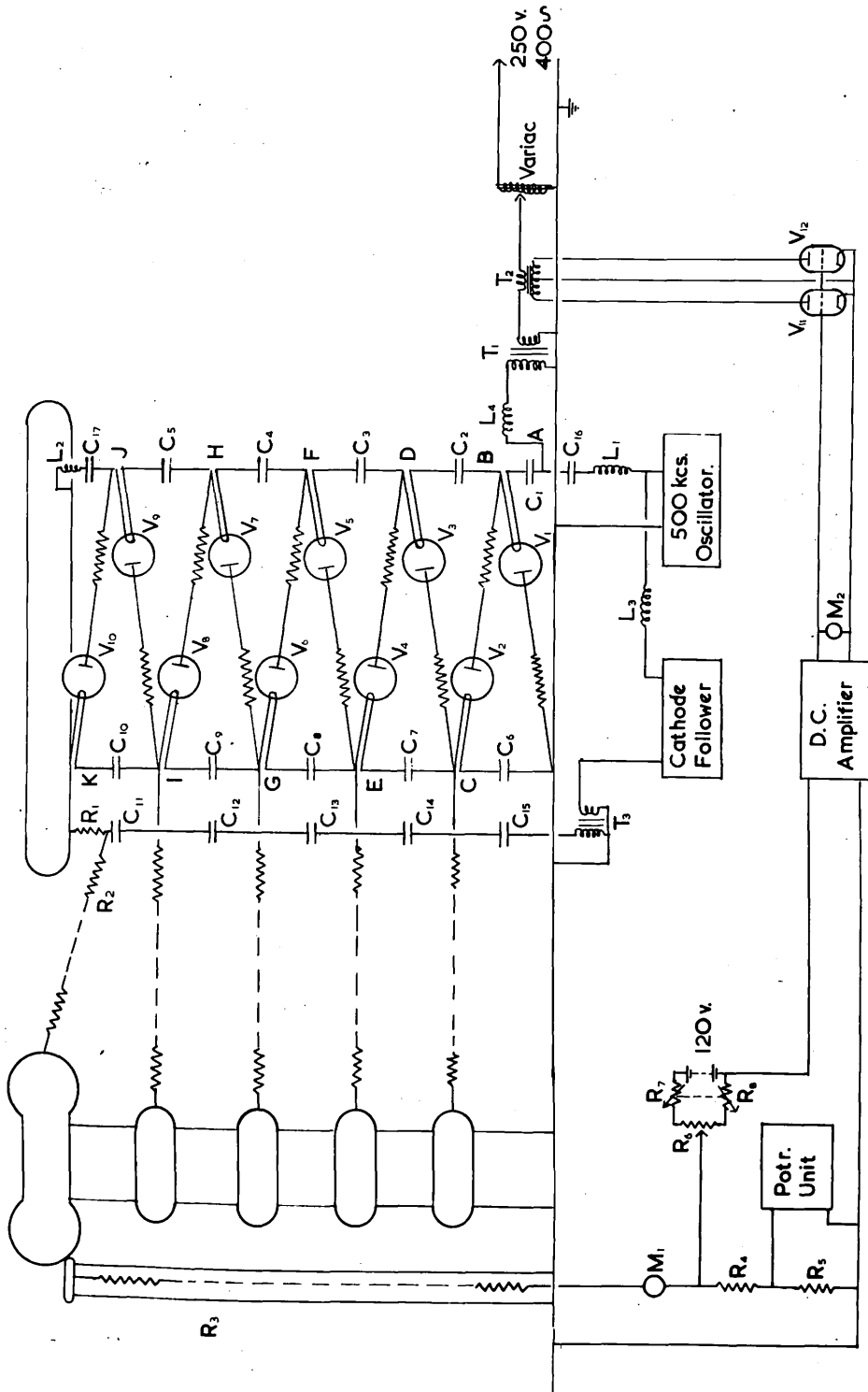


Figure 2.2. Circuit, Cascade Generator.

transformer oil which is circulated by a pump.

The temperature and voltage coefficients of the resistors are appreciable. Measurements on a typical batch of resistances gave the values:

Voltage coefficient $\alpha_v = -2.6 \times 10^{-5}$

Temperature coefficient $\alpha_T = -9 \times 10^{-5}$

$$R_{v,t} = R_o [1 + \alpha_v V] [1 + \alpha_t t]$$

$R_{v,t}$ = resistance at $t^\circ\text{C}$
with V volts
applied.

R_o = resistance at 0°C
with 0 volts
applied.

In addition to these variations, the resistance has shown a tendency to increase in value with time and on several occasions has become open circuited. These failures are attributed to the action of the transformer oil on the resistors: the protective varnish softens and the unprotected carbon film then disintegrates. Once a break has occurred, spark discharges take place under the oil and these usually result in the rapid destruction of adjacent resistors.

The effect of temperature and voltage changes on the resistors could be reduced by earthing the lower end of the resistance and measuring the potential across a few of the lower resistances; this would lead, however, to some

complications in the stabilising and measuring circuits and in view of the present unreliability of the resistance, has not been considered worth while.

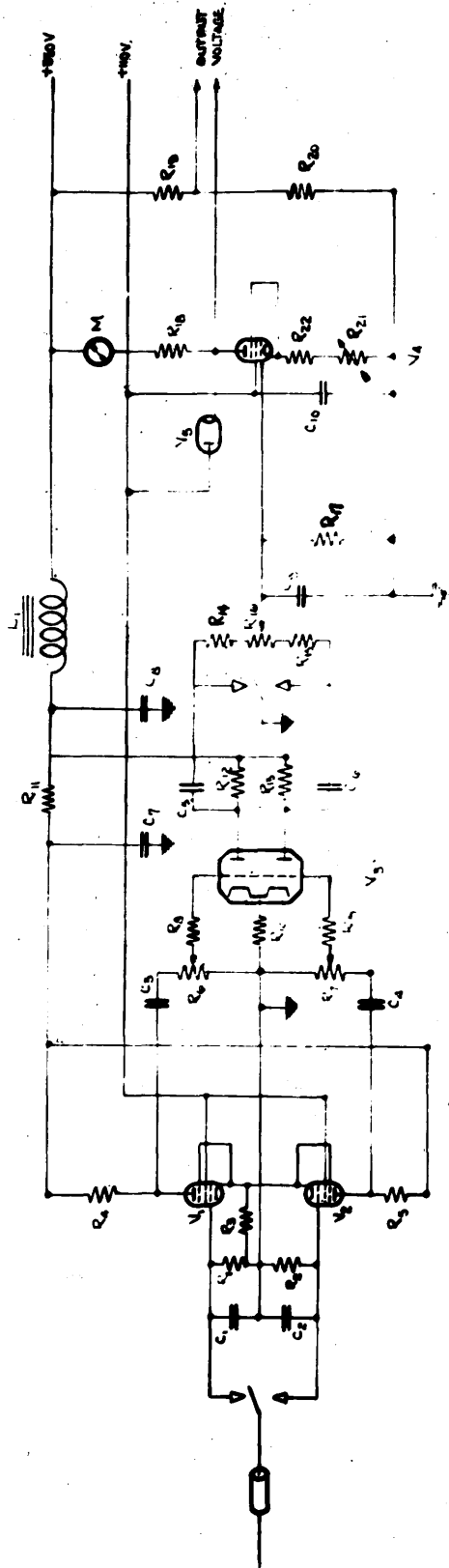
No attempt has been made to make absolute voltage measurements. The volt-meter is frequently calibrated by comparison with known nuclear resonances. Uncertainties of effective proton energy which arise from the possible presence of surface films on a target and the energy spread of the beam due to ripple on the generator voltage, have usually been greater than those due to the variations of the measuring resistance.

II. 2.4. Voltage Stabilisation.

In the absence of any stabilisation the H.T. voltage applied to the accelerating tube varies considerably as a result of changes in the mains supply voltage, changes in beam current and fluctuations in the rectifier valves. The effect of these variations was reduced by the stabilising circuit shown in figure 2.3. A constant fraction of the voltage on the accelerating tube is developed across R_2 and R_3 and the difference between this voltage and a reference voltage is amplified and applied to the grids of the control valves V_1 and V_2 . The reference voltage is derived from a 120 volt dry battery by means of the potentiometer R_4, R_5, R_6 .

In order to minimise drifts in the D.C. amplifier a "chopper" amplifier was designed. In this type of amplifier the input D.C. signal is converted by a rotary switch to a square wave. The square wave is amplified in a push-pull A.C. amplifier and then synchronously rectified by a second pair of contacts on the rotary switch. Thus the only source of drift will be changing contact potentials or thermal voltages in the input circuit, and these will be smaller than the changes experienced when using thermionic valves as D.C. amplifiers. In the present amplifier an A.S.B. radar aerial switch used as a "chopper" to generate a square wave at a frequency of 30 cycles. The circuit is shown in figure 2.4.

The rectified signal is amplified by V and fed to the grids of the control valves. These valves (V_1 and V_2 in figure 2.3.) are 250 watt triodes which conduct on alternate half cycles of the 400 cycle supply to the cascade generator and act as a variable resistance. The valve anodes are connected to the high ratio transformer T_1 the primary of which is in series with the supply to the cascade generator. The high resistance of the valves will then appear as a low resistance in series with this supply and variation of this resistance by variations in the grid voltage of V_1 and V_2 will control the voltage developed by the cascade generator. The overall response time is 1/10 sec.



L_1	100 μ H, 10 mA current
C_1	100 μ F, 500V
C_2	100 μ F, 500V
C_3	2 μ F, 50V
C_4	2 μ F, 50V
C_5	2 μ F, 50V
C_6	2 μ F, 50V ELECTROLYTIC
C_7	2 μ F, 50V ELECTROLYTIC
C_8	2 μ F, 50V ELECTROLYTIC
C_9	2 μ F, 50V
C_{10}	2 μ F, 50V

M	0.2 mA METER
V_1	6.5V 7
V_2	6.5V 7
V_3	6.5V 7
V_4	1A 50
V_5	350V
R_1	100 Ω 5W
R_2	100 Ω 5W
R_3	22 Ω 5W
R_4	100 Ω 5W
R_5	100 Ω 5W

R_6	100 Ω 500V POTENTIAL
R_7	10 Ω 5W
R_8	10 Ω 5W
R_9	10 Ω 5W
R_{10}	220 Ω
R_{11}	41 Ω 1W
R_{12}	100 Ω 5W
R_{13}	100 Ω 5W
R_{14}	22 Ω 5W
R_{15}	22 Ω 5W
R_{16}	50 Ω POTENTIAL

R_{17}	220 Ω 5W
R_{18}	100 Ω 5W
R_{19}	10 Ω
R_{20}	220 Ω
R_{21}	2 Ω POTENTIAL
R_{22}	22 Ω 5W

CHOPPER AMPLIFIER

Figure 2.4. D.C. Amplifier Circuit.

The stabilising circuit will reduce slow changes in the cascade generator output by a factor of 100 and has a controlling range of 10% of the generator voltage.

II. 2.5. Ripple Voltage.

The effective zero-frequency impedance of the cascade generator is given by the expression

$$Z = \frac{2n^3}{3fc}$$

$n =$ number of stages $= 5$
 $f =$ frequency $= 400 \text{ } \checkmark$
 $c =$ capacity of reservoir condensers in microfarads $= .015.$

$$\underline{=} 1.4 \text{ M}\Omega .$$

The generator is connected to the accelerator tube by a $2\text{M}\Omega$ resistor which protects the generator in the event of a discharge occurring in the accelerating tube. The normal current drain on the set including that due to the measuring resistor is about 1.5 m/a, resulting in a voltage drop from the unloaded figure of about 30 KV.

The ripple voltage due to the rectifying action of the circuit is given by the expression

$$\delta v = \frac{i}{fc} \frac{n(n+1)}{2} \quad i = \text{current taken from generator.}$$

$$= 2.5 \text{ KV per m/a.}$$

In the present generator, however, this ripple voltage is smaller than that due to capacitive

diagram of the generator and its equivalent circuit.

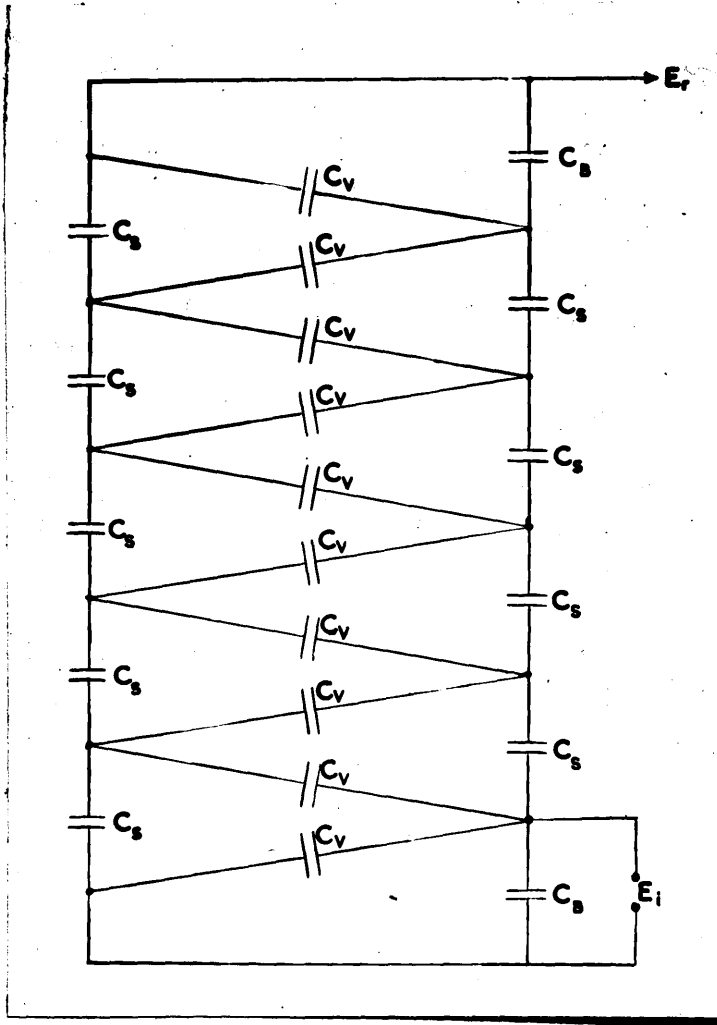


Figure 2.5. Equivalent circuit of generator for production of ripple.

pickup of the input voltage by various paths. The most important of these is that via the valve capacities and the bridging condenser necessary to complete the circuit carrying the R.F. current which heats the rectifying valves. The effect of these may be calculated as follows ...

Let C_v = valve capacity = 30 pf

C_B = capacity of Bridging condenser = 120 pf

C_S = capacity of main stack condensers =
 $.015 \mu F$

The relevant part of the generator circuit is shown in figure 2.5. As $C_v \ll C_S$ the A.C. voltage on the A.C. side of the generator will be constant, and we may add the individual contributions of each valve capacity to obtain the total ripple.

We have:

$$E_r = E_i \left[\frac{2C_v}{C_S} + \frac{2C_v}{C_S/2} + \frac{2C_v}{C_S/3} + \frac{2C_v}{C_S/4} + \frac{S/C_S}{\frac{1}{C_v + C_B} + \frac{9}{C_S}} \right]$$

where the last term, due to the capacity of the bridging condenser C_B and the top valve capacity in parallel, is the largest.

$$\therefore E_r = E_i \left[\frac{20C_v}{C_S} + \frac{5 [C_v + C_B]}{C_S + 9 [C_v + C_B]} \right]$$

which leads to $E_r = .09 E_i$, or for a H.T. voltage of 500 KV a peak to peak ripple of 9 KV.

II. 2.6. Smoothing Circuit.

For most experiments it is desirable that the ripple voltage on the generator should be reduced to a minimum. This is particularly true for excitation curves and experiments involving accurate measurement of the energies of charged particles produced in nuclear reactions. The energy spread of the particles reaching the target can, of course, be reduced using a high resolution in the resolving magnet; this, however, will involve serious loss of beam intensity if the unresolved beam has a large spread in energy. The ultimate limit to the homogeneity of the beam obtainable depends on the spread in energy of the protons leaving the source; in the case of the high voltage sources this spread will amount to several thousand electron volts. With the R.F. ion source used, the normal extraction voltage is about 1600 volts, which sets an upper limit to the possible energy spread. In fact, as most of the plasma is at the extraction potential, the majority of ions will be accelerated with full extraction volts; the energy of the ions in the plasma due to the R.F. discharge is small.

Most of the energy spread of the proton beam is due to the ripple discussed in paragraph 2.5. A reduction in this ripple is, therefore, very desirable and it is practicable to achieve this with a resistance capacity filter. The capacity used consists of five

.015 μ fd condensers in series; these condensers are similar to those used in the cascade generator itself. The smoothing resistance is limited in value by the permissible voltage drop; a value of 10M Ω was chosen. This results in a voltage drop of 20 KV at a total drain of 2ma; while the ripple will be reduced by the ratio

$$K = \frac{1}{w C R}$$

where $w = 2 \pi \times 400$

$$R = 10 M \Omega$$

$$\approx \frac{1}{75}$$

$$C = .003 \mu \text{Fd.}$$

Owing to the limited space available considerable difficulty was experienced in the installation of the smoothing condenser stack. Originally it was placed about 60 cms. from the D.C. side of the cascade generator; the intermediate points on the smoothing condenser were presumed to adjust themselves to the correct voltage by corona action and were left floating. The top of the condenser stack was connected to the set by an oil immersed 10M Ω resistor protected by a spark gap. The intermediate electrodes were connected direct to the appropriate points on the cascade generator.

This arrangement proved to be unsatisfactory. When a discharge occurred, surges in the cascade generator resulting from the direct connection (via the spark gap) to the top of the smoothing condenser, caused sparks to occur between the valve cases,



Figure 2.7. Spark to smoothing condenser.

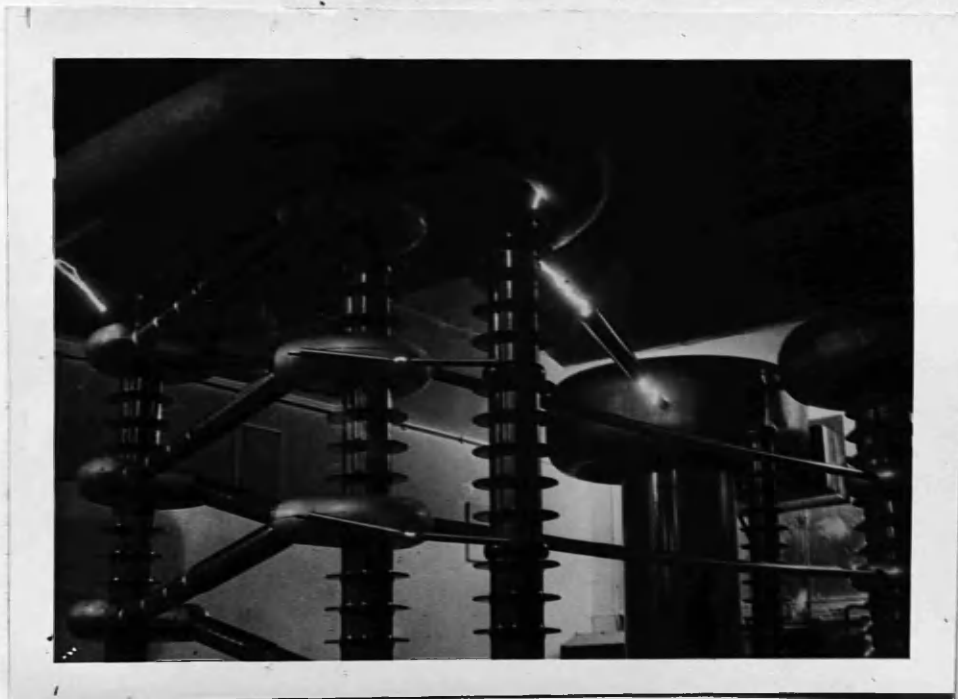


Figure 2.8. Spark along surge limiting resistor.

puncturing the bakelite condenser sections of which they are built. (Figure 2.6.).

A position for the smoothing stack roughly equi-distant from the generator and power stack with each section of the condenser tied to the appropriate point on the cascade generator and to the corresponding accelerator tube electrode was next tried. This would undoubtedly be the best arrangement, were more room available, but with the greatest spacing possible it was found that if a tube discharge took place at voltages above 600 KV. breakdown occurred between the top of the accelerating column and the smoothing stack. (A typical spark is shown in Fig.2.7.).

Next an arrangement, similar to that originally used, was tried, but with the junctions of the condensers in the D.C. side of the cascade generator by the short spark gaps. This arrangement was successful in preventing the internal spark-over of the generator previously noted, but the surges produced now resulted in spark-over along the length of the resistance from the smoothing condenser to the accelerating column.

Finally, the generator was moved so as to increase this distance to 12 ft. and this arrangement proved satisfactory up to 700 KV. Above this voltage the surge limiting resistor was still liable to breakdown, and fig.2.8. is a photograph of such a failure. In addition to this spark along the length of the resistance (the central portion of

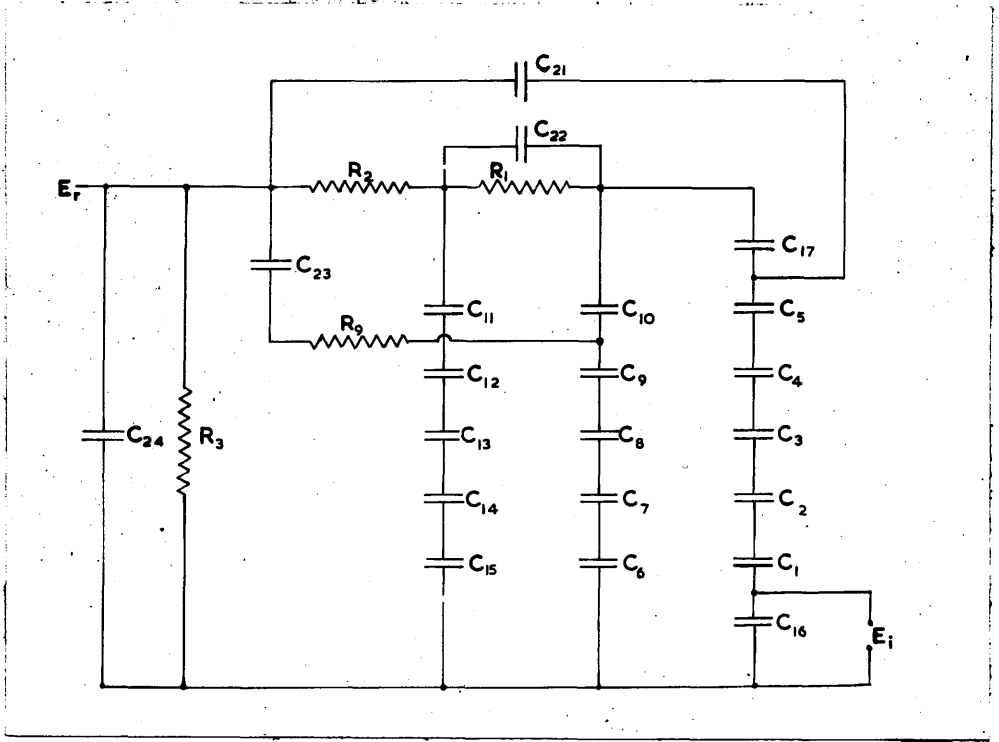


Figure 2.9. Equivalent circuit of generator, smoothing stack and accelerator tube.

which is concealed by the paxolin corona shield) discharges across the gaps tying the sections of the smoothing stack to the D.C. side of the generator, and two sparks across the gap protecting the upper bridging condenser (C_{17} in fig.2.2.) are clearly shown.

Unfortunately the effect of the RC filter is reduced by a ripple voltage fed from the A.C. side of the cascade generator to the top of the accelerator column owing to the stray capacities that exist between the various parts of the installation. For instance the capacity between the top of the accelerator tube and the A.C. side of the generator is approximately 1.5 μ f, and the impedance of such a capacity at 400 cycles is not negligible compared with the impedance to ground. Another important path whereby ripple voltage reaches the high tension terminal is that due to the interelectrode capacity of the accelerating column. The electrodes are connected to the junctions of the condensers on the D.C. side of the generator by $10M\Omega$ resistances. The ripple voltages on each of these will be $1/5$, $2/5$, $3/5$ and $4/5$ respectively of the ripple on the top of the set. As the capacity between the top electrode and the top of the set is about 20 pf, and the impedance of the top of the set to ground is very nearly that of R_2 i.e. about $1.5M\Omega$ this effect is important. Further possible paths for ripple pickup exist, particularly the distributed

capacity between both the A.C. and D.C. sides of the cascade generator and the top feed resistor. The major paths are represented in the simplified circuit of fig.2.9.

C_{21} = Capacity A.C. side of generator to top of accelerating tube ≈ 15 pf.

C_{22} = Capacity from A.C. side of generator to top of smoothing condenser ≈ 10 pf.

C_{23} = Capacity from first accelerating electrode and connecting resistor to top of accelerating tube ≈ 2 pf.

C_{24} = Capacity from top of accelerating column to ground ≈ 25 pf.

C_{22} will not be important as it is small compared with the smoothing condenser made up of $C_{11} - C_{15}$ in series. C_{21} and C_{23} have impedances at 400 cycles, which are high compared with R_2 and R_3 . The impedance of R_3 and C_{24} is high compared with $C_{11} - C_{15}$ in series with R_2 . Consequently, the ripple voltage will be given by:

$$E_r = E_1 \omega C R_2 + 4/5 \cdot E_5 \omega C R_{23}$$

E_r = RMS ripple voltage out.

E_1 = RMS ripple voltage on secondary of input transformer.

E_5 = RMS ripple voltage on D.C. side of generator.

$$\frac{1}{10} E_1 \text{ (Section II. 2.5.)}$$

$$E_R \approx E_1 \omega R_2 [C_{21} + 0.08 C_{23}]$$

$$1.4 \times 10^{-2} E_1$$

$$C_{21} \approx 1.5 \text{ pf.}$$

$$C_{23} \approx 20 \text{ pf.}$$

$$R_2 \approx 2 \text{ M}\Omega.$$

$$\text{H.T. Voltage} = E_{D.C} = 10 \sqrt{2} E_1$$

$$E_R = 10^{-3} E_{D.C.}$$

or the peak to peak ripple voltage is approximately one third percent of the H.T. voltage. This corresponds to about 1.6kV at 500kV and will be much greater than the ripple fed via the coupling resistance and smoothing condenser from the generator.

It is difficult in the space available to reduce the stray capacities responsible for this ripple and it was, therefore, decided to cancel the ripple by feeding a voltage of the opposite phase to the bottom of the smoothing condenser.

A suitable voltage is derived from the earthy end of the bridging condenser C_{16} (figure 2.2.) A choke L_3 offers a high impedance to the radio-frequency valve heating current, and after a phase correcting network the voltage is fed to the grid of a cathode follower. This in turn feeds the voltage via a step-up phase reversing transformer T_3 to the bottom of the smoothing condenser.

By adjusting the phase and amplitude controls it was found possible to reduce the ripple to less than .05% of the H.T. voltage.

II. 2.7. Operation of the generator.

The control desk for the generator is situated in a room next to the beam room, on the floor below the generator itself. An interlock is provided on the door of the H.T. room and a safety key (which prevents operation of the set when it is removed) is used to protect anyone working on the set. A thermostatic heating system maintains the temperature of the H.T. room above 20°C., the minimum operating temperature for the rectifier valves.

When the generator is switched on two minutes are allowed for the filaments to heat and the H.T. voltage gradually raised to the operating value. While this is done the Pennig vacuum gauge is watched to ensure there is no dangerous rise in pressure likely to cause a tube discharge. Once the tube has been thoroughly outgassed the full H.T. voltage can normally be applied after a few minutes of operation; though if air is admitted to the tube several days operation is required before the tube is completely normal.

The corona current becomes noticeable above 600kV and at 750kV the total D.C. load on the set is about 1.5 ma., of which about 600 μ a is due to the measuring resistance, about 600 μ a to the ion beam and the remainder to corona. The corona current is increased by the presence of dust particles or other irregularities and as large quantities of soot are precipitated on to the set

and walls of the room by the electrostatic field, frequent cleaning is necessary.

2.8. Reliability

Though this type of generator has proved in the past to be capable of trouble free operation over long periods of time⁽¹⁰⁶⁾; the present installation has not been good in this respect. The troubles have mainly been due to difficulties experienced in the Philips factory in obtaining the same quality materials that were used in the pre-war generators.

The three main types of faults that have been experienced are:-

(a) Failure of condensers in the generator. Now that the original condensers have been replaced by others of later manufacture no further failures have occurred.

(b) Failure of rectifier valves.

These troubles were due to breakdown of the cases of the mercury vapour rectifiers. These cases are built up of a number of bakelite sections, each suitably metallised to form a condenser of about 150 pf. These condensers serve to distribute the inverse voltage evenly along the length of the valve. The moulding powder from which these condensers were made differed slightly from the original and the sections frequently puncture with consequent failure of the valve.

(c) Failure of measuring resistor.

This resistor is constructed of a large number of one watt

spiral film carbon resistors. The varnish protecting these resistors is softened by the transformer oil in which they are immersed and this leads to their failure. Once one resistor has reached a high value sparking occurs and rapidly destroys neighbouring resistors. Several such breakdowns have occurred.

II. 2.9. Servicing of Generator.

In order to facilitate the maintenance of the generator three winches were fixed in the roof of the H.T. room, one each above the actual generator, the accelerating column, and the power stack. A special servicing trolley of welded angle-iron was constructed to enable access to be gained to the high tension terminals. This trolley may be seen in the background of fig.2.7.

The location of faults in the generator itself proved to be comparatively simple. The first sign of trouble was usually either a high current in the primary of the main H.T. transformer or the development of jitter of the H.T. voltage. A high primary current can be caused either by a soft valve or a short-circuited condenser. A valve fault can usually be detected by the consequent heating of the limiting resistance in series with it. If either of the bridging condensers C_{16} or C_{17} in fig.2.2. fails the primary current will be high when the valves are cold. If one of the reservoir condensers C_1 to C_{10} fails the current will be normal when the rectifiers are cold but high when they are hot and the two valves connected across the

condenser will over-heat (i.e. if C_7 fails V_3 and V_4 will over-heat).

The second type of fault is associated with intermittent striking of one of the rectifier valves. Should one of these valves cease to conduct the voltage on the top of the set will decay exponentially and at the same time a reverse voltage will build up across the faulty valve. Should the valve be completely non-conducting (as a result, for example, of the failure of its heater supply) the full set voltage may develop across this valve. This is likely to cause further damage and care must be taken to see that the primary voltage of the input transformer is never dangerously higher than that appropriate to the D.C. voltage indicated on the set voltmeter.

The faulty valve is identified by measuring the voltage on each stage of the cascade generator, commencing with the voltage on C_1 . The voltmeter used consists of a 500 microamp meter and a $200M\Omega$ resistor made up of 170 2 watt carbon resistors mounted in series on a long pole. With a total H.T. voltage of about 150 kV the voltage developed by each valve can rapidly be checked and compared with that expected for normal operation. Failure to strike correctly may be due to the room temperature being below 20°C ., or to some internal fault in the valve. In particular, if one or more of the condenser sections in the valve case is faulty

this will cause incorrect distribution of voltage across the valve and may result in jittery operation. Occasionally a sudden overload on the generator may cause the mercury to become irregularly distributed in one of the valves; it will usually recover after several minutes operation with a load current of 2 ma or more.

Though various other faults have occurred from time to time these have usually been easily rectified. The effect of a failure in the measuring resistance is worth noting: when a large number of resistors have become open-circuited the fault is immediately manifest by a spectacular and noisy brushing discharge down the side of the resistance assembly. In its initial stages the fault can only be detected by examining the current down the resistance with an oscilloscope. If a fault is present, superimposed on the normal 400 cycle ripple there will be a sawtooth waveform of irregular amplitude and duration.

2.3. Accelerator Tube.

1. General

The tube is required to produce a high intensity parallel beam of high energy ions at the target. This problem is similar in some ways to that of producing a high intensity beam of electrons for use in a cathode ray tube. A great deal of work has been carried out on the design of both magnetic and electrostatic electron lenses and the techniques thus developed may readily be adapted for use in the design of suitable lenses for proton beams^{(31) (32)}. As the focal length of magnetic lenses is proportional to the mass of the particle being focussed, while the focal length of electrostatic lenses depends only on the charge, the latter lenses are, therefore, more convenient for focussing positive ions.

Probably the most important practical difference to be noted in the design of these lenses is the relatively large effect of space charge, due to the smaller velocity of the positive ions. As the velocity of the ions for a constant accelerating voltage is inversely proportional to the square root of their mass, the space charge effects experienced with proton beam currents are comparable with those of electron beam currents $\sqrt{1837} = 43$ times as large. It is, therefore, important that the proton beam is initially accelerated to a high voltage in the shortest possible distance, and that cross-over points resulting in regions of high space charge are

avoided as far as possible.

Owing to the large mass of the proton, compared with that of the electron, relativistic variation of mass with velocity, which leads to difficulties in the design of lenses for energy electrons, is negligible for 1 MeV protons (a 1 MeV proton has a velocity of 1.38×10^9 cms. per second and a De Broglie wavelength of 2.86×10^{-12} cms.).

In the design of the accelerating tube, attention must also be paid to the reduction of the reverse electron current travelling up the tube. These electrons cause an additional drain on the generator, produce X-rays on impact with the high voltage electrode, resulting in an undesirable background radiation near the target, and may over-heat the ion source.

The electrode surfaces must be smooth and suitably rounded to prevent the occurrence of local high fields resulting in the cold emission of electrons. It is also desirable that all insulating surfaces shall be completely shielded from the ion beam, otherwise surface charges may accumulate and deflect the beam.

II. 3.2. Construction of tube.

The accelerating tube used is built up with steel electrodes insulated with porcelain cylinders, the joints being sealed with rubber gaskets. A sectional diagram of the final arrangement is shown in fig.2.10. The acceleration

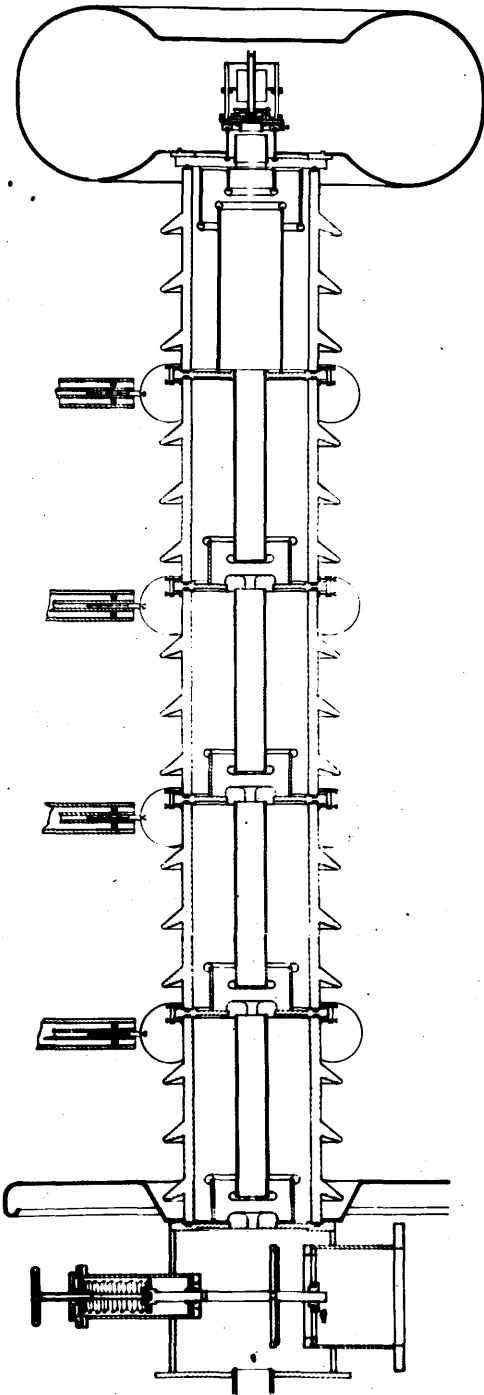


Fig.2.10. Sectional
Diagram of Accelerating
Column. Scale 1/20.

takes place in five stages, the intermediate electrodes being held at appropriate potentials by connection to the corresponding stages of the cascade generator. These connections are made with $10M \Omega$ resistors constructed from over 200 $\frac{1}{2}$ watt carbon resistors soldered end to end. These resistors are contained inside a one-inch diameter paxolin tube. This tube is covered with a similar tube two inches in diameter to reduce corona effects.

The accelerating electrodes are a copy of those successfully used by Messrs. Philips in an installation at Eindhoven. As this installation had a high-voltage ion source similar to that of Oliphant and Rutherford⁽³³⁾, the top electrode was modified to allow the installation of a R.F. type source (section II. 2.4.). The electrodes have comparatively small diameter apertures; this reduces the secondary electron current travelling up the tube.

Two main difficulties have arisen with this tube. Firstly, chiefly owing to mechanical inaccuracies especially of the porcelain insulating cylinders, considerable trouble was experienced in aligning the tube. Secondly, several modifications had to be made to the first accelerating stage before a reasonable proportion of the exit current from the source could be focussed on the target.

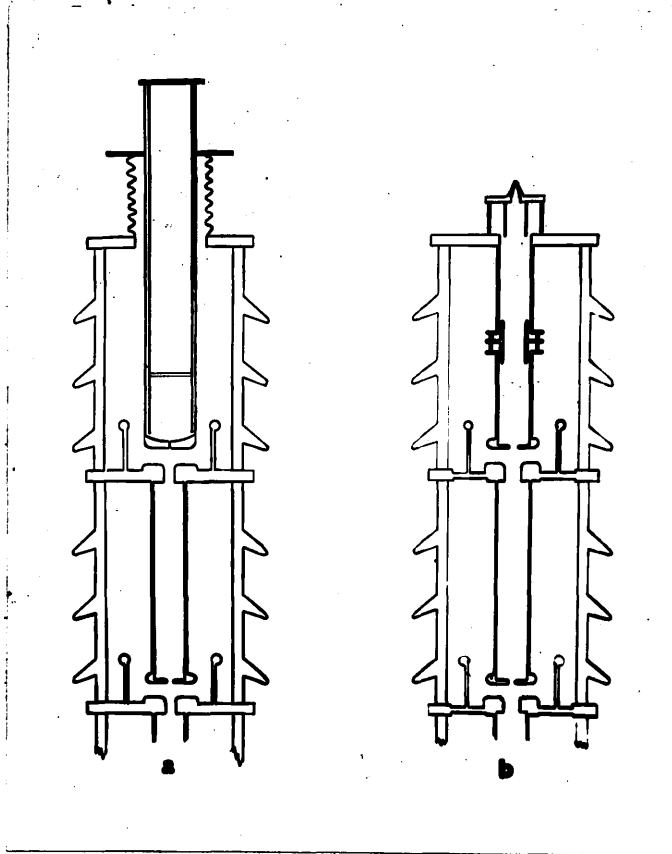


Figure 2.11. Experimental Focussing Arrangements.

II. 3.3. Initial Installation.

The original design of the tube with the high voltage ion source is shown in fig. 2.11 (a). For test purposes the ion source and first lens were set up on their own and tested with the aid of a 50kV D.C. generator. In the arrangement of the first accelerating lens originally tested the ion source was mounted on the top plate of the tube. In this arrangement the exit beam from the ion source is accelerated to a potential of up to 8kV and brought to a focus near the focal point of the first main accelerating gap. As this gap accelerates the ions to one-fifth of the main H.T. voltage it has a high voltage ratio and a short focal length. Consequently, the 8kV beam from the ion source has to travel about 50 cm. to a cross-over point, and space charge effects become troublesome. Further as the main H.T. voltage increases the strength of the lens formed by the first gap increases and the magnification and hence the size of the spot on the target increases.

The first modification to this system consisted of the introduction of an auxiliary electrode approximately half-way between the ion source and the first main lens. This was maintained at a voltage more positive than the adjacent electrode and thus formed a symmetrical lens in which the ions are first retarded and subsequently accelerated to their original energy. This arrangement is shown in figure 2.11 (b) and it was in this form that the

top electrode was first fitted to the accelerating tube. After further modification to allow the auxiliary electrode to be adjusted laterally without disassembling the tube it was found possible to obtain a total beam current at the target of 100 μ a at 300kV. The image size, however, varied with the H.T. voltage and the beam current decreased seriously as the voltage was raised to 600kV.

II.3.4. Modified Accelerating Tube.

In order to overcome this difficulty the first accelerating stage was completely re-designed so as to eliminate the cross-over point before the first main accelerating lens.

In this arrangement shown in figure 2.12. the ions emerging from the ion source canal are first accelerated by the focus voltage (0 to 16kV). Electrodes F and G form a positive lens but the focussing effect of this lens is small, as the object (the end of the ion source canal) will lie very near to the image side principal plane of the lens. Thus a virtual image smaller than the object will be formed close to the object. The main effect, therefore, of varying the focus voltage will be to alter the voltage ratio across the next lens. This lens is of large aperture so as to accept as much as possible of the diverging beam from the ion source, and consists of a four-inch diameter cylinder I followed by a six-inch diameter cylinder J. This lens will have one-fifth of the

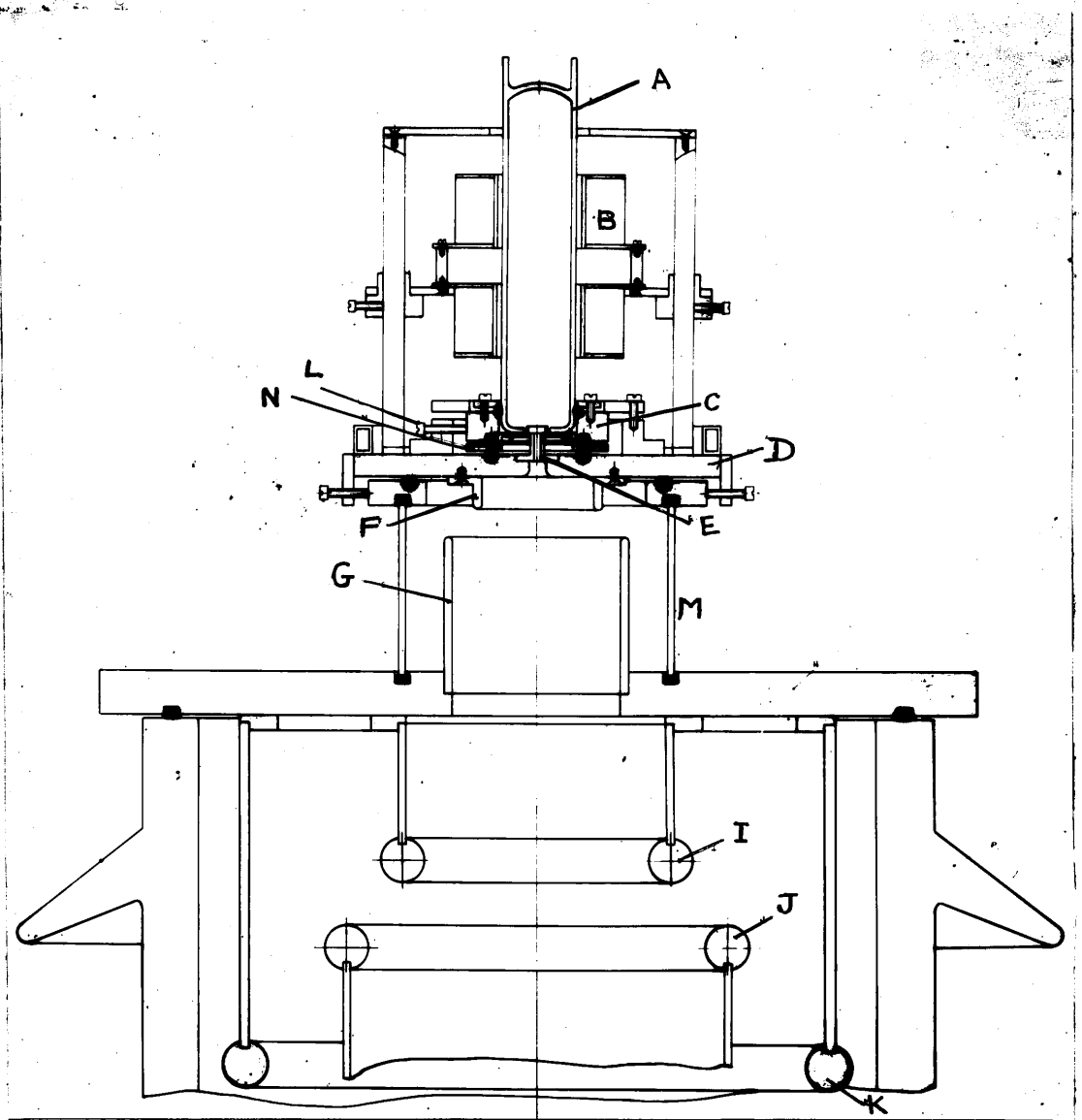


Figure 2.12. Ion Source and first accelerating lens.

main H.T. voltage across it. By adjustment of the focus voltage the voltage ratio and hence the focal length of this lens may be kept constant as the main H.T. voltage is varied. This ratio is normally maintained at about 15:1. Published curves show that this lens can be considered as a thin lens 3.2 inches in front of the accelerating gap with an object side focal length f_1 of 2 inches and an image side focal length f_2 of 9 inches, and it will, therefore, produce an image above the second accelerating gap. In a similar manner the effect of the successive accelerating gaps may be determined. Only the first gap will act as a strong lens, however, the voltage ratio across the remaining gaps becoming successively smaller.

The image positions and magnifications calculated in this way are only true for paraxial rays (rays whose angle with and position from the axis remains small) and if space charge effects are negligible. Neither of these conditions is closely fulfilled, and an accurate determination of the image by the above methods is not possible. However, it is found in practice that most of the beam that passes the first electrode reaches the target: the loss of beam to this electrode is due partly to the effects of space charge considered in the next section. An improvement might be obtained by inverting all the lower electrodes, thus shortening the path inside the first electrode and reducing the

size of the image produced by the first lens. It is hoped to try this modification later.

II. 3.5. Effect of Space Charge.

The importance of space charge effects in the focussing of ion beams was noted in section II. 3.1. An estimate of the magnitude of these effects can be obtained by making the following assumptions:

- (1) The charge and current densities are uniform across the beam. (This would be true for a beam diverging from a point source. The actual ion beam has a fairly uniform central core surrounded by a comparatively large fringe of low intensity).
- (2) The electric potential does not change along the length of the beam. (This condition will hold for the sections between actual accelerating gaps).
- (3) The potential difference (due to the space charge) between the centre and edge of the beam is small compared with the potential corresponding to the velocity of the particles. (This condition is satisfied closely).
- (4) The angle of convergence or divergence of the ion beam is small. (The actual angles are small except in the initial focussing lenses).

Let

- E = Radial electric field due to space charge.
 v = Velocity of ions.
 x = Distance travelled by beam.

and

$$\begin{aligned}\rho &= \text{Charge density.} \\ r &= \text{Radius of beam.} \\ j &= \text{Current density.}\end{aligned}$$

where the subscripts 0 and 1 refer to the initial and final values.

Then

$$E = 2\pi r \rho$$

If the ions have charge e and mass m , then the radial acceleration due to space charge will be:

$$\text{Put } R = \frac{r}{r_0} \quad \frac{d^2 r}{dt^2} = \frac{2\pi r \rho e}{m}$$

$$\text{Then } \frac{d^2 R}{dx^2} = \frac{1}{v^2 r_0} \cdot \frac{dr}{dt^2} \quad \left(v = \frac{dx}{dt}\right)$$

$$R \cdot \frac{d^2 R}{dx^2} = \frac{r}{v^2 r_0^2} \cdot \frac{2\pi r \rho e}{m}$$

$$\text{As } \pi r^2 \rho = \pi_0 r_0^2 \rho_0$$

$$R \frac{d^2 R}{dx^2} = \frac{2\pi \rho_0 e}{m v^2}$$

$$= \frac{2\pi j_0 e}{m v^3}$$

$$= \text{constant.}$$

The evaluation of the integrals resulting from the solution of this equation has been performed by several authors. A useful graph giving the divergence of a parallel beam has been published by

Smith, Parkins and Forrester⁽³⁵⁾. For converging and diverging beams, expressions derived by Borries and Dosse⁽³⁶⁾ for electron beams may be used, making allowance for the greater mass of the ions.

In this manner it can be shown that space charge effects are negligible except in the initial focussing section and in the path between the final accelerating lens and the target. When the beam leaves the ion source it diverges rapidly and the space charge increases this divergence. This increase cannot be calculated exactly as the current distribution in the beam is not known. The effect is not very great, however, as in a distance of only a few centimetres the beam is accelerated to the potential of the focussing electrode. If the beam is assumed to leave the canal with a divergence of 30° , the effect of space charge will be to increase the diameter by 5% in a distance of 3 cms. If the beam is supposed to leave the exit canal of the ion source (radius 0.16 cms.) as a parallel beam it would increase in radius to 0.4 cms. in the same distance. In either case the space charge divergence is small compared with the aperture of the focussing lens.

After the final accelerating gap the beam travels about 3 metres before reaching the target. Consider, for example, a $500 \mu\text{a}$ beam of protons of an energy of 500 keV. If the beam is initially parallel and has a radius of 0.25 cm., space charge

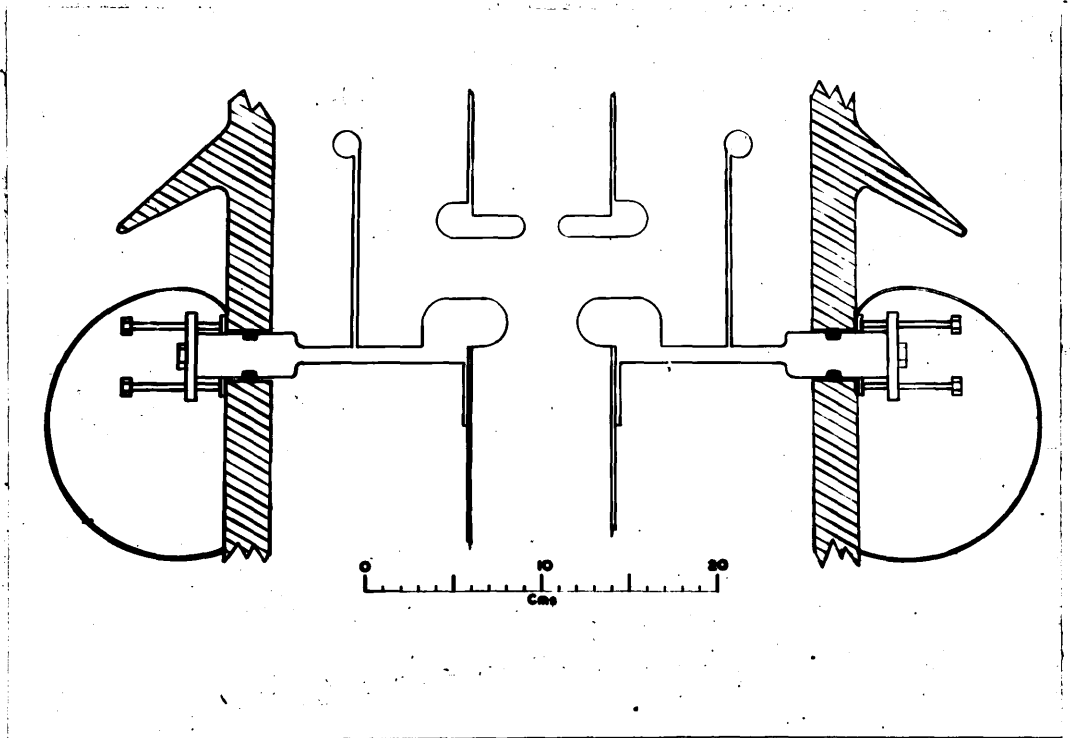


Figure 2.13. Section of accelerating lens.

will cause the beam to diverge to 0.4 cm. before the target is reached.

Thus for the beam currents achieved with the present accelerating tube space charge defocussing is not thought to be serious, though for much larger beam currents modifications in the design of the electrodes would be necessary.

II. 3.6. Initial Alignment of Tube.

When the accelerator tube was first erected the centring of the electrodes was accomplished optically. A pointolite lamp at the focus of a weak convex lens was placed in the beam room below the accelerating tube so as to project a vertical beam of light up the tube. The H.T. room was darkened and the shadow of the lowest aperture marked on the ceiling. The accelerating column was then built up section by section and each electrode adjusted in turn so that both its top and bottom apertures were concentric with the light beam. Some difficulty was experienced in achieving this as the porcelain insulating sections had not been cut accurately and their ends were not parallel. This was counteracted as far as possible by setting the actual electrodes at a slight angle to the supporting spiders.

II. 3.7. Subsequent Adjustment of Tube.

With the tube aligned as described in the last section it was found possible to obtain a small beam current on the target, but the majority of the current from the ion source was intercepted by the intermediate electrodes. It was, however, found that the necessary lateral adjustments to the electrodes could be made without disturbing the vacuum by sliding the electrodes relative to the porcelain cylinders. Each joint was adjusted by the movement of four $\frac{1}{4}$ inch screws bearing on brass shoes resting against the porcelain (figure 2.13.).

Microammeters were placed in series with the resistors connecting the electrodes to the cascade generator and viewed from a safe distance through a telescope. Starting with the top electrode and with a H.T. voltage of 350kV each gap was adjusted in turn to give minimum current to the electrode below it. Though the currents recorded are greatly affected by secondary emission to and from adjacent electrodes this criterion of minimum current was found to be the most reliable of several tried. The final positions of the electrodes were critical to $\pm \frac{1}{2}$ mm. Adjustment of the lowest gap enables the position of the beam on the target to be altered.

II. 3.8. Typical Operating Conditions of the Tube.

After the above adjustments had been made the currents reaching the various electrodes were as follows:

H.T. Voltage	= 500 kV
Focus Voltage	= 7.5 kV
Current to first accelerating electrode	= 300 μ a
Current to second accelerating electrode	= 15 μ a
Current to third accelerating electrode	= 3 μ a
Current to fourth accelerating electrode	= -90 μ a
Total current to resolving chamber	= 420 μ a
Total current passing 2 cm. diameter aperture	= 400 μ a
Total load current on generator (measured in earth return)	= 1000 μ a
Current in measuring resistor	= 450 μ a
\therefore Total load due to accelerating tube	= 550 μ a
Resolved proton beam reaching target	= 160 μ a
Resolved H_2^+ beam reaching target	= 40 μ a
Resolved H_3^+ beam reaching target	= 25 μ a
Total of resolved beams due to splitting of molecular ions while passing down tube	= 80 μ a

The total exit current from the source could not be measured directly but was estimated from previous measurements to be about 600 μ a. The currents to the intermediate electrodes are largely due to secondary emission. Measurements of the resolved beam currents are not subject to this error.

II. 4. Ion Source.

II. 4.1. General.

The ion source on the present equipment has been used to produce proton and deuteron beams; apart from a small difference in space charge effects the operation of the source is identical in the two cases. The desirable characteristics for the ion source include:

- (a) High output.
- (b) High proton percentage.
- (c) Low gas consumption.
- (d) Small energy spread of the ions.
- (e) Long life.
- (f) Low power consumption.

A comparative survey of ion sources used with high voltage accelerating tubes has recently been made by Hoyaux and Dujardin⁽³⁷⁾. The types most frequently used have been the high voltage D.C. arc similar to that described by Oliphant⁽³³⁾ (38) and the low voltage capillary arc originally used by Tuve⁽³⁹⁾ (40). The high voltage sources are simple and reliable but the emergent ions have a large spread in energy. The capillary sources produce more nearly mono-energetic ions but tend to be more complicated and difficult to adjust. A different type of source was developed in 1946 by Thonemann⁽⁴¹⁾ in which the ionisation is produced by a high frequency discharge. Several sources of

this type have recently been described and these give a high current for low gas consumption and low power input. The ion beam has a very small spread in energy and as these sources have a long life they are more satisfactory than the older types. This type of ion source was, therefore, used in the present equipment.

II. 4.2. First Type Source.

The source originally installed was similar to that described by Rutherglen and Cole⁽⁴²⁾. In order to make the source more compact the magnetic field coils were combined with the R.F. electrodes. The coils were wound on brass formers which are connected to a short-circuited stub made from $\frac{1}{4}$ inch diameter copper tubing. The balanced pair of coaxial cables connecting the coil to the 200 Mc/s oscillator was tapped at a suitable point on the stub to match the load to the oscillator.

This source was found to have a rather short life, usually less than 20 hours. Failure was found to be due to the sputtering of metal from the exit canal to the surrounding glass. This produced an unfavourable potential distribution near the exit canal and caused a large reduction in the beam current.

II. 4.3. Modified Source.

In order to overcome these difficulties a new source with a new extraction arrangement was

developed. This is a development of the arrangement of Baly and Ward⁽⁴³⁾ and is shown in figure 2.12.

The discharge is maintained in the pyrex tube (A). The ion extraction potential is applied between the canal (E) and a concentric aluminium electrode (C) that takes the place of the probe at the top of the source used in the earlier version. The top of this electrode projects through a hole in the base of the discharge tube and is slightly higher than the canal. This electrode (subsequently referred to as the probe) is insulated from the steel base of the ion source by a glass plate (N) $\frac{1}{8}$ inch thick. The vacuum seals either side of this plate are made with "O" rings. The exit current through the canal is sensitive to small lateral movements of the canal relative to the probe and adjusting screws (L) are, therefore, provided to allow the canal to be positioned for maximum output. This can be accomplished while the source is in position on the accelerating tube by using the first accelerating electrode as a collector for the ion beam.

II. 4.4. Gas Supply.

Hydrogen or deuterium is supplied from one litre brass containers to the source at the rate of about 15 ccs. per hour. These reservoirs are connected through taps to two electrically heated palladium tubes either of which can be used to feed the gas through the supply pipe in the base

of the source. The pressure in the source is controlled by varying the current to the palladium leak. This is controlled by a helically wound variable series resistance. In practice it is found that as the pressure in the reservoir falls the temperature of the heater rises owing to the reduced cooling effect of the gas, and this rise in temperature is sufficient to keep the gas supply very nearly constant.

II. 4.5. Power Supplies for the Ion Source.

The power for the ion source is supplied by a type U.O. generator and its associated carbon pile regulators. This generator has a maximum output of 1.2kW at 80 volts 2000 cycles and 3kW at 27 volts D.C. It is supported on the top of a paxolin cylinder 2.7 metres high and 80 cm. diameter and belt driven by a 4 H.P. 3-phase motor at the base of the column. The corona shield at the top of this column (made, like that on the accelerating column, from papier-mache rendered conducting with "aquadag") contains the R.F. oscillator and necessary power packs supplying the ion source and focussing voltages.

II. 4.6. Performance of the Ion Source.

The performance of the present source may be considered in relation to the desired characteristics noted in section II. 4.1.

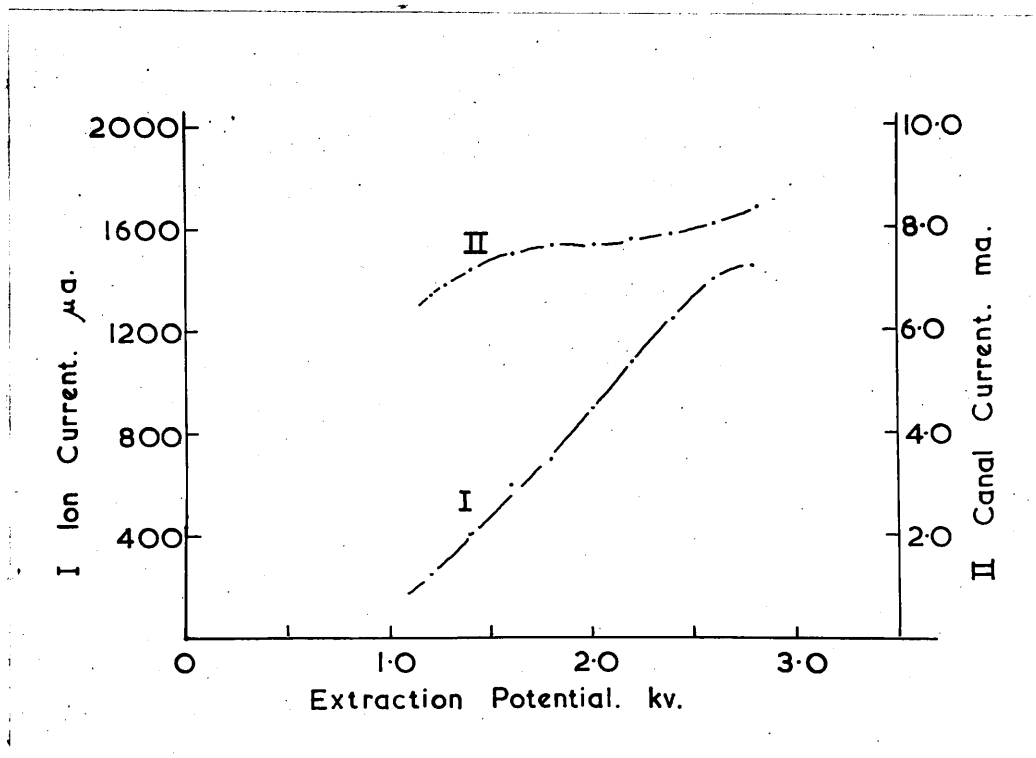


Figure 2.14. Performance of Ion Source.

(a) High output current.

A curve showing the dependance of output current on probe voltage is shown in figure 2.14. The ion current was measured in a Faraday cage immediately below the exit canal. The extraction voltage is limited to 2.5kV by the permissible heat dissipation.

(b) High proton percentage.

In the discharge three types of ions, H_1^+ , H_2^+ , H_3^+ occur together with uncharged hydrogen atoms and molecules. H_3 , formed by the recombination of H_3^+ ions with free electrons immediately dissociates into H_2 and H_1 as H_3 is unstable. In order that there shall be a high proportion of protons in the output, it is necessary to maintain a high proportion of atomic hydrogen in the source, despite its continual disappearance by recombination to molecular hydrogen. This can be achieved by maintaining a high rate of ionisation, and as recombination occurs chiefly on the walls, by making these of a suitable material. The ionisation is due to collisions with free electrons oscillating in much ing the source. A further improvement is secured by the axial magnetic field, which by causing the electrons to spiral round the lines of force, compels them to travel a greater distance in the gas, and hence make more ionising collisions before being lost to the walls.

Recombination of atomic hydrogen to molecular hydrogen was found to be high on all metallic surfaces. Fortunately, recombination is low on clean pyrex glass and this is, therefore, used for the discharge vessel. The only metal exposed to the discharge is that forming the extraction electrodes and is of small area. In this way a proton percentage of over 50% is achieved.

(c) Low gas consumption.

Hydrogen is supplied to the source at 15 cc. per hour; about 2% of this gas emerges from the source as protons.

(d) Small energy spread of ions.

The energy acquired by a charged particle in the R.F. field is inversely proportional to its mass. In the discharge in the source an electron will attain an energy of about 50eV so that the maximum energy acquired by a proton will be about 0.3eV; consequently any spread in energy of the emergent beam will be due solely to imperfections in the extraction system.

The life of the present source is determined by the slow sputtering of the aluminium extraction electrodes on to the pyrex envelope. After several hundred hours of operation sufficient metal has been deposited to lower the proton

percentage appreciably, and the pyrex enveloped must then be cleaned or replaced. This can be done without disturbing the adjustment of the extraction electrodes.

(f) Low power consumption.

The probe current is shown as a function of probe voltage in figure 2.14. In addition power is required for the R.F. oscillator, the magnetic field, and blowers for air cooling, resulting in a total power consumption of about 250 watts.

II.5. Vacuum System.

II. 5.1. General.

The high-vacuum system consists of the accelerating tube itself, the resolving chamber and target assembly and the necessary pumping equipment. The total volume of the system is about 500 litres and the operating pressure is maintained by continuous pumping. Most vacuum joints are made with rubber rings and a series of valves is provided to facilitate leak detection and allow for rapid target changing.

II. 5.2. Pumps.

The main backing pump is a type DVD 8810
minute.
required
for normal running it has proved of great value when
air is admitted to any part of the system, as, for
example, when changing a target. There are two oil
vapour pumps; a 16 inch pump with a speed of 2000
litres per second backed by a 4 inch pump with a speed

of 75 litres per second. The pumps are charged with Apiezon B oil and to reduce the amount of oil vapour reaching the accelerating tube a baffle cooled with "Drikold" is mounted directly above the large pump. These pumps maintain an operating pressure of approximately 5×10^{-6} mm. of mercury.

II. 5.3. Valves and Interlocks.

Interlocks are provided to switch off the heaters of the diffusion pumps should the cooling water fail or the backing pressure rise. Air may be admitted to the resolving chamber or to the resolving chamber and accelerating tube and pumped out through by-pass valves without admitting air to the vapour pumps. The pressure is monitored with a Pennig type gauge, whose indicating microammeter is protected from overload with a neon discharge tube, and this arrangement has proved very convenient and reliable. Pirani hot-wire gauges are also fitted and are useful in locating leaks. The gauges were originally calibrated against a Macleod gauge: for normal operation of the tube the calibration of the gauge is unimportant.

After acceleration the beam consists of protons and molecular ions having an energy corresponding to the full H.T. voltage, and a number of groups of slower ions produced by the break-up

of molecular ions at various stages in their passage down the accelerating tube. In order to separate the protons from the other ions, the beam is magnetically deflected through 30° before reaching the target. It should be noted that an electrostatic analyser cannot be used to separate protons and molecular ions. The velocity v of an ion of mass m and charge e accelerated by a voltage P is given by:

$$Pe = \frac{1}{2}mv^2$$

If the ions are bent into an arc of radius ρ by a radial electric field E or a magnetic field H then:

$$\frac{mv^2}{\rho E} = Ee \quad \text{Electric deflection}$$

$$\frac{mv^2}{\rho H} = Hev \quad \text{Magnetic deflection}$$

whence

$E\rho_E = 2P$ and is independent of the nature of the ion and $H\rho_H = \sqrt{\frac{2Pm}{e}}$ allowing ions having different values of m/e to be separated.

The choice of the angle of deflection is
get,
and
the resolution required. It is usual to employ an angle of 90° so that the resolved beam travels horizontally, this being most convenient for the target and detecting apparatus. For this angle of deflection a parallel beam will be brought to a

focus at the edge of the magnet pole. (This arrangement is analagous to one half of a conventional 180° spectrometer), and if, as is usual, the target is some distance from the magnet the beam will be diverging when it reaches the target. In the present equipment a resolving angle of 30° is employed. This has the advantage of requiring a smaller and cheaper deflecting magnet. In addition the beam is brought to a focus about 30 cm. beyond the poles. By the addition of suitable shims to the magnet poles so as to allow the magnetic field to fall off as $r^{-1/2}$ some degree of focussing in the plane normal to the deflecting plane can be achieved. The focal length of the magnetic lens is also increased and the beam brought to an approximate point focus at about 50 cm. from the edge of the poles. These shims have been used when the target was further than 30 cm. from the resolving chamber. Without the shims, the beam focusses to a narrow ribbon about 2 mm. wide and 2.5 cm. long. By using narrow defining slits the energy of the ions reaching the target can be precisely defined; for most experiments, however, all that is required of the resolving magnet is to define the energy of other ions, which can be obtained by stabilising the accelerating voltage.

The general arrangement of the lower end of the accelerating tube, together with the resolving chamber is shown in figure 2.15. In order to centre

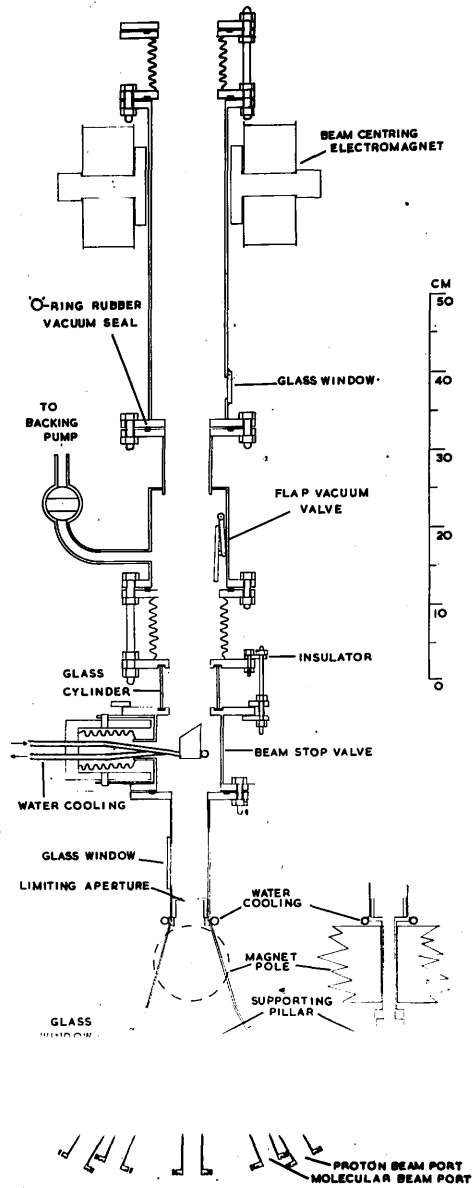


Figure 2.15. Lower end of accelerating tube.

the beam on the target, two flexible metal bellows sections are inserted above the resolving chamber. Small shifts of the beam can be counteracted by means of the beam centring magnet shown.

II. 5.5. Leak Detection.

When the system was first erected the usual troubles were experienced in locating leaks; several which were due to porosity in the steel castings being especially troublesome. Various methods of leak detection were tried, including the use of a mass spectrograph. A simple spectrograph was constructed using a R.F. ion source and opposed magnetic and electric deflection. The electrostatic field was varied at 50 cycles and the output from a collector cup behind a slit amplified and displayed on a cathode ray tube. The trace clearly separated the peaks due to ions of masses 1, 2, 3, and 4. Various probe gases were tried by supplying them to the vacuum through a known small leak. Helium was found to be satisfactory but unfortunately was not available in sufficient quantity to be used for tracing actual leaks. Hydrogen is not nearly so effective, as it was always present, to some extent, in the system before the probe gas was applied. Descriptions of several devices of this type have recently been published and the detection of one part of helium in 150,000 of air is claimed.

During the course of these tests it was noticed that the change in colour of the R.F.

discharge in the ion source gave almost as sensitive an indication when hydrogen was used as probe gas as did the mass spectrometer itself. This colour change was made the basis of subsequent leak testing. A portable 30 watt 30 mc/s oscillator was used to excite a discharge in a convenient glass part of the system (the discharge can be maintained down to a pressure of one micron or less). Coal gas was used as a probe gas and the colour of the discharge watched.

After the initial troubles had been overcome the main part of the system has not given further trouble. Most of the subsequent leaks have been in the resolving chamber and target assemblies where constant changes are necessarily being made.

II. General Purpose Auxiliary Equipment.

II. 6.1. General.

Directly associated with the accelerator is a large amount of electronic apparatus, some of which has already been described (Sections II. 2.3. and II. 2.4.). The complexity of this apparatus is a direct result of the attempt to make precision measurements; for example to locate resonances in nuclear reactions with an accuracy of the order of 100eV such devices as current integrators and H.T. voltage stabilisers become virtual necessities.

II. 6.2. Layout.

Most of this equipment, together with the greater part of the electronic apparatus involved in the particular experiment being performed, is assembled in the control room. Thus, while the set is operating it is not normally necessary to remain in the beam room for any length of time. Though the intensity of radiation in this room is usually low, in some cases it may be dangerous. This is particularly true of deuteron induced reactions when a flux of fast neutrons may be present.

The equipment is, as far as possible, rack mounted; with the H.T. stabilising and measuring units occupying the rack nearest to the cascade generator control desk. An adjacent rack carries

the pressure gauges and a further three racks are filled with amplifiers, scaling units, power supplies for counters, cathode-ray monitors and similar equipment.

II. 6.3. Current Integrator.

The proton beam reaching the target fluctuates in intensity due to various small disturbances in the accelerator tube. The total charge reaching the target in any given time is measured by an automatic integration of this fluctuating current. In order that this shall be a true measure of the number of protons it is necessary to prevent secondary emission electrons either leaving or being collected by the target. This is usually achieved by means of a special electrode held at a potential of 100 volts negative with respect to the target and so placed in front of the target that it cannot be struck by the beam. Alternatively, a magnetic field of a few hundred gauss in the immediate vicinity of the target will suppress all secondary emission.

The circuit designed for us with the present equipment will integrate currents from $1\mu\text{a}$ to $150\mu\text{a}$ with an accuracy of 1% or better. The current to be measured is fed into the grid of a valve connected as a Miller integrator. At the end of the Miller run-down a unistable multivibrator discharges the integrating condenser and the action repeats. The number of cycles is recorded on a post

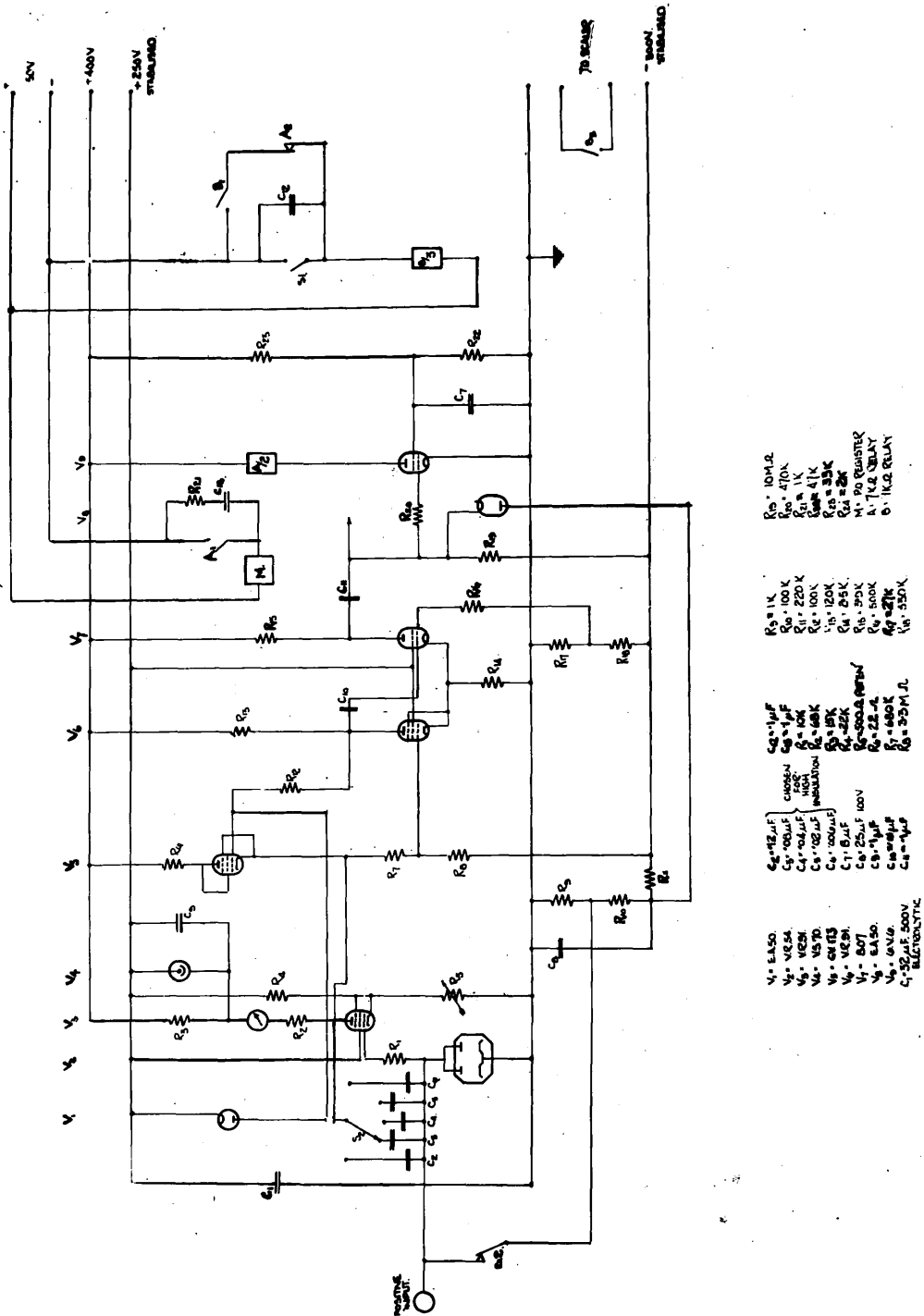


Figure 2.16. Circuit of Current Integrator.

office register. The circuit diagram is shown in figure 2.16. and the operation of the circuit is described in Appendix II.

II. 6.4. Timing Unit.

In many experiments it is necessary to make simultaneous counts on a number of channels. For example, when investigating the energy spectrum of alpha-particles from a particular reaction it might be necessary to record the following:

- (a) The duration of the count.
- (b) The number of alpha-particle counts.
- (c) The number of counts in a monitor gamma-ray counter.
- (d) The charge received by the target.

To enable such experiments to be performed rapidly and accurately an automatic timing unit is used. This unit is based on a clock which gives pulses every half second, the pulses being recorded on a special register which makes one complete revolution for every 120 counts. Two such registers are incorporated in the unit, so that it will simultaneously switch on any number of scaling units, and switch them off again after the arrival of 1 to 14,400 pulses. These pulses may be half-second pulses from the clock, pulses from the current integrator or pulses from a monitor counter. Thus runs may be made for a predetermined time,

charge or monitor count.

II. 6.5. Resolving Magnet and Power Supplies.

The magnet used to deflect the proton beam has poles 10 cm. in diameter and produces a field of 10,000 gauss in a 2 cm. airgap. For this field the power consumption is 8 amps. at 60 volts. It was originally intended to use the deflection of the molecular ion beam by the resolving magnet as a measure of the energy of the accelerated particles, thereby deriving from suitable collector plates a signal voltage that could be applied to the input of the accelerator voltage stabiliser (Section II. 2.4.). Consequently, a stable ripple-free power supply was built for the resolving magnet. Full wave rectification of the 50 cycle mains supply results in an A.C. component of 5% of the magnet current. To reduce this ripple, the inductance of the magnet was increased from 0.33H to 0.7H by slotting the aluminium end plates of the coil spools, and the rectifiers were supplied from an aircraft type alternator at a frequency of 2000 cycles. A voltage proportional to the magnet current is obtained from an air-cooled 0.5 ohm. resistance wound with low temperature coefficient "minalpha" wire. The difference between this voltage and a reference voltage is amplified with a "chopper" amplifier similar to that shown in figure 2.4., but with an extra stage of amplification.

The A.C. input to the rectifier circuit is controlled in a similar manner to the H.T. stabiliser, using six 6L6 valves as a variable impedance. This circuit maintains the current through the magnet coils constant to better than 0.1%.

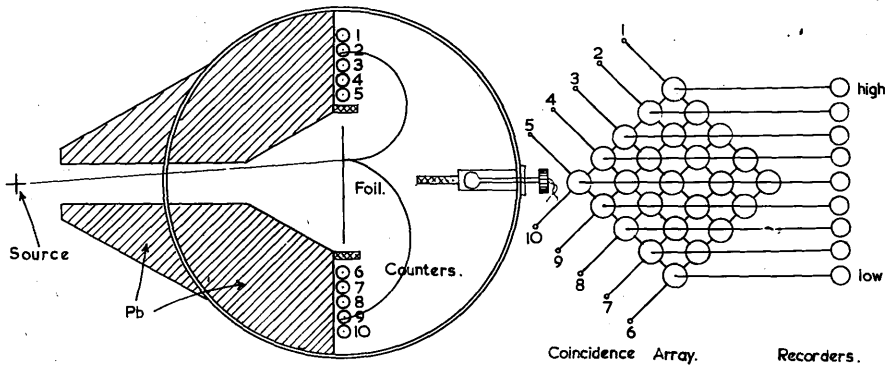


Figure 3.1. Arrangement of Pair Spectrometer.

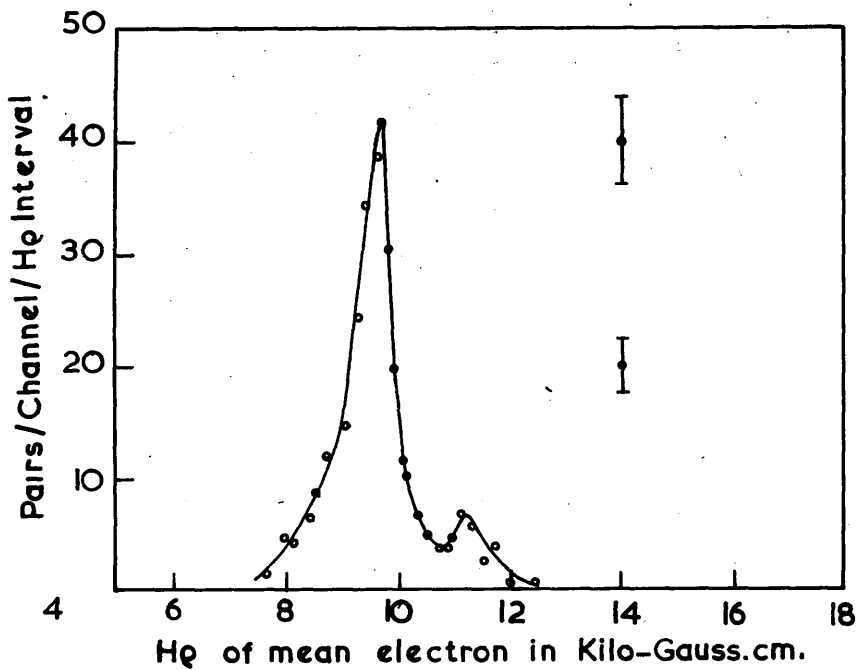


Figure 3.2. Spectrum of gamma radiation from 340 KeV resonance of the reaction $F^{19}(p, \alpha, \gamma) O^{16}$

Part III. Experimental Results.

III. 1. Hard Gamma-Radiation.

III. 1.1. General.

The measurement of the energy of gamma-radiation from excited states of nuclei is one of the ways of determining the location of these levels. (See Section 1.5.). The positions of many of the levels known in light nuclei depend on coincidence absorption or cloud chamber measurements. These measurements are not very precise, and are liable to give misleading results if several gamma-rays of differing energy are present simultaneously. In the experiments described below, a "pair" spectrometer was used to make some more precise measurements of some of these gamma-rays.

III. 1.2. Principle of Operation of Spectrometer.

The probability that a gamma-ray will produce a pair in a foil, thin enough not to scatter or absorb the resultant positron and electron, is rather small. A useful sensitivity can only be achieved by making use of a foil of large area. In the design of spectrometer used, based on that of Walker and McDaniel⁽¹⁴⁾, this is made possible by measuring the sum of the momenta of the positron and the electron. Their curvature in a magnetic field is proportional to their momentum and as the pairs are ejected from the foil in nearly the same

direction as the incident gamma-ray, it is possible to use an array of counters that automatically provides the summation of momenta required.

In this instrument, shown diagrammatically in figure 3.1., the positron-electron pairs, produced from a thin foil placed at right angles to the flux of gamma-rays, are deflected in semicircular arcs by a magnetic field and detected by small Geiger counters located in the plane of the foil.

The distribution of the surplus energy between the positron and electron has been calculated by Heitler⁽⁴⁵⁾, who shows that in the energy range considered here, that is from 4 MeV. to 25 MeV., the energy spectrum is nearly rectangular. The pair particles are projected forwards so that the majority of them lie within a cone of solid angle $m_0 c^2/hf$, whose axis is the direction of the incident gamma-ray (m_0 is the rest mass of the electron, hf the energy of the incident quantum).

If the momentum and total energy of the electron are p_1 and E_1 , respectively, and those of the positron are p_2 and E_2 , then in a magnetic field H the two particles will be bent into two opposite semicircular arcs of radii r_1 and r_2 such that:

$$Hr_1 = p_1/e$$

$$Hr_2 = p_2/e$$

$$r_1 + r_2 = \frac{(p_1 + p_2)}{He}$$

Thus if 4ρ is the distance between the two points where the positron and electron returned to the plane of the foil, a mean radius ρ may be defined, and this mean radius will be a measure of the total momentum and hence of the energy of the particles.

$$2\rho = (r_1 + r_2)$$

$$p_1 + p_2 = 2 \text{ He} \rho$$

If the energy of the gamma-ray producing the pair is E_γ

$$E_\gamma = E_1 + E_2$$

$$E_1^2 = p_1^2 c^2 + (m_0 c^2)^2$$

$$E_\gamma = (p_1^2 c^2 + (m_0 c^2)^2)^{1/2} + (p_2^2 c^2 + (m_0 c^2)^2)^{1/2}$$

$$\therefore E_\gamma = (p_1 + p_2) c \left[1 + \frac{(m_0 c^2)^2}{2 p_1 p_2} \right] \quad \left[\begin{array}{l} p_1 c \gg m_0 c^2 \\ p_2 c \gg m_0 c^2 \end{array} \right]$$

Thus to a first approximation the energy of the gamma-ray is directly proportional to the sum of the momenta of the positron and electron, and hence to ρ . The "correction" term $\frac{(m_0 c^2)^2}{2 p_1 p_2}$ depends on the relative distribution of energy between the two particles and will be large only for very unequal distributions of energy. Pairs of this type are not accepted by the spectrometer. From the geometry of the spectrometer the correction for pairs produced at various points along the foil may be calculated and an average correction found. This correction is very small, and for the spectrometer used the expression

$$E = 600 H \rho \left[1 + 2.5 a^2 \right]$$

where $a = \frac{\text{Energy corresponding to rest mass of electron}}{\text{Energy of the gamma-ray.}}$

$E =$ energy of gamma-ray in electron-volts

$H =$ magnetic field in gauss

$\rho =$ mean electron radius in centimetres.

is accurate to within 0.5% over the energy range considered.

The most important factors which determine the resolving power of the spectrometer are:

- (1) The width of the detecting counters. Not only is the actual width of the counters appreciable, but it is not easy to define their effective width precisely, owing to the scattering of electrons by the counter walls and windows.
- (2) The thickness of the radiator. A compromise is necessary between the conflicting requirements of the higher yield from a thicker foil and the consequent loss of resolution due to the scattering and energy loss of the emergent electrons. A lower useful limit to the foil thickness is reached when the scattering due to the foil is less than the angular divergence which occurs in any case in the pair production process.

The effect of these imperfections is to produce a low energy tail to the observed peak in the spectrum. In consequence of this the precise energy of a particular gamma-ray was determined from the half

amplitude point on the high energy side of the peak rather than from the position of the peak itself.

The actual construction of the spectrometer is described in Section III. 1.7.

III. 1.3. Target Arrangements and Experimental Procedure

The resolved beam from the accelerator, emerged from the resolving chamber down the axis of a pyrex glass tube inclined at 30° to the vertical. The targets used were prepared on thin brass or copper sheet and clamped to the base of a small water cooled brass cup, sealed to the end of the glass tube. The current reaching the cup was fed to the input of the current integrator. The secondary emission from the target was found to be negligible under these conditions. A G.E.C. Type G.M.4. Geiger counter was fixed inside a block of aluminium and mounted at a fixed distance from the target. The effective thickness of the aluminium walls of the counter was one inch, and all runs were made for a fixed number of counts in this counter. Any deterioration of the target was then detected by the resultant variation in current integrator counts.

For each gamma-ray spectrum a number of runs were made, each at a different setting of the magnetic field. Each run gave nine counts corresponding to the nine energy channels, the spacing between channels being 5.8% of the energy of the centre channel. Successive runs were chosen so

that the centre channel shifted only one or two channel widths, a number of counts from different channels thus being obtained for each momentum interval. This tended to reduce errors due to slight differences between channels which might be present, for example, as a result of small discrepancies in the resolving times of the coincidence circuits.

The fluxmeter was calibrated by observations of the 6.13 MeV. gamma-ray from the 340 KeV. resonance of the $F^{19} (p, \alpha, \gamma) O^{16}$ reaction and the 17.6 MeV. gamma-rays from the 441 KeV. resonance of the $Li^7 (p, \gamma) Be^8$ reaction. These gamma-ray energies have been accurately determined by Walker and McDaniel. These two calibrations differed by less than 0.5% and the mean value was used in the calculation of the results below.

The spectrum of the 6.13 gamma-rays from the $F^{19} (p, \alpha, \gamma) O^{16}$ reaction used for calibration is shown in figure 3.2. The small peak at an $H\rho$ value of 11.2 kilogauss-cms. is due to the smaller intensity gamma-ray at 7.0 MeV. The errors shown in this and subsequent spectra are standard deviations of the actual counts. An estimate for the relative yield of the various gamma-rays measured can be obtained from the current integrator count and the count per channel recorded with the spectrometer.

Each counter in the spectrometer will accept particles having a range of momenta

proportional to the effective counter width and to the magnetic field H . As the energy spectrum of the positrons (and hence also of the electrons) is approximately rectangular, the number of counts recorded in each similarly spaced pair of coincidence counters will be the same, irrespective of any asymmetry with respect to the origin of the pair. In order to normalise the counts at a particular field H , it is, therefore, only necessary to weight the counts from each output channel according to the number of coincidence channels (see Section III. 1.7.) and multiply by the ratio H_0/H where H_0 is some arbitrary standard field. The ordinates in figure 3.2. and subsequent figures are counts per channel per standard $H\rho$ interval calculated in this manner.

Thus, provided that the radiating foil is sufficiently thin, the relative intensities of two gamma-rays can be determined by measuring the areas under the two peaks and correcting for the relative values of the pair cross-section in lead at the energies of the two gamma-rays.

III. 1.4. The Reaction $F^{19}(p, \gamma) Ne^{20}$

The gamma-rays resulting from the bombardment of fluorine have been extensively studied. The yield from this reaction is high, compared with most other reactions resulting from proton bombardment of light nuclei. The gamma-radiation was shown by Dee et al. ⁽⁴⁶⁾ to originate from the excited oxygen

nucleus, formed by alpha-particle emission from the compound Ne^{20} nucleus, rather than from direct de-excitation of the compound nucleus. The excitation energy of the levels formed in the compound Ne^{20} nucleus by the capture of low energy protons will lie in the neighbourhood of 13.5 MeV. At such a high excitation energy, though the emission of a charged particle will normally be more probable than the emission of a gamma-ray, such radiation may still occur from particular levels. (Section 1.3.). Walker and McDaniel⁽¹⁴⁾ searched for such hard radiation with their pair spectrometer, but were unable to detect it, setting an upper limit to its intensity of 0.3% of that of the 6 MeV. gamma-rays resulting from the emission of alpha-particles. Their value refers to the bombardment of a thick target with 1.15 MeV. protons. Devons and Hereward⁽⁴⁷⁾ also made a search for this radiation, and by making use of the photo-nuclear effect in Cu^{63} , which has a threshold at about 11 MeV., were able to investigate the reaction at a number of different bombarding energies. They found that gamma-radiation hard enough to activate Cu^{63} was emitted at a proton energy of 660 KeV., an energy corresponding to one of the known alpha-emitting levels of Ne^{20} . Using a thick target they were unable to find any further resonances at bombarding energies below 960 KeV. the yield increasing only very slowly as the bombarding energy was raised from

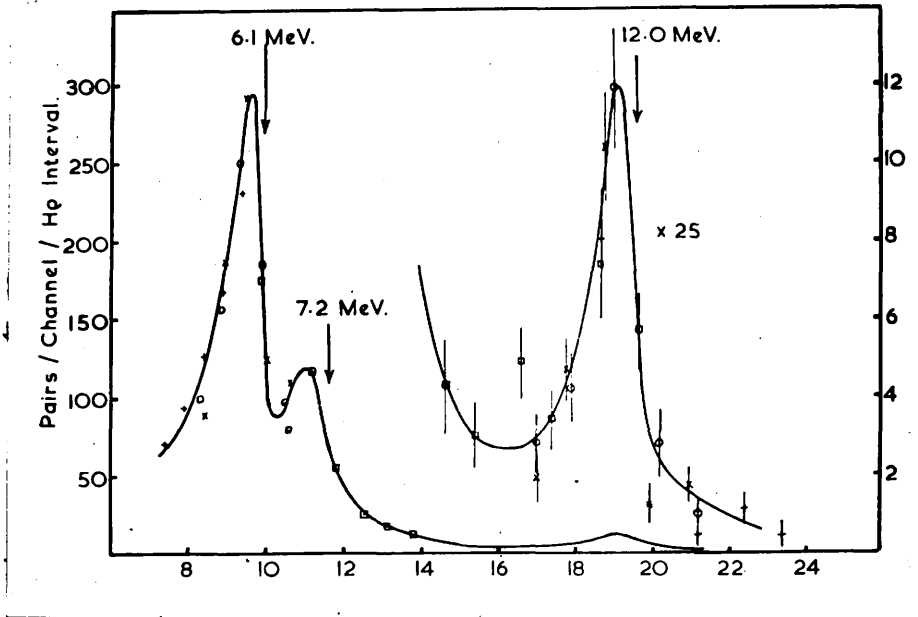


Figure 3.3. Spectrum of gamma-rays from $(F^{19}+p)$. 660 KeV. resonance.

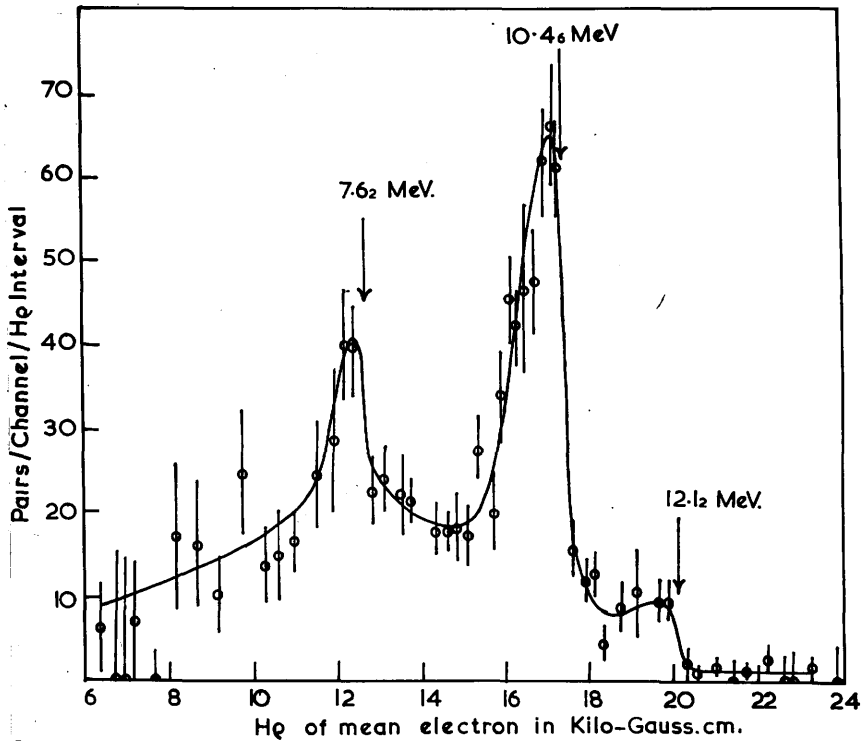


Figure 3.4. Spectrum of gamma-rays from $Al^{27} + p$ at $E_p = 750$ KeV.

700 KeV. to 960 KeV.

They assumed that the gamma-radiation observed was due to a transition to the ground state and, therefore, had an energy of 13.4 MeV. Its intensity was estimated from the cross-section of the photo-nuclear effect in Cu^{63} , to be $2.2 \pm 0.8\%$ of the intensity of the 6 MeV. radiation at the same bombarding energy of 660 KeV.

As a result of the work of Devons and Hereward, it was possible to use the pair spectrometer to measure the energy of the hard gamma-radiation, by using a thin target and a proton bombarding energy just above 660 KeV. The background of 6 MeV. radiation was then greatly reduced compared with that of McDaniel and Walker, while the intensity of the capture radiation remained approximately the same. The targets used, about 50 KeV. thick, were prepared on brass discs by deposition in a vacuum by the evaporation of calcium fluoride.

The spectrum obtained is shown in figure 3.3. It will be seen that, in addition to the gamma-rays at 6.1 MeV. and 7.2 MeV. from excited states in O^{16} , there is a peak corresponding to an energy of 12.0 MeV. When the experiment was repeated at a bombarding energy corresponding to the 340 KeV. resonance, this high energy peak was absent. The intensity of the 12 MeV. radiation was estimated to be 2% of the radiation from the excited O^{16} in good agreement with the results of

Devons and Hereward. The energy of the gamma-ray which was estimated at 12.0 ± 0.2 MeV. is not, however, consistent with the transition to the ground state of Ne^{20} which they assumed to be the origin of the radiation. The energy release in the transition to the ground state should be 13.4 MeV., and it, therefore, seems that this ground state transition is forbidden, and a transition occurs instead to an intermediate level about 1.4 MeV. above the ground state. Such a state is known to be excited in the decay of F^{20} (48), the reaction $\text{F}^{19}(\text{d},\text{n})\text{Ne}^{20}$ (49), and the inelastic scattering of protons in neon (50), and it is reasonable to suppose that the same level is involved in the $\text{F}^{19}(\text{p},\gamma)\text{Ne}^{20}$ reaction.

The results presented here were first published in a joint letter to the editor of the "Proceedings of the Physical Society" (51). Subsequently the energy of the hard gamma-radiation was confirmed by Carver and Wilkinson (15), who obtained the value 12.09 ± 0.29 MeV. at a bombarding energy of 669 KeV., using a method based on the photo-disintegration of deuterium.

III. 1.5. The Reaction $\text{Al}^{27}(\text{p},\gamma)\text{Si}^{28}$.

The thin target excitation curve of the gamma-radiation resulting from the bombardment of aluminium with protons has been investigated by a number of workers, and shows a large number of sharp resonances. The only previous measurement

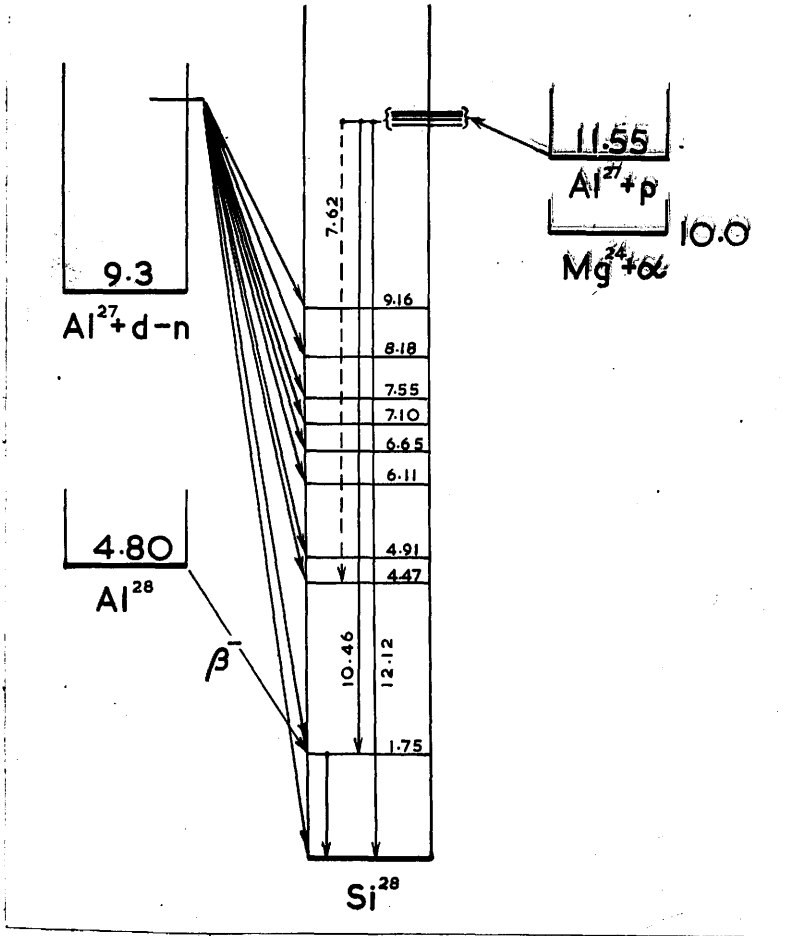


Figure 3.5. Energy level diagram of Si^{28} .

of the energy of the radiation is that of Plain et al. (52), who used a coincidence absorption technique. They concluded that the effective energy of the radiation was about 6.5 MeV., at a bombarding energy of 700 KeV., but the method used is inaccurate in the presence of several gamma-rays of differing energy, as is the case for this particular reaction.

It was, therefore, decided to use the pair spectrometer to measure the energy of these gamma-rays. In order to obtain sufficient intensity it was necessary to use a thick target so that all the resonances below 750 KeV. were excited. Even so the total gamma-ray yield was only about one-fifteenth of that produced by the 340 KeV. resonance of $F^{19}(p, \alpha, \gamma)O^{16}$. The measured spectrum under these conditions is shown in figure 3.4. It will be seen that three gamma-rays of energies 12.12 ± 0.1 MeV., 10.46 ± 0.07 MeV. and 7.62 ± 0.1 MeV. are clearly resolved, but the background both above and below the 7.6 MeV. peak suggests the presence of other weak gamma-rays. The low intensity of the reaction prevented a more detailed investigation of this region.

The interpretation of these gamma-rays can be discussed in terms of the energy level diagram of Si^{28} shown in figure 3.5. The only reactions which are energetically possible in this case are $Al^{27}(p, \gamma)Si^{28}$ and $Al^{27}(p, \alpha)Mg^{24}$ and only

the former has a sufficiently large Q -value to produce the observed gamma-rays. The most energetic gamma-ray is presumed to correspond to the direct transition to the ground state of Si^{28} . From the results of Brostrom et al.⁽⁵³⁾ on the relative intensities of the resonances below our bombarding energy of 750 KeV. we assume the mean effective bombarding energy to be 630 KeV., which corresponds to an additional excitation energy of 610 KeV. in centre-of-mass coordinates. Although it is known that the spectrum is not identical for all resonances⁽⁵⁴⁾ the above assumption cannot be in error by more than ± 100 KeV. We thus obtain a value of 11.51 ± 0.2 MeV. for the Q -value of the ground state transition. This Q -value may be calculated by two other methods. First, the reactions $\text{Al}^{27}(\text{d}, \text{p}) \text{Al}^{28}$, $Q = 5.45 \pm 0.05$ MeV.⁽⁵⁵⁾ and $\text{Al}^{28}(\beta^-) \text{Si}^{28}$, $Q = 4.80 \pm 0.05$ MeV.⁽⁵⁶⁾ predict a Q -value of 11.70 ± 0.1 MeV. for $\text{Al}^{27}(\text{p}, \gamma) \text{Si}^{28}$. Second, the reaction $\text{Al}^{27}(\text{d}, \text{n}) \text{Si}^{28}$, $Q = 9.08 \pm 0.2$ MeV.⁽⁵⁷⁾ predicts a Q -value of 11.31 ± 0.2 MeV. It will be seen that there is no serious discrepancy between these three determinations and they yield a weighted mean value of 11.55 ± 0.07 MeV.

The gamma-ray of energy 10.46 ± 0.07 MeV. is almost certainly due to a cascade transition which proceeds through a level of Si^{28} in the region of 1.8 MeV. On this assumption the measurements give a value of 1.66 ± 0.2 MeV. for this level. The reaction $\text{Al}^{28}(\beta^-) \text{Si}^{28}$ proceeds via a level at

1.80 \pm 0.05 MeV. and the reaction $^{27}\text{Al}(d, n) ^{28}\text{Si}$ proceeds via a level which has been measured as 1.78 \pm 0.13 MeV. from the neutron groups⁽⁵⁷⁾, and as 1.72 \pm 0.08 MeV. from the gamma-radiation⁽⁵⁸⁾. Thus, all the determinations are consistent with a weighted mean value of 1.75 \pm 0.04 MeV. for the energy of this level in ^{28}Si .

The interpretation of the 7.6 MeV. gamma-ray is less certain, but it seems probable that it is due to a cascade transition which proceeds through a level in ^{28}Si at 4.50 \pm 0.15 MeV. This interpretation is consistent with the level at 4.47 \pm 0.13 MeV. found by Peck⁽⁵⁷⁾ in the $^{27}\text{Al}(d, n) ^{28}\text{Si}$ reaction.

In the present measurements six excited states in ^{28}Si were excited simultaneously. It is virtually certain that the radiation from each state separately is less complex. The results of measurements on the $^{27}\text{Al}(p, \alpha) ^{24}\text{Mg}$ reaction, discussed in Section III. 3.2., indicate that at least two different kinds of level are present. It would, therefore, be of interest to make measurements of the energy of the radiation from each separate resonance. As the intensity of the radiation from the individual resonances is too low for these measurements to be practical with the existing spectrometer, a crystal pair spectrometer is now being constructed. In this instrument the incident gamma-quanta produce pairs in a sodium iodide

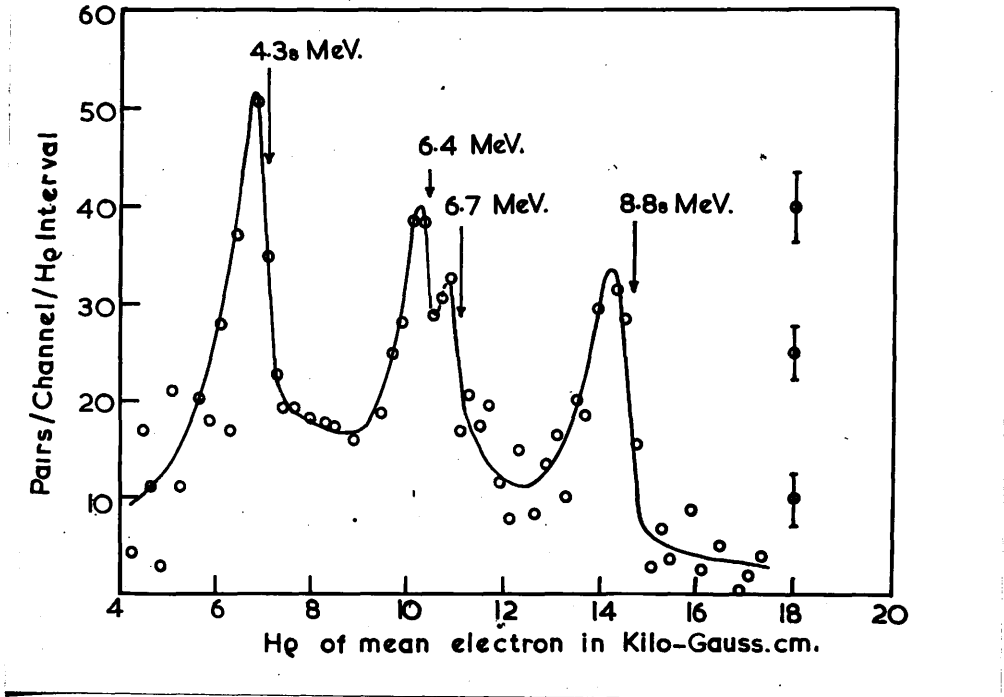


Figure 3.6. Spectrum of gamma-rays from B + d at Ed = 600 KeV.

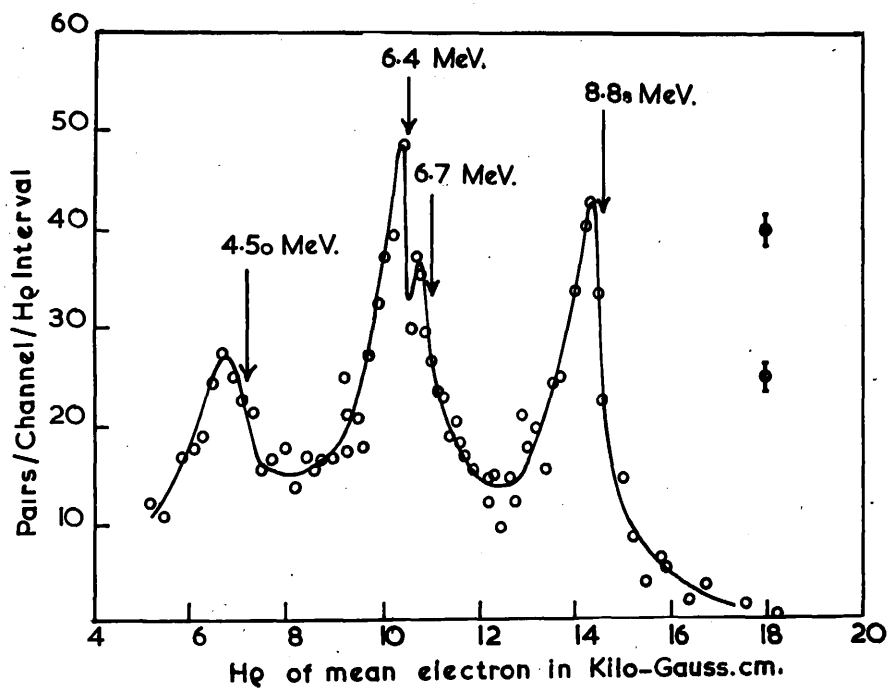


Figure 3.7. Spectrum of gamma-rays from $B^{10} + d$ at $E_d = 600$ KeV.

crystal sufficiently large to stop the electron and positron within the crystal. The energy of the gamma-ray can then be determined from the pulse size produced by a photomultiplier receiving the scintillations from the crystal. In order to avoid the very large background due to photoelectrons and Compton electrons the pulses are fed to the pulse analyser via a gate circuit. This gate is only opened when a coincidence is recorded in two counters placed either side of the sodium iodide crystal, such coincidences being produced by the annihilation radiation resulting from the decay of a positron from a positron-electron pair. Calculations show that the sensitivity of such a spectrometer should be five times as great as the existing spectrometer, while still possessing sufficient resolution to identify the various gamma-rays present.

The measurements of the gamma-rays from the $Al^{27}(p, \gamma) Si^{28}$ reaction have been published elsewhere (59).

III. 1.6. Gamma-Radiation Resulting from the Bombardment of Boron by Deuterons.

Natural boron consists of the two isotopes B^{10} and B^{11} which are present to the extent of 10% and 90% respectively. When it is bombarded with deuterons a number of reactions occur and in most of these the emission of high energy gamma-radiation is possible. Previous measurements of

this radiation by Gaerttner et al.⁽⁶⁰⁾ and Halpern and Crane⁽⁶¹⁾ indicated the presence of three gamma-ray lines (see Table 3.1.). These results were obtained by measuring the curvature of the tracks of positron-electron pairs in a cloud chamber. As the energies and origins of these gamma-rays give much information on the energy levels of the residual nuclei involved, it was decided to use the pair spectrometer to investigate this reaction. In addition to the better statistical accuracy obtainable with the pair spectrometer, the availability of separated boron isotopes prepared in the electromagnetic separator at the Atomic Energy Research Establishment at Harwell, enabled the reactions of the two isotopes to be investigated separately.

First, the gamma-ray spectrum from a natural boron target was measured. The target was prepared by making a paste of finely divided amorphous boron with xylene, spreading it on a brass plate and allowing it to dry. A bombarding energy of 600 KeV. was used and the resulting spectrum is shown in figure 3.6. At this time the spectrometer had not been fitted with the baffles shown in figure 3.1. and the background coincidence rate due to the neutrons was of the same order of magnitude as that due to pairs produced by gamma-rays in the foil. This background was subtracted to give the spectrum shown in figure 3.6., but as a result the statistical errors were rather large.

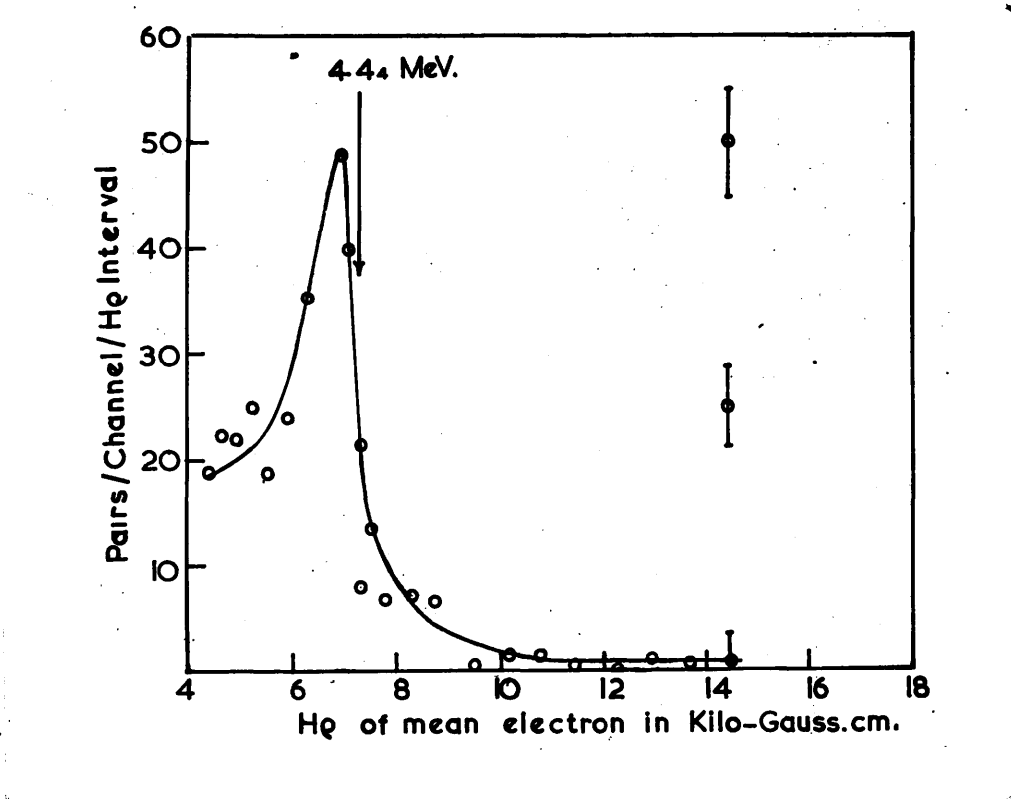


Figure 3.8. Spectrum of gamma-rays from $B^{11} + d$ at $E_d = 600$ KeV.

The separation between the two groups of deposits on the left is

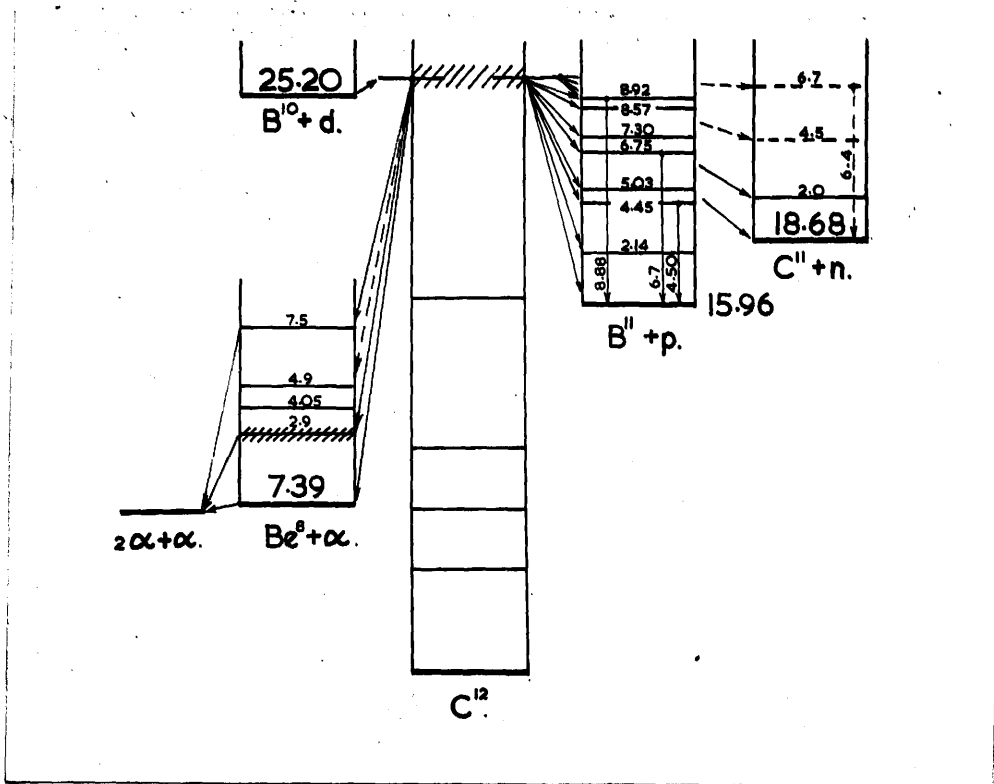


Figure 3.9. Energy level diagram for C^{12} .

The separated isotopes from Harwell were in the form of deposits on brass plates and could be used as targets without further preparation. The spectrum from B^{10} at a bombarding energy of 600 KeV. is shown in figure 3.7. The background was considerably smaller on this run, partly because of the baffles which had been fitted to the spectrometer. The gamma-ray yield was also greater because of the use of an isotopic target. The statistical accuracy was, therefore, very much better on this run than on the previous one.

A third run was then made with a target of separated B^{11} under similar conditions and the gamma-ray spectrum is shown in figure 3.8. The background on this run was of the order of magnitude of one third of the true coincidence rate at the peak of the spectrum and has been subtracted to give the spectrum shown.

The results of these three runs are summarized in Table 3.1., together with the measurements of previous workers on the same reaction. It will be seen that the majority of high energy gamma-rays from $B + d$ reactions are due to the B^{10} isotope and that $B^{11} + d$ does not produce any gamma-rays of energy greater than 4.44 MeV. The spectrum from $B^{10} + d$ is clearly complex in the region between 6 and 7 MeV. and is not completely resolved. However, both the $B + d$ and $B^{10} + d$ runs indicate two gamma-rays of the same order of intensity at 6.4 and 6.7 MeV. There is also a

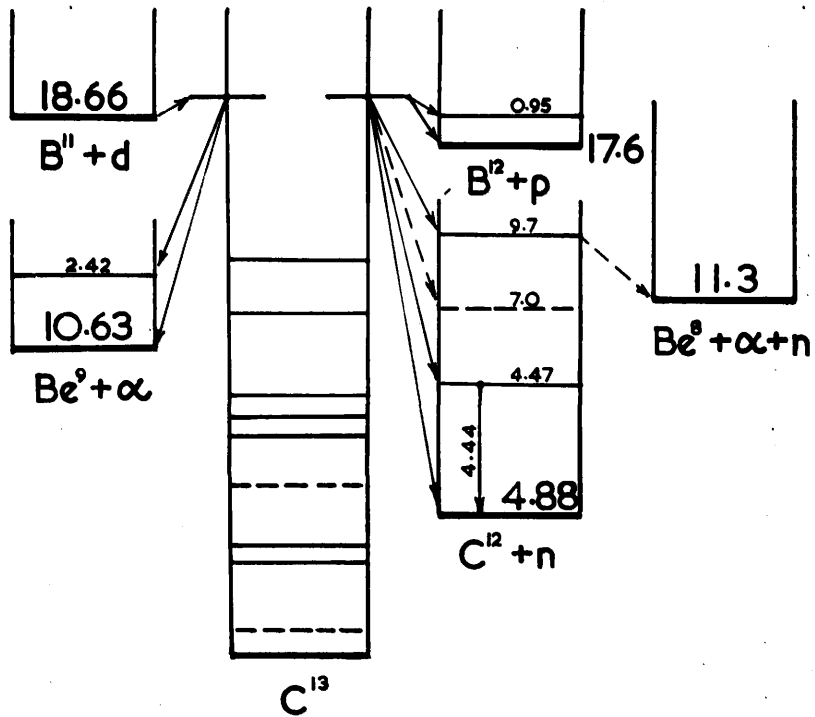


Figure 3.10. Energy level diagram for C^{13} .

pronounced 'tail' on the high-energy side of these peaks which suggests the presence of a gamma-ray of smaller intensity at about 7 MeV.

The interpretation of these results is complicated by the number of possible competing reactions. In the case of $B^{10} + d$, three reactions are energetically possible, as shown in the energy level diagram for C^{12} , figure 3.9. These are $B^{10}(d,p)B''$, $Q = 9.24$ MeV.; $B^{10}(d,\alpha)Be^8$, $Q = 17.81$ MeV.; and $B^{10}(d,n)C^{11}$, $Q = 6.53$ MeV.

The reaction $B^{10}(d,p)B''$ leads to a number of excited states in B'' . The most precise measurements of the energies of the proton groups from this reaction have been made by Van Patter Buechner and Sperduto⁽⁶⁷⁾, using a bombarding energy of 1.5 MeV. and the energies of the levels in B'' thus found are given in Table 3.4. In order to correlate proton groups associated with the formation of particular excited states with the gamma-radiation resulting from their de-excitation, measurements were made of the relative intensities of these proton groups at a bombarding energy of 600 KeV. These measurements are described in Section III. 3.2. and the results are included in Table 3.4. It will be seen that the energies of the measured gamma-rays at 4.5, 6.7 and 8.9 MeV. are in good agreement with the energy levels predicted by the three most intense proton groups. The intensities of the remaining proton groups are too small to give observable gamma-rays in this work,

but the proton group corresponding to the 7.3 MeV. level may be responsible for the shape of the gamma-ray spectrum on the high energy side of the 6.7 MeV. peak.

The $B^{10}(d,\alpha)Be^8$ reaction is known to lead to levels in Be^8 at 7.5 MeV. and 2.9 MeV. ⁽⁶²⁾ but it is almost certain that these levels decay with the emission of two alpha-particles and would not, therefore, contribute to the observed gamma-radiation.

The neutrons from $B^{10}(d,n)C^{11}$ have been studied by Gibson ⁽⁶³⁾ at $E_d = 0.93$ MeV. and by Swann and Hudspeth ⁽⁶⁴⁾ at $E_d = 1.4$ MeV. The former find neutron groups corresponding to the ground state and to a 2.0 MeV. excited state in C^{11} . The latter find evidence for only two levels in C^{11} at 4.5 MeV. and 6.7 MeV., but there is a possibility that the corresponding neutron groups were due to contamination. If a level exists in the region of 6.7 MeV. it may be responsible for the complexity of the gamma-ray spectrum observed in this region.

We may summarize these reactions by saying that the majority of the high energy radiation from $B^{10}+d$ arises from transitions between excited states of B^{10} and the ground state, following the $B^{10}(d,p)B^{10}$ reaction, but that there may be some gamma-radiation of energy about 6.4 MeV. from the $B^{10}(d,n)C^{11}$ reaction. This conclusion is

Table 3.1. Summary of Gamma-ray Measurements.

Reaction	Present Work		Gaerttner et al. 1939		Halpern and Cranz 1939		Terrell and Phillips 1951		Bame and Bagget 1951
	Ex. MeV.	Rel. Int.	Ex. MeV.	Rel. Int.	Ex. MeV.	Rel. Int.	Ex. MeV.	Rel. Int.	
B+d	888±0.06	1	9.1±0.4	1	8.6	1	9.0±0.2	1	
	6.7±0.15	0.8	6.9±0.4	3	6.0	2	6.7±0.2	1.8	
	6.4±0.15	0.9							
	438±0.05	2.9	4.4±0.3	10	4.2	6	4.5±0.1	8.7	
¹⁰ B+d	888±0.06	1					9.04±0.18	1	8.93±0.07
									7.34±0.20
	6.70±0.15	0.8							6.75 ± 0.13
	6.40±0.15	1					6.71±0.13	1.6	6.51 ± 0.13
	4.50±0.05	0.9					4.52±0.1	2.8	4.43±0.07
B+d	4.44±0.05						4.5 ± 0.1		

supported by the observations of Thirion⁽⁶⁶⁾, and Curling and Newton⁽⁶⁵⁾, who observed proton-gamma coincidences but no alpha-gamma coincidences from this reaction.

In the case of $B^{10} + d$, we must consider the reactions $B^{10}(d,n)C^{12}$, $Q = 13.78$ MeV.; $B^{10}(d,p)B^{11}$, $Q = 1.1$ MeV. and $B^{10}(d,\alpha)Be^8$, $Q = 8.03$ MeV., as shown in the energy level diagram for C^{13} (figure 3.10.). The first reaction has recently been studied by Gibson⁽⁶³⁾ and is found to yield neutron groups leading to excited states of C^{12} at 9.72 ± 0.15 MeV. and 4.47 ± 0.10 MeV. with relative intensities of $0.67 : 1$. The second group corresponds well with the gamma-ray energy of 4.44 ± 0.05 MeV. measured in this work. However, there is no evidence of a gamma-ray at 9.7 MeV. This is not unexpected, since this level can decay by the emission of an alpha-particle to the ground state of Be^8 , with an energy release of 2.3 MeV., and one would expect the lifetime for this process to be very much shorter than that for the emission of a gamma-ray. Malm and Buechner⁽⁶⁸⁾ have also observed this level in the reaction $N^{14}(d,\alpha)C^{12}$ and find that it has a greater width than the lower levels in C^{12} which is consistent with the assumption that it decays by alpha-emission. The possibility of a cascade transition through the 4.5 MeV. level seems to be ruled out by the fact

that a gamma-ray of energy 5.2 MeV. is not observed.

The reaction $B^{11} (d,p) B^{12}$ need not be considered because of its low Q -value. The reaction $B^{11} (d,\alpha) Be^9$ has recently been studied by Van Patter et al. (69) and has been found to lead only to the 2.4 MeV. level in Be^9 . It would, therefore, not be expected to contribute to the gamma-radiation observed in this work.

We may summarize these conclusions by saying that the high energy gamma-radiation from $B^{11} + d$ arises from the transition from the 4.47 MeV. level in C^{12} to the ground state and the 9.7 MeV. level in C^{12} decays by alpha-particle emission to Be^8 .

Since these experiments were completed, further measurements have been reported by Terrell and Phillips (70) and Bame and Baggett (108). Their results are included in Table 3.1. Terrell and Phillips, using a similar type of pair spectrometer, measured the energies and relative intensities of the three main gamma-rays but were unable to resolve the 6.4 MeV. and 6.7 MeV. lines. Bame and Baggett used a magnetic lens spectrometer to detect internal pairs and were thus able to avoid the loss of resolution consequent on the use of a comparatively thick external radiator. Their results verify that the radiation at an energy of about 6.7 MeV. is due to two gamma-ray lines, and also confirm the presence of a gamma-ray line at about 7 MeV. as suggested in

this work. Their measurements of the energies of the other lines are also in excellent agreement with those described here.

The present results were first published in a joint paper in the Proceedings of the Physical Society (1951)⁽⁵⁹⁾.

III. 1.7. Constructional Details of Spectrometer.

The vacuum chamber of the spectrometer consisted of a circular copper cylinder 12 in. in diameter and $2\frac{1}{4}$ in. long with circular steel end plates 14 in. in diameter and $\frac{1}{2}$ in. thick sealed to the cylinder on one side with a soldered joint and on the other by a rubber gasket. The gamma-rays from the target were collimated by the lead shielding blocks and allowed to fall on a lead foil 0.003 in. thick placed at the centre of the vacuum chamber. This foil was mounted on a light frame which could be rotated about an axis through one edge by means of a rod passing through a rotary vacuum seal. Thus, it was possible to take measurements of the background coincidence counting rates by rotating the foil through 90° , so that it lay against the vertical end plate of the vacuum chamber. These background rates were negligible when measurements were made on proton reactions, but were often serious in deuteron reactions because of the difficulty of providing adequate screening of the counters from

the gamma-rays produced by the accompanying neutrons.

The chamber was placed between the 12 in. diameter poles of an electromagnet of conventional design which provided a field of up to 7,000 gauss. This field was sufficient to measure gamma-ray energies up to 30 MeV. The field was measured by means of a flip coil and fluxmeter. The relative accuracy of this measurement was estimated to be within approximately 0.3%. A magnet current of 50 amperes at 50 volts was required for the maximum field and this was supplied by a D.C. generator. The current was stabilized and controlled to an accuracy of within 0.1% by a feedback circuit operating on the field current of the generator.

The electrons and positrons were detected by two sets of five miniature Geiger counters placed in the plane of the foil. These counters⁽⁷¹⁾ were constructed from brass tube, $\frac{1}{2}$ in. in diameter and of $\frac{1}{32}$ in. wall thickness. The tube walls were cut away over 180° along their operating length and replaced by 0.001 in. copper foil to allow electrons or positrons to enter the counters with a minimum of scattering. The counter wires were supported on Kovar seals soldered to one end of the counter tubes. The other ends of the tubes were sealed up and provided with short helical springs which were located in blind holes recessed in the side plate of the spectrometer. The ends provided with Kovar seals projected through clearance holes in the other side plate of the

spectrometer and were sealed to it with 'Q' compound. A gap of 1 in. was left between this plate and the magnet pole to allow connection to be made to the counters.

The counters were screened from direct gamma-radiation by lead blocks. Baffles were placed in the vacuum chamber to reduce the background due to electrons produced by gamma-rays from (n, γ) reactions in the counter walls and the lead shielding behind them, which could otherwise traverse the spectrometer and cause spurious coincidences.

The output pulses from the counters were fed via cathode followers and shaping circuits to twenty-five coincidence circuits each with a resolving time of about 2μ sec. The arrangement of these circuits is shown in the schematic diagram of figure 3.1. The output pulses from the coincidence circuits were grouped into nine different energy channels, and the output of each channel was recorded on a mechanical counter.

The counts recorded on these nine energy channels must be weighted according to the number of coincidence channels connected to each output channel. It will be seen from figure 3.1. that there is only one pair of counters (5 and 6) having the smallest spacing and one pair (1 and 10) having the largest spacing, whereas the central output channel is connected to five pairs of counters (1 and 6, 2 and 7, 3 and 8, 4 and 9 and 5 and 10). Therefore, in order

normalise the counts recorded on the nine channels they must be divided by 1, 2, 3, 4, 5, 4, 3, 2, 1 respectively.

The pulses from the monitor Geiger counter were recorded on a scale of 100. The output of this scaler was fed into the timing unit described in Section II. 6.4. and all runs were made for a fixed number of monitor counts, the duration of each run being automatically recorded.

III. 2. Soft Gamma-Radiation.

III. 2.1. General.

The investigation of the gamma-radiation from the excited states of light nuclei has been principally concerned with gamma-rays having energies greater than 250 KeV. The part of the spectrum below this has been less thoroughly explored, chiefly because there are good theoretical grounds for supposing such radiation to be unlikely, but also because the detecting instruments used (mainly Geiger counters) were of low sensitivity at these energies.

With the development of the proportional counter in this laboratory a sensitive method became available for the detection of soft electromagnetic radiation. It was, therefore, possible to re-examine some of the reactions involving light nuclei to see if such radiations were present.

III. 2.2. Origin of Soft Gamma Radiation.

The emission of gamma-radiation of energy less than 100 KeV. implies the existence of two levels spaced by less than this amount. The level spacing at low excitations in light nuclei is usually about 1 MeV. and though the levels are sufficiently close at an excitation energy of 10 MeV. or so, a transition between these is improbable. For instance, consider a compound nucleus ($Z \approx 20$) excited by proton capture to an excitation energy of about

10 MeV. The level density at this energy can be calculated on the basis of particular nuclear models, for example, by considering the nucleus as a degenerate Fermi gas of protons and neutrons⁽⁷²⁾. In addition direct evidence for the spacing in a number of nuclei can be obtained by the resonance capture of protons, for example, aluminium shows an average level spacing of about 30 KeV. at an excitation energy of 12 MeV.⁽⁵³⁾. This level spacing is rather greater than that predicted by the nuclear models, but it is possible that other levels not excited by proton capture may exist. If a light nucleus excited in this manner emits gamma-radiation it would normally do so by making a transition to the ground state. It is possible, however, that it might first make a transition to an adjacent level emitting radiation of an energy of 100 KeV. or less and then emit a second quanta of high energy.

The width Γ_1 for the emission of the 100 KeV. gamma-ray would, however, normally be small compared with the width Γ_2 for the emission of a high energy gamma-ray of about 10 MeV. to the ground or first excited state of the nucleus, since for an electric dipole transition the probability of gamma-ray emission is proportional to the cube of the quantum energy. If, however, the emission of the hard gamma-ray is prevented by powerful selection rules the lower energy transition may occur.

The emission probability for electromagnetic radiation from a nucleus, can be calculated by

classical electromagnetic theory by assuming the radiation to be due to the motion of electric charge within the nucleus⁽⁷³⁾.

The expression obtained for the radiation field can be split up into a number of terms. The first term corresponds to the field of electric dipole radiation. The second term can be split into two parts, one corresponding to the field of an electric quadrupole, and the other corresponding to the field of a magnetic dipole. Similarly the next term may be regarded as the sum of an electric octupole and a magnetic quadrupole and so on.

Each term is smaller than the preceding one by a factor (x/λ^2) where $2\pi\lambda$ is the wavelength of the emitted radiation and x is a distance not greater than the nuclear diameter.

The result for the radiation width, for dipole radiation is:

$$= 4/3 \frac{\omega^3}{c^3} \left| M_{mn}^e \right|^2$$

where $M_{m\eta}^e$ is the matrix element of the electric moment of the nucleus for the transition mn .

Similarly for magnetic dipole

$$= 4/3 \frac{\omega^3}{c^3} \left| M_{mn}^m \right|^2 \quad \text{where } M_{mn}^m \text{ is the}$$

matrix element of the magnetic moment for the transitions mn .

For the estimation of the matrix elements M_{mn}^e and M_{mn}^m some particular nuclear model must be

L.	$\frac{\Gamma_1}{\Gamma_2}$	
	Lowen	Bethe
2	10^{-8}	10^{-10}
3	8×10^{-6}	5×10^{-8}
4	10^{-2}	5×10^{-5}
5	20	8×10^{-2}

= width for emission of electric quadrupole radiation of 100 KeV. energy.

= width for emission of electric 2 -pole radiation of 10 MeV. energy.

Table 3.3. Relative probability of emission of high and low energy gamma-ray radiation for A = 28.

assumed. For example, Lowen⁽⁷⁴⁾ has calculated for the liquid droplet model that for 2^L -pole radiation

$$\Gamma_{\gamma} = \frac{3}{4} \cdot \frac{\hbar Z^2 e^2}{c} \cdot \frac{L+1}{AM \Gamma_0^2} \cdot \frac{(\hbar \omega)^{2L}}{1^2 3^2 5^2 \dots (2L-1)^2}$$

while Bethe⁽⁷⁵⁾ obtained the approximate expression

$$\Gamma_{\gamma} = \left(\frac{\omega}{c}\right)^{2L+1} e^2 \eta^2 \frac{r^{2L}}{1^2 3^2 5^2 \dots (2L-1)^2}$$

where r = nuclear radius

M = mass of proton

Z = atomic number

e = electronic charge

$\hbar \omega$ = quantum energy

$$\eta^2 \approx 1$$

Of these expressions, that due to Bethe is a better fit of the experimental data. Experimentally it is found that gamma-rays that may be identified as dipole and quadrupole by measurement of their internal conversion coefficients seem to show no systematic difference in intensity. This is assumed to be due special symmetry properties of nuclei, resulting in a reduction in the expected dipole moment. However, higher order transitions show the expected decrease in probability. Therefore, by substitution in the above expressions on the assumption that the 100 KeV. transition is dipole or quadrupole the ratio of the widths Γ_1/Γ_2 may be calculated for various multi-polarities of the 10 MeV. transition.

The results are shown in Table 3.3. From

this table it may be seen that, in order that the 100 KeV. transition be of appreciable intensity, the transition to the ground state and any low lying excited states must be of an order higher than octupole. For this to occur the excited level in the compound nucleus must have a high spin and will, therefore, be correspondingly difficult to excite.

Hence soft radiation from this process is improbable but might be detected under special circumstances.

If, on the other hand, the first excited level of a nucleus is within 100 KeV. of the ground state, comparatively weak selection rules will suffice to cause the low energy transition to be favoured in a cascade de-excitation of the compound nucleus.

No such low-lying levels, however, are at present known for nuclei with $Z < 15$ (with the exception of Al^{28} - see Section III.2.7.). Theoretical predictions of the positions of energy levels may be made on the basis of some nuclear models, but though most of these give an estimate of the level density at high excitation energies, prediction of the position of the first level is more difficult. Guggenheimer⁽⁷⁶⁾ and Preiswerk⁽⁷⁷⁾ have calculated the energies of levels due to the rotation of the whole nucleus and particles rotating round it. There is evidence that some

levels of light nuclei may correspond to rotation levels. On this picture the lowest levels of the rigid rotator system are given by:

$$E = \frac{2.5 \hbar^2 A^{2/3} K (K + 1)}{2M_0 r_0^2}$$

A = number of nucleons.

M₀ = mass of hydrogen atom.

K = small integer.

radius of nucleus = r = r₀ A^{1/3}.

which would place the lowest level at about 170 KeV. for A = 20 and correspondingly higher for lighter nuclei.

"One particle" models of the nucleus such as that due to Mayer⁽⁹²⁾ have been successful in predicting the ground state properties of nuclei. The first excited level can then often be regarded as a member of a doublet made up of this level and the ground state. An estimate of the magnitude of the splitting can be made; it is of the order of 1 MeV. for light nuclei.

Thus the existence of a low-lying level in light nuclei capable of emitting 100 KeV. quanta is rather improbable.

Assuming for the moment that radiation of this energy by either of the processes suggested above does in fact occur; the difficulty of its detection may be increased by internal conversion of the gamma-ray. For light nuclei and energies of

less than 100 KeV., transitions of a higher order than quadrupole are almost totally internally converted.

III. 2.3. Radiation by Extra-Nuclear Electrons.

When the search for soft gamma-radiation was commenced it became apparent that a lower limit to the intensity of radiation that could be detected would be set by the radiation from the atomic electrons. Two main types of radiation were detected, characteristic X-radiation and a diffuse background of lower intensity. The X-radiation resulting from the proton bombardment of such an element as copper is, for example, so intense that the presence of 0.1% of copper as impurity in the target will produce more radiation than any probable nuclear reaction.

Therefore, in order to avoid confusion caused by these radiations, before continuing the search for gamma-radiation the excitation of these radiations was investigated. Section III. 1.4. deals with the characteristic X-radiation and Section III. 1.5. with the "white" background radiation.

III. 2.4. Characteristic X-radiation.

When fast moving protons or other ions are stopped in the target material they make large numbers of ionising collisions resulting in the

ejection of low energy electrons. J.J. Thomson was the first to study electrons expelled in this process, the bombarding particles in his case being alpha-particles from polonium. The electrons were called Delta rays and were investigated in detail in the succeeding years. A summary of the results has been made by Rutherford, Chadwick and Ellis⁽⁷⁸⁾. The majority of the delta-rays will originate in the outer shells of the atoms of the target, but a small number of inner shell electrons will be ejected, and when these ionised atoms de-excite characteristic X-radiation will be emitted. This characteristic radiation was first detected by Chadwick⁽⁷⁹⁾ and later studied by Slater⁽¹⁰⁷⁾.

A detailed examination of the X-radiation produced by absorbing alpha-particles from Polonium in a number of different elements was made by Bothe and Franz⁽⁸⁰⁾ in 1928. Gerthsen and Reusse⁽⁸¹⁾ (1933) measured the K X-rays produced by proton bombardment of Aluminium at energies from 30 KeV. to 100 KeV., and a similar investigation was made subsequently by Peter⁽⁸²⁾. Henneberg⁽⁸³⁾ (1933) calculated the cross-section for the ionisation of K-shell electrons by low energy heavy charged particles. His calculation was based on the use of the Born approximation, i.e. the ionising particle is represented before and after the collision by plane waves. This ignores the polarisation of the atomic shell caused by the incoming particle and is normally only justified when the velocity of the latter is large

compared with the velocity of the K-electrons in the atomic shell. In this particular instance, however, Henneberg showed that the errors introduced by using the Born approximation to calculate the ionisation probability are small even though the above condition is far from being satisfied. In this manner he obtains for the total ionisation probability for K-shell electrons:

$$\Phi(E) = \frac{6\pi}{5\alpha^4} e^{-\frac{4\eta}{1+\eta}} \left[\frac{4\eta}{1+\eta} \right]^4 \left[\frac{1}{4} + \frac{1}{2} \left(\frac{4\eta}{1+\eta} \right) + \dots \right] \dots (1)$$

where $\eta = \frac{4E}{\alpha^2 M}$

E = energy of ionising particle in Rydberg units.

M = mass of ionising particle in units of electron mass.

α^2 = actual ionisation energy of K-shell in Rydberg units.
 $\approx Z^2$

α^2 is slightly smaller than Z^2 owing to the screening effect of the outer electrons. For aluminium $\alpha^2 = 0.68 Z^2$ and for copper $\alpha^2 = 0.78 Z^2$. For small values of η (η is less than 0.1 for the experiments to be described later) this expression shows:

$$\begin{aligned} \Phi(E) &\propto \frac{\eta^4}{\alpha^4} \\ &\propto \frac{E^4}{Z^{12}} \dots (2) \end{aligned}$$

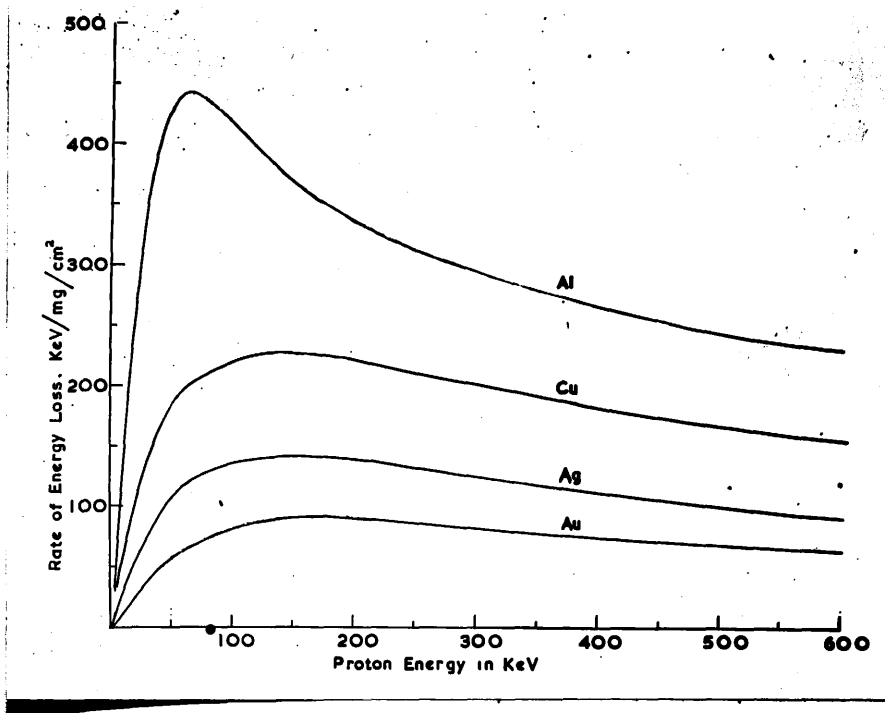


Figure 3.11. Rate of energy loss of protons in metals.

The number dI of K-shell electrons ejected by the incident particle in a path length ds (measured in milligrams per square centimetre) is given by:

$$dI = 2Na^2\bar{\Phi}(E) ds$$

N = number of atoms of target element per milligram
 ($2N$ = number of K-electrons per milligram)

a = radius of hydrogen atom in centimetres
 (arises from the use of atomic units).

Thus

$$dI = 2 N a^2 \bar{\Phi}(E) \frac{ds}{dE} dE$$

$$I = \int_0^E 2 N a^2 \bar{\Phi}(E) \cdot \frac{ds}{dE} dE \quad \dots (3)$$

$\frac{dE}{ds}$ = rate of loss of energy of ionising particle in target in Rydberg units per milligram per square centimetre

I = total number of K-electrons produced by stopping particle of energy E , Rydberg units.

In the energy range investigated $\frac{dE}{ds}$ is approximately constant so that for low energy protons for which

$$\bar{\Phi}(E) \propto \frac{E^4}{Z^{12}}$$

$$I \propto \frac{E^5}{Z^{12}}$$

The actual variation of $\frac{dE}{ds}$ with energy for various metals is shown in figure 3.11., which is drawn from the experimental data of Warshaw⁽⁸⁴⁾. An accurate expression for I can be calculated by graphical integration but the results in the cases considered

in this thesis differ little from those obtained by assuming $\frac{dE}{ds}$ to be constant.

The number of K-electrons per milligram of stopping material is approximately proportional to Z^{-1} , but $\frac{ds}{dE}$ increases with increasing Z , so that for $29 < Z < 50$:

$$N \frac{ds}{dE} \approx \text{constant.}$$

The number of X-ray quanta emitted will be lower than the number of K-shell ionisations owing to the Auger effect. For light elements the majority of de-excitations do not result in the radiation of a quanta but the ejection of an electron from an outer shell. A theoretical expression for the magnitude of this Auger effect has been obtained by Burhop⁽⁸⁵⁾. He shows:

$$P = 1 - (1 - bZ^4)^{-1} \quad \dots (4)$$

where P = probability of emission of K X-ray

Z = atomic number

b = constant.

The most accurate value for b to fit the available experimental data has been given by Martin and Egglestone⁽⁸⁶⁾ as $b = 7.7 \times 10^{-7}$.

P varies very rapidly for elements of atomic number less than 40, and in consequence the observed variation of K X-ray yield with atomic number will differ from the variation of K-shell ionization. If Z is less than 20, bZ^4 is small

compared with unity and therefore:

$$P \propto bZ^{-4}$$

and the observed X-radiation would be expected on the basis of Henneberg's theory to be proportional to Z^{-8} .

The agreement between these theoretical predictions and experiment is not good. The original results of Bothe and Franz⁽⁸⁰⁾ show the cross-section rising more rapidly than E^4 and the variation of the yield of K X-ray with atomic number was less than predicted. In these experiments, however, the interpretation is complicated by the fact that γ is not always small.

The experiments of Gerthsen and Reusse⁽⁸¹⁾ and Peter⁽⁸²⁾ on the excitation of K X-rays by protons of energies between 40 KeV. and 150 KeV. both show a thick target yield proportional to E^4 ; instead of the E^5 relationship expected on the basis of Henneberg's calculation.

Livingston, Genevese and Konopinski⁽⁸⁷⁾ carried out experiments with protons of energies up to 1.8 MeV. using the beam from a cyclotron. Again these experiments show a thick target yield proportional to E^4 . The intensity of K X-radiation from different target materials was estimated to be proportional to Z^{12} . A correction was made for the absorption in the target of X-rays originating below the surface (this correction is small, even

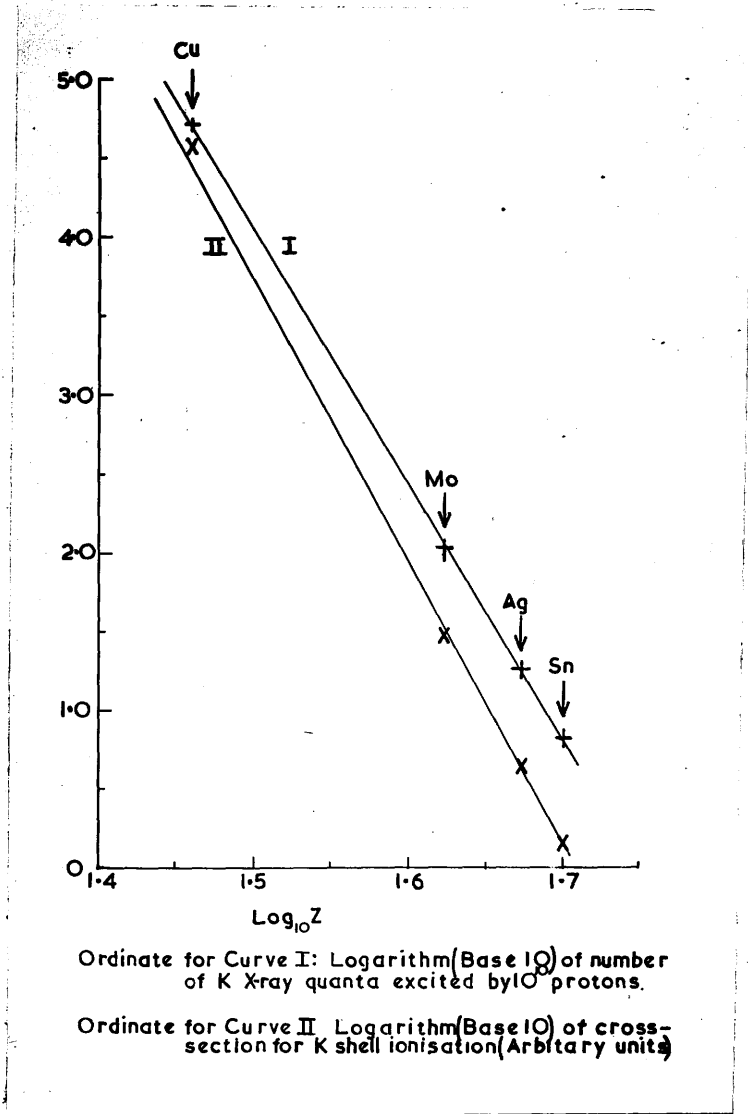


Figure 3.12. Variation of intensity of characteristic X-radiation excited by proton bombardment with atomic number of target nucleus.

even for the high bombarding energy used). If allowance is made for the variation of Auger coefficient with Z , these results indicate that the cross-section for K-shell ionisation decreases more rapidly than Z^{-12} .

The present results are also in disagreement with Henneberg's theory. The determination of the cross-section for K-shell ionisation as a function of Z involves a knowledge of the relative efficiencies of the proportional counters used as detectors at the energies of K X-rays of the elements investigated. The efficiency of the counters may be estimated from the known absorption of the window and the gas filling. As this efficiency for any one counter varies very greatly over a comparatively small range of energies it is difficult to compare the yields from targets of very different atomic numbers, particularly as these yields differ by several powers of ten. The experimental results for the yield of X-rays and the relative cross-section for K-shell ionisation are shown in figure 3.12. The relative cross-section was calculated from the experimental thick target yield of X-rays by allowing for the Auger effect and the variation of $\frac{ds}{dx}$ and N with Z . In this figure the experimental results lie close to a straight line of slope 18, indicating that for Z between 29 and 50 the K-shell ionisation is proportional to $Z^{-18 \pm 2}$.

The excitation of K X-rays from copper and molybdenum as a function of proton energy is shown

in figure 3.13. Curves 1 and 2 were obtained with thick targets of copper and molybdenum respectively, and curve 3 with a thin copper target (approximately 15 KeV. thick) electroplated on to a silver backing. In each case the yield was recorded as the number of counts in a pulse analyser, set on the peak of the K X-ray pulse distribution. The thick target yields are proportional to E^7 and the thin target yield proportional to E^6 , as would be expected if the cross-section $\bar{\Phi}(E)$ were proportional to E^6 .

A measurements was also made of the efficiency of singly charged hydrogen molecules in excitation K X-rays. A molecular ion will be equivalent to a proton and a neutral hydrogen atom, each having half the kinetic energy of the molecular ion. The ionisation produced by the proton will be the same as that due to an isolated proton accelerated by a voltage half as great. The hydrogen atom will become ionised as it passes through the material and will thereafter contribute to the ionisation. A 500 KeV. molecular ion would, therefore, be expected to produce between one and two times as much radiation as a 250 KeV. proton. The experimental value for this ratio, using a thick copper target, was 1.15 ± 0.05 .

The K X-radiation excited by deuterons is more difficult to measure, owing to the larger background effects. Since the ionising effect of protons and deuterons should be the same for particles of similar velocities, it is to be expected

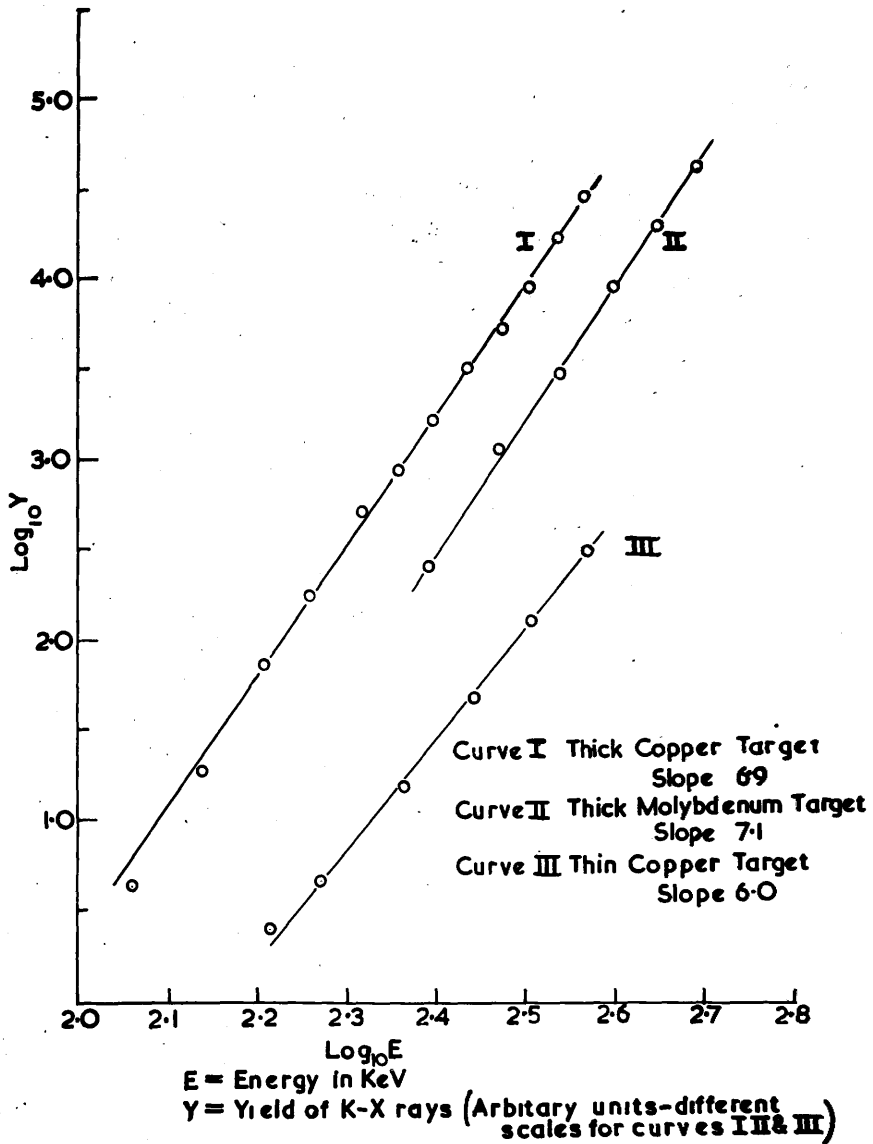


Figure 3.13. Excitation of characteristic X-radiation by proton bombardment.

that a deuteron will produce twice the ionisation of a proton of half the energy. The X-ray yield from copper and molybdenum, bombarded with deuterons of an energy of 500 KeV., was in approximate agreement with this prediction.

III. 2.5. "White" Background Radiation.

An initial examination of the radiation of energy between 5 KeV. and 20 KeV. resulting from the bombardment of a thick aluminium target by protons showed the presence of radiation of an intensity of the order of that expected from a nuclear reaction. However, this radiation proved to be of two kinds, neither nuclear in origin. The greater part was characteristic X-radiation from traces of impurity (mainly copper) present in the aluminium target, and the rest consisted of a continuous background of radiation whose intensity fell off rapidly with increasing energy. In order to reduce the characteristic X-radiation, it was necessary to use spectroscopically pure aluminium sheet as a target material. (The cross-section for the production of copper X-rays is nearly a thousand times that for the white background, so that the proportion of copper in the aluminium should be less than 0.01%). The spectrum of the radiation resulting from the bombardment of a thick aluminium target with protons of an energy of 500 KeV. is shown in figure 3.14. As the efficiency

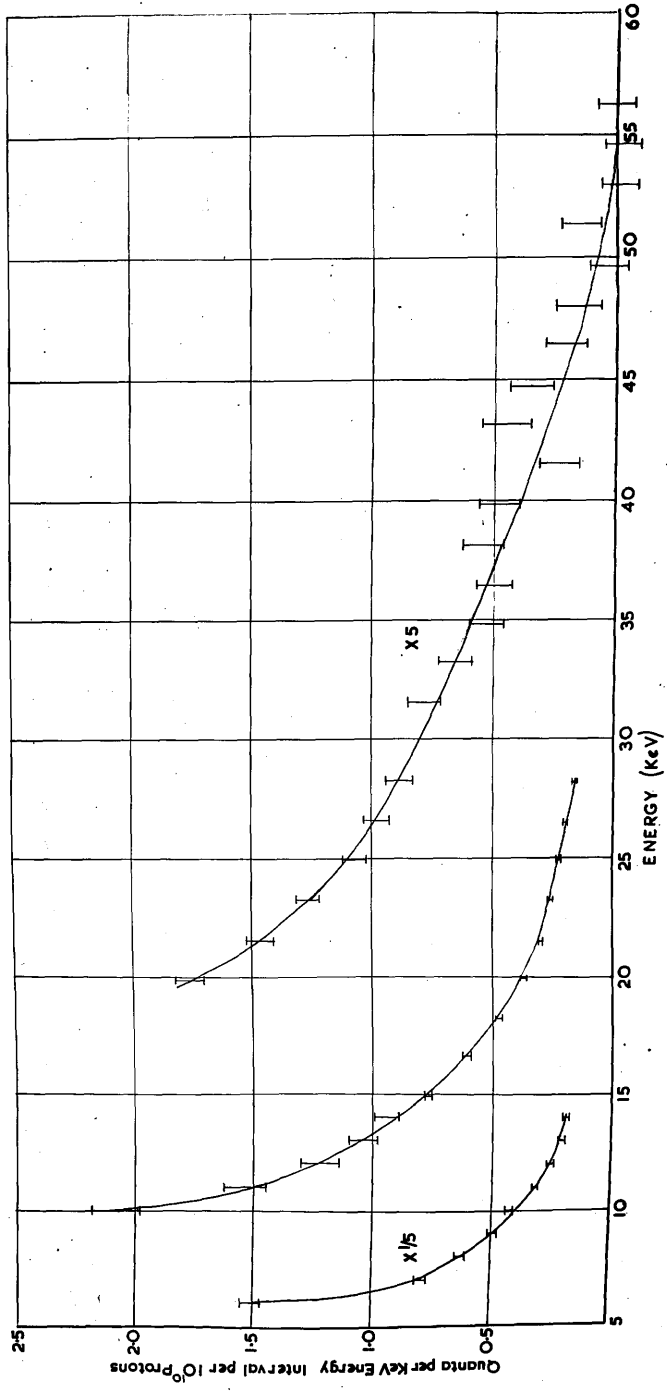


Figure 3.14. Spectrum of "white" radiation resulting from proton bombardment of aluminium.

of the counter used varies rapidly with energy (see figure 3.16.) it was necessary to use two different counters to obtain the curve shown in figure 3.14. The lower part of the spectrum was obtained with counter 'A' (see Section III.2.9.) and was fitted to that for the more energetic part of the spectrum, for which counter 'B' was used, at 20 KeV. The errors shown are standard deviations of the actual counts and do not include systematic errors.

This "white" radiation resulting from proton bombardment has not been previously reported. Its intensity is many times too great for it to be attributed to "Bremstrahlung" radiation from the protons: most probably it originates as radiation from electrons ejected by the incident protons. These electrons, or at any rate those contributing to the more energetic part of the spectrum, must originate in the K-shells of the target atom, as only tightly bound electrons will receive sufficient energy as a result of the impact of the protons. The excitation of this radiation will, therefore, be closely related to the excitation of characteristic K X-rays.

III. 2.6. Low Energy Nuclear Radiation.

After the magnitude of the effects due to radiation from the atomic shells had been established, a preliminary search for low energy

gamma-radiation was made. Thick targets of copper, aluminium, magnesium, fluorine, carbon and boron, were bombarded with 700 KeV. protons, but no radiation that could be attributed to radiation from atomic shells was detected. At this time a level at 31 KeV. in Al^{28} was reported by Enge et al. (88) and a more systematic search for radiation due to proton bombardment was deferred until the reaction $\text{Al}^{27}(\text{d},\text{p})\text{Al}^{28}$ had been investigated (Section III.1.7.).

III. 2.7. The Reaction $\text{Al}^{27}(\text{d},\text{p})\text{Al}^{28}$.

The Q-value of the reaction $\text{Al}^{27}(\text{d},\text{p})\text{Al}^{28}$ has recently been accurately determined by Enge et al. (88) (89). Using a high resolution magnetic analyser with photographic plate detection, they were able to determine the Q-value of a large number of reactions involving light nuclei with accuracies of the order of 1%. The most energetic proton group from the reaction $\text{Al}^{27}(\text{d},\text{p})\text{Al}^{28}$ was found to be a doublet and this was attributed to the presence of an excited state in Al^{28} at an excitation energy of 31 ± 2 KeV.

Al^{28} is an unstable nucleus and decays by beta emission to an excited state in Si^{28} (figure 3.5.). A level at 31 KeV. in Al^{28} may, therefore, either emit a gamma-ray and decay to the ground state of Al^{28} , or emit a beta-particle, the residual Si^{28} nucleus being left either in an excited state or in its ground state.

If the spin difference between the 31 KeV. state and the ground state of Al^{26} is small the gamma-ray transition is the more probable, and, provided that the internal conversion of the gamma-ray is not too large, it should be of sufficient intensity to be detected with a proportional counter.

A search was, therefore, made for radiation of an energy between 20 KeV. and 40 KeV. resulting from the bombardment of a thick aluminium target with deuterons⁽⁹⁴⁾. A bombarding energy of 700 KeV. was used as this was the highest voltage available at the time of the experiment. Enge et al.⁽⁸⁸⁾ used energies of 1.2 MeV. and 1.8 MeV. and found that the yield of the 31 KeV. state was 55% of the ground state at both energies. Though it was not certain that the 31 KeV. state would be excited at an energy of 700 KeV. as deuteron reactions do not usually show resonance effects, it was assumed that the relative intensities of the two proton groups forming the doublet would not change greatly.

It had originally been intended to use the proportional counter technique for the investigation of proton induced reactions only, owing to the high background of neutrons and gamma-rays produced by deuteron bombardment. However, as in this case, only a limited energy range was to be examined, it was found possible to search for soft radiation despite the high background. This background was found to originate in part from the

target and in part from the resolving chamber. That from the resolving chamber is due to part of the ion beam that strikes the collimators and walls of the chamber. In addition to the metal of the walls of the chamber, carbon from the vapour pump oil and absorbed deuterium are always present on these surfaces and the resultant reactions give rise to a high flux of gamma-rays and neutrons. This background is liable to vary greatly during the course of an experiment owing to slight shifts of the beam and changes in the surface films present. In order to minimise this background the counter was surrounded with three inches of lead and the ion beam was carefully centred in the resolving chamber. Attempts to reduce the neutron flux by interposing paraffin wax and cadmium sheet between the counter and resolving chamber were not successful, as there was insufficient space to make an effective shield.

Four counts were made at each setting of the pulse analyser. The first and fourth counts were made with a lead foil, thick enough to absorb over 90% of 30 KeV. radiation, inserted between the target and the counter. The second and third counts were made with an aluminium absorber of surface density equal to that of the lead. The difference between the sum of counts two and three and the sum of counts one and four was plotted as a function of pulse analyser setting. By taking four counts in this order errors due to the steadily

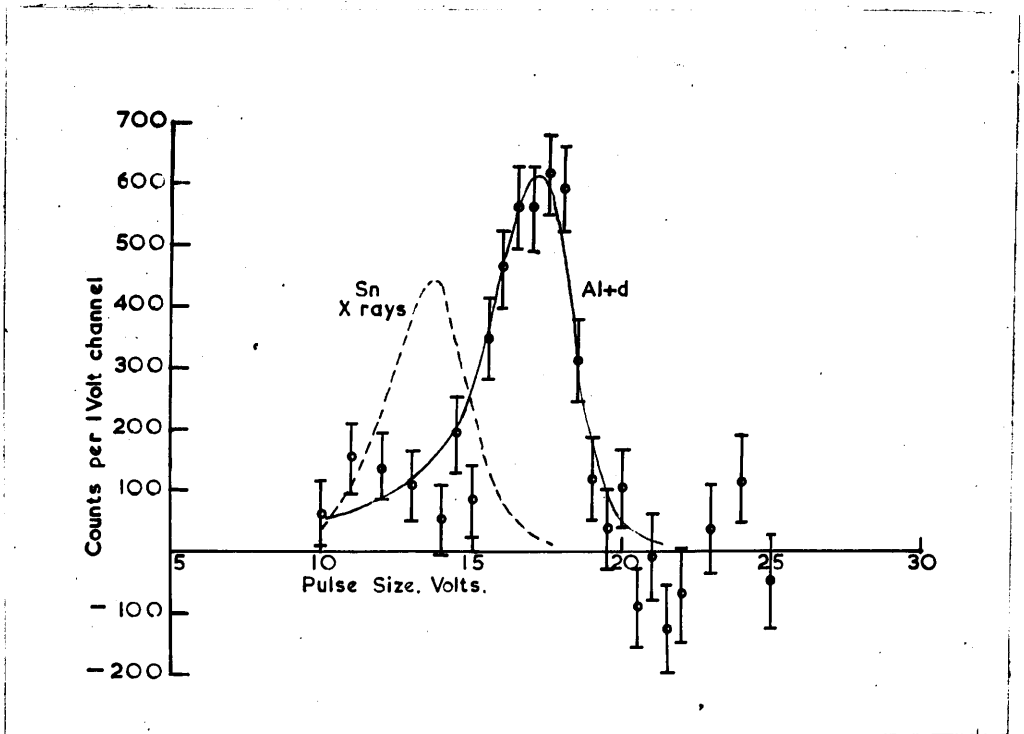


Figure 3.15. Spectrum of low-energy gamma-radiation from $Al^{27}(d,p)Al^{28}$ obtained with proportional counter.

increasing background caused by the build up of radioactivity in the counter and surrounding objects were minimised. By taking the difference between counts with lead and aluminium absorbers, errors due to electrons or soft gammas in the absorbing foil were reduced. The beta-particles from the decay of Al^{28} were prevented from reaching the counter by the combination of a strong magnetic field (of a magnetron magnet) and a polythene absorber. The difference between counts with aluminium and lead absorbers is plotted as a function of pulse amplitude in figure 3.15. The spectrum of the K X-rays of tin produced by proton bombardment of a tin target is shown for comparison. A peak, corresponding to radiation of an energy of 31 KeV., is clearly shown.

In order to confirm that this peak was due to radiation of this energy a series of absorption measurements were made using solutions containing tin, antimony, tellurium, iodine and caesium. The K-absorption edges of these elements lie between 29 KeV. and 36 KeV. Thus if the energy of the gamma-ray were, for example, 30 KeV., the radiation would be much more strongly absorbed by tin than by any of the other elements mentioned. The results obtained in this way indicated that the energy of the radiation was between 30.4 KeV. and 31.8 KeV. (the absorption edges of antimony and tellurium) though owing to difficulties due to variation of the background and the low residual true counting rate, this result was not conclusive.

is a line graph showing a distribution with a peak around 18-20 Volts. The y-axis is labeled 'Counts per 7mc.' and ranges from -200 to 500. The x-axis is labeled 'Pulse Size, Volts.' and ranges from 5 to 35. The data points are represented by circles with vertical error bars. A smooth curve is drawn through the data points, peaking at approximately 18-20 Volts. The label 'Al²⁷(d,p) Al²⁶' is placed in the upper right area of the plot.

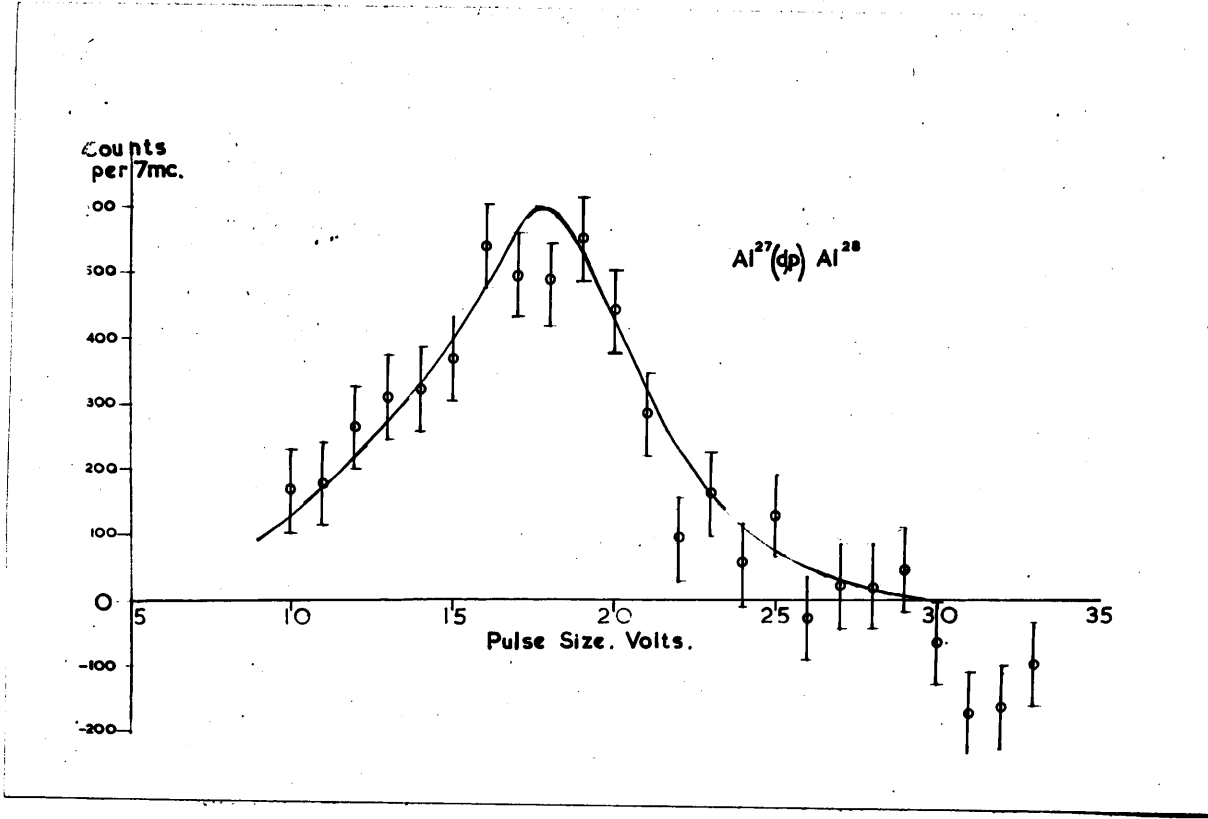


Figure 3.16. Spectrum of Al²⁷ (d,p) Al²⁶ obtained with scintillation crystal.

As a final check a scintillation method was used to detect the gamma-ray. A thallium-activated sodium iodide crystal, 1 cm. square and 1 mm. thick, was mounted on an E.M.I. type 5311 photomultiplier and screened with 3 inches of lead. The beta-particles from the target were absorbed with polythene (the magnet used in the counter experiment was omitted as its stray field affected the performance of the multiplier). As the crystal had a much smaller volume than the multiplier but still was nearly as efficient as a detector of 30 KeV. radiation it was hoped that the background would be relatively less. This proved to be so and the spectrum obtained with the crystal is shown in figure 3.16. This curve is a difference curve, taken with aluminium and lead absorbers in the same way as that in figure 3.15.

The resolution of the crystal method is inferior to that of the counter method and the latter was, therefore, used for the determination of the energy of the gamma-ray. The K X-rays of tin and barium were used for calibration. The weighted mean of a number of observations gave the value 31.4 ± 1.0 KeV.

The yield of the reaction was calculated from the estimated efficiencies of the crystal and the counter. The two methods agreed within the experimental error and a mean value of $1.2 \pm 0.5 \times 10^3$ gammas per microcoloumb was obtained.

III. 2.8. The Reaction $P^{31}(d,p)P^{32}$.

Measurements by Strait et al. (89) on the proton groups from this reaction indicated the presence of an excited state in P^{32} at an energy of 77 KeV.

A copper phosphide target was bombarded with deuterons of an energy of 700 KeV. and a search made for 77 KeV. gamma-radiation. The sodium iodide crystal and multiplier described in Section III. 1.7. were used as a detector.

No such gamma-radiation was detected. An upper limit to the thick target yield was estimated from the efficiency of the crystal to be 2.5×10^2 gammas per microcoulomb.

III. 2.9. Apparatus.

The use of proportional counters for the investigation of soft radiations was developed in this laboratory by Curran, Angus and Cockroft (90), and basically similar counters were used in the experiments described here.

The amplifier used was standard Type 1008A, but in order to avoid overshoots, a shorted delay line was used for shaping the pulses. The delay line was of special low loss construction and was inserted between the head amplifier and main amplifier giving a pulse width of 3 μ s.

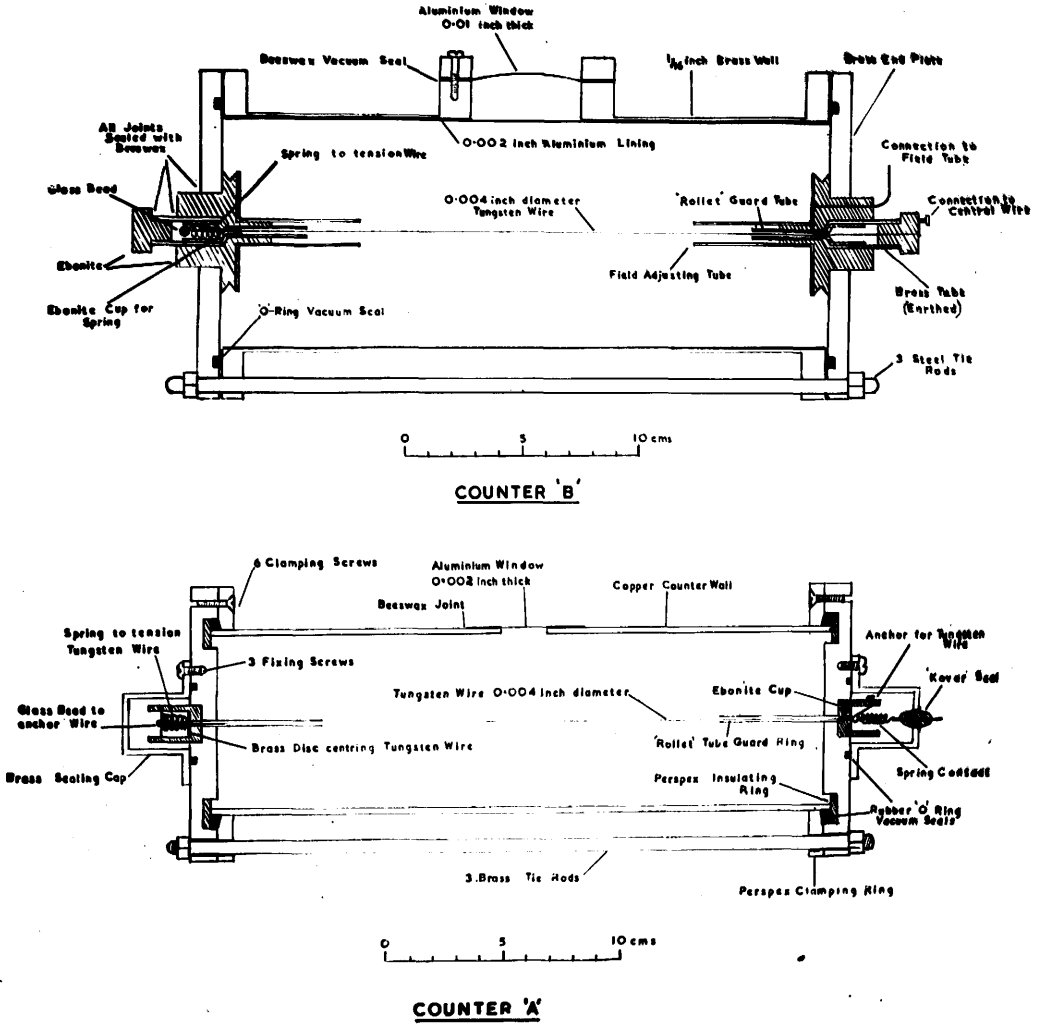


Figure 3.17. Constructional details of counters 'A' and 'B'.

Some difficulties not encountered in work with radioactive sources were encountered. In the first instance, as the target room was electrically very "noisy" very careful screening and rigorous elimination of common earths was necessary to avoid unwanted pickup; the R.F. oscillator used to heat the rectifier filaments in the cascade generator was a particularly serious source of trouble.

Secondly, the film method of analysing the pulse output used by Curran et al. was found to be inconvenient, especially for excitation curves. Instead, a single channel pulse analyser with a resolving time of $10 \mu s$ was built and used for all the early experiments until a commercial five channel analyser ("kicksorter") became available. This A.E.R.E. Type 1074A pulse analyser suffers from the disadvantage of a long resolving time, the analyser being inoperative for $60 \mu s$ after a pulse has triggered the lowest discriminator. (The analyser consists essentially of five discriminator circuits whose triggering levels are accurately spaced. Pulses whose amplitude corresponds to the interval between adjacent discriminators are fed to four scaling circuits; all pulses larger than these actuate the fifth scaling circuit). The long resolving time of this instrument limits the maximum permissible counting rate to one sixth of that for the single channel analyser and hence for fast rates the five channel

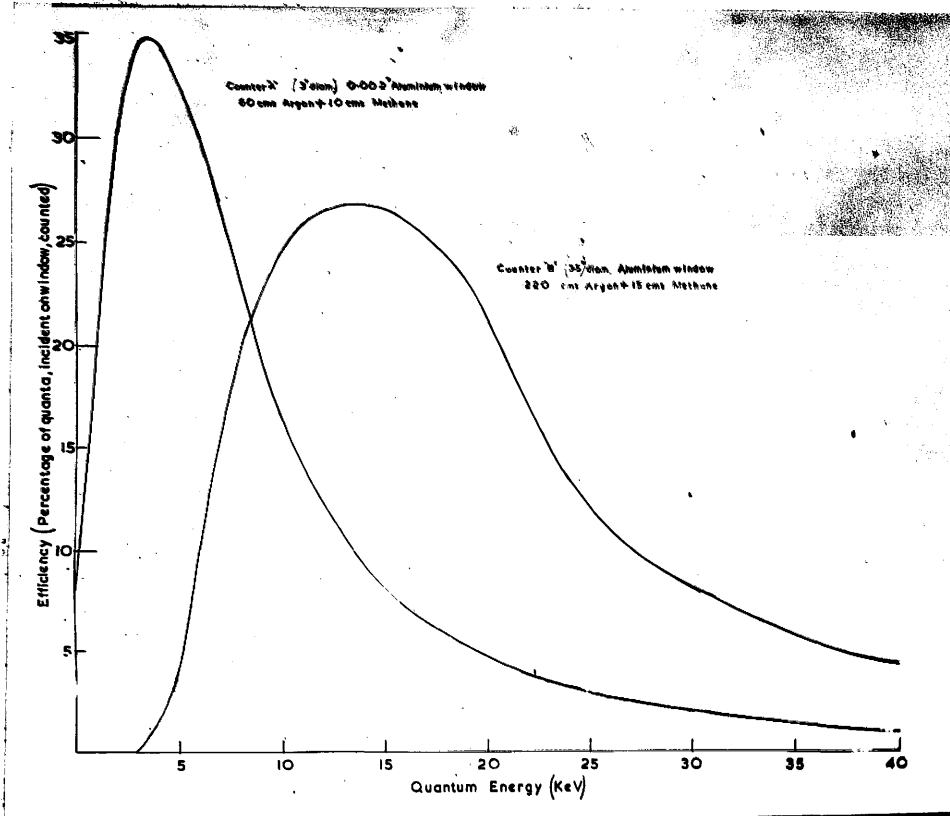


Figure 3.18. Calculated efficiencies of counters 'A' and 'B'.

analyser is actually slower. In order to overcome this difficulty a "low pass amplitude discriminator" was built. This consists of a trigger circuit set to operate just above the level of the upper discriminator of the five channel analyser. When this circuit was triggered it closed a diode gate through which the signal had to pass to reach the analyser, the signal being delayed $3\ \mu\text{s}$ by a length of delay cable. In this way only those pulses falling in the band of pulse sizes covered by the particular setting of the analyser were allowed to trigger it, and as the low pass amplitude discriminator had a dead time of only $6\ \mu\text{s}$, high counting rates could be accepted.

A disadvantage of the pulse analyser technique compared with the film method of analysis is the greater stability of gain of the counter and amplifier required. In order to avoid errors from this cause, it was necessary to build a special high stability high voltage power supply for the counter. The characteristics of the counters themselves were found to vary with time, and as a general rule they were freshly filled each day and their calibration checked before and after each set of measurements.

A number of different counters were used in the course of the experiments but most of the measurements were made with one or other of two counters, referred to as counters A and B. (figure 3.17.). Counter A was three inches in

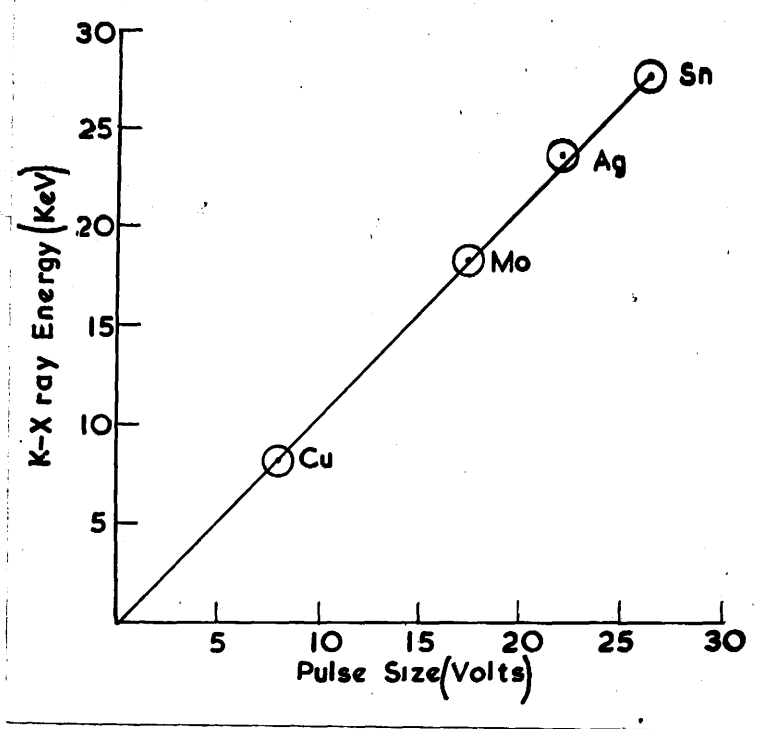


Figure 3.19. Calibration curve for proportional counter.

diameter and arranged so that the cylindrical counter wall forming the cathode could easily be changed, thus allowing the use of several different window arrangements. With a thin aluminium tube as cathode and a high pressure filling the counter can be used up to energies of 50 KeV. or more. However, the performance of the counter was found to deteriorate considerably within a few hours after filling when spun aluminium tubes were used as cathodes. The cause of this deterioration was not established with certainty, but it is believed that the aluminium used was porous and released traces of gases with a high electron affinity into the body of the counter. Highly polished rolled aluminium sheet, such as was used to line Counter 'B', does not show this effect, Counter 'A', therefore, was normally fitted with a copper anode and the window covered with a 0.002 inch aluminium foil. It was used for radiation having a quantum energy between 5 KeV. and 20 KeV. Counter 'B' was four inches in diameter and was fitted with 'Field Tubes'⁽⁹¹⁾ to eliminate end effects. It was filled to a pressure of 30 lbs. per sq. in. and was used for harder radiation. The efficiencies of these counters, expressed as a percentage of the quanta incident on the window recorded as counts, were calculated from the absorption coefficients of the windows and the counter gas and are plotted as a function of energy in figure 3.18.

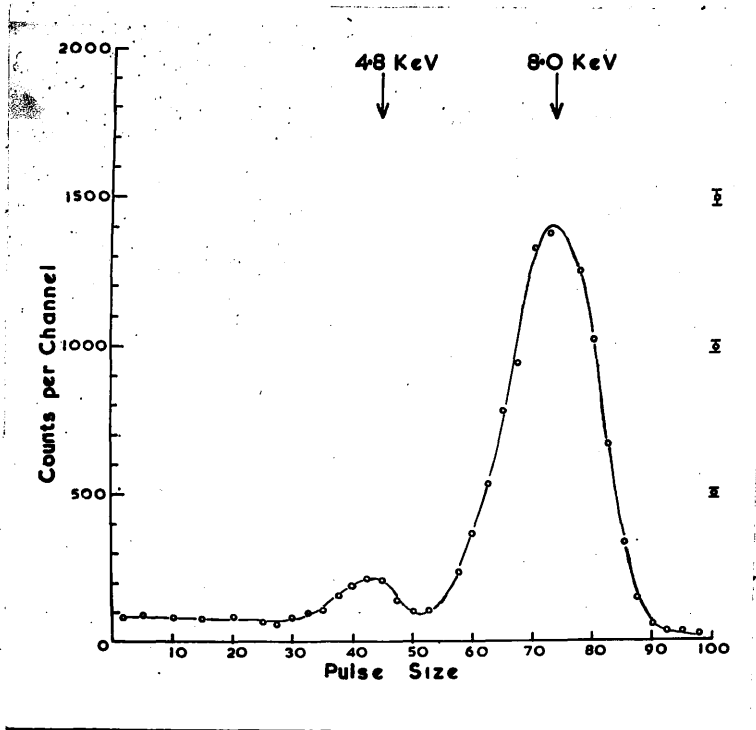


Figure 3.20. X-rays from proton bombardment of copper.

The pulse size produced is accurately proportional to the energy of the incident X-ray quanta. The X-rays produced by proton bombardment of metallic targets were used for calibration purposes. A typical calibration curve taken with counter 'B' is shown in figure 3.19.

A typical pulse size distribution obtained by bombarding copper with protons is shown in figure 3.20. The main peak is due to the K_{α} (8.03 KeV.) X-rays of copper: the K_{β} X-rays were filtered out with a thin nickel foil. The peak at an energy of 4.8 KeV. is due to the escape of argon X-rays from the counter. The absorption of a copper X-ray from the counter results in the ejection of an electron from an argon atom, leaving the atom in an excited state. This atom will normally emit an Auger electron and as both this electron and the original photo-electron have a short range in the gas filling the counter the full energy of the initial X-ray quanta will appear as ionisation in the counter. If, however, the excited argon atoms emit a quanta, as argon has a low absorption coefficient for its own radiation, the quanta will normally escape to the walls and not contribute to the ionisation. The ejected photo-electron will then give a pulse corresponding to an energy smaller than the original X-ray quanta by the energy of the K_{α} X-ray of argon. That the small peak is not due to an energy smaller than the main peak was confirmed by measuring the

absorption of the radiation incident on the counter with a polythene absorber. The absorption was found to be the same for the two peaks, whereas 4.8 KeV. radiation has an absorption coefficient three times as great as that of 8 KeV. radiation. This result was confirmed by careful comparisons of the positions of the peak for copper and zinc radiation.

The size of this small "escape peak" is a measure of the Auger coefficient for argon. From figure 3.17. and several similar curves an estimate of $93.5 \pm 2\%$ was obtained for this coefficient. For a more accurate determination the geometry of the experiment would need to be improved and the shape of the low energy "tail" of the main peak accurately determined. (This might be done, for example, by absorbing the argon X-rays inside the counter with chlorine in some form such as carbon tetrachloride).

The value of $93.5 \pm 2\%$ is in good agreement with the accepted value of 92.5% based on an experimental result of Martin et al.⁽⁹²⁾ and the theoretical expression derived by Burhop⁽⁸⁵⁾ referred to in Section III. 1.4.

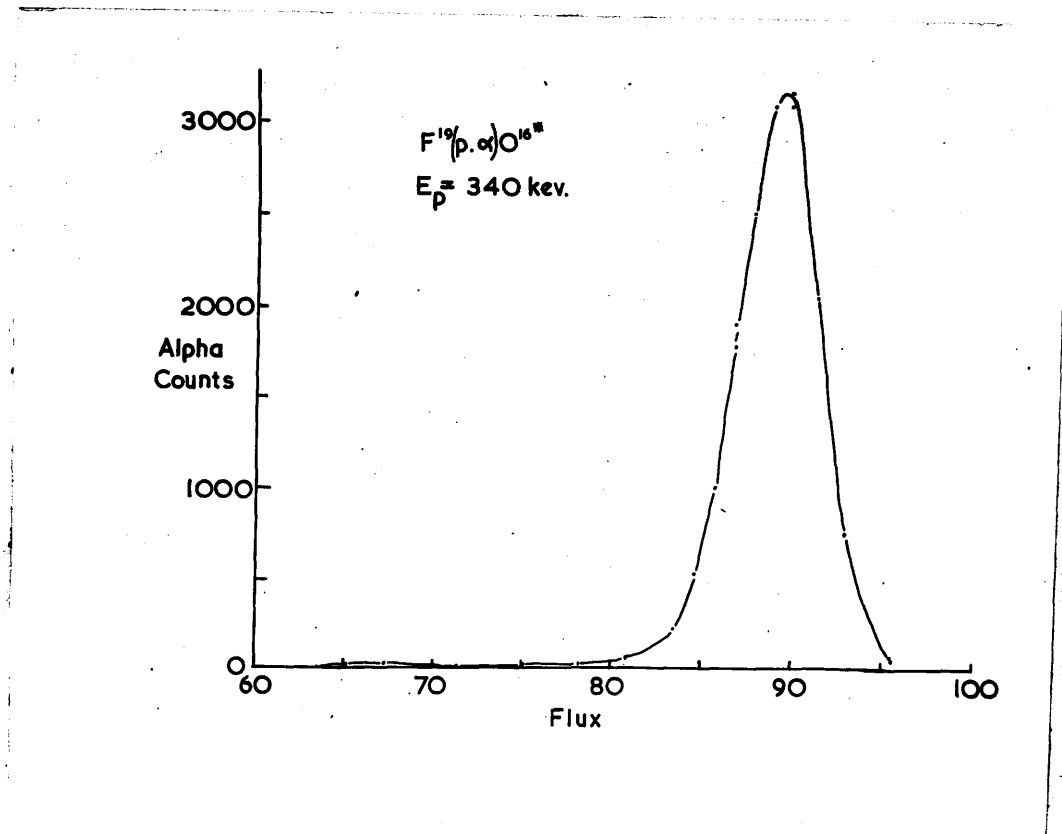


Figure 3.21. Spectrum of 1.84 MeV. alpha-particles from 340 KeV. resonance of $F^{19}(p,\alpha,\gamma)O^{16}$

III. 3. Emission of Charged Particles.

III. 3.1. General.

In Section I. 6.3. it was shown that the measurement of the energies of charged particles in magnetic spectrometers forms one of the most accurate methods of locating energy levels. For all but the very slowest particles, however, such spectrometers require very large electromagnets, especially if high resolution is to be achieved. No such spectrometer was available in this laboratory, but a smaller instrument proved suitable for some measurements made in connection with the gamma-ray measurements described in Section III. 1. The spectrometer used had a comparatively high sensitivity, and was capable of focussing alpha-particles of energies up to 2 MeV. The resolution of the instrument is illustrated in figure 3.20., which shows the spectrum obtained with the 1.84 MeV. alpha-particles from the 340 KeV. resonance of the $F(p, \alpha) O^{16*}$ reaction. In the two reactions to be described below, the main interest lay, in one case, in the measurement of the relative intensities of particular proton groups and in the other in the excitation function of an alpha-particle group. These measurements were complementary to those on the gamma-radiation from the same reactions described in Section III. 1.

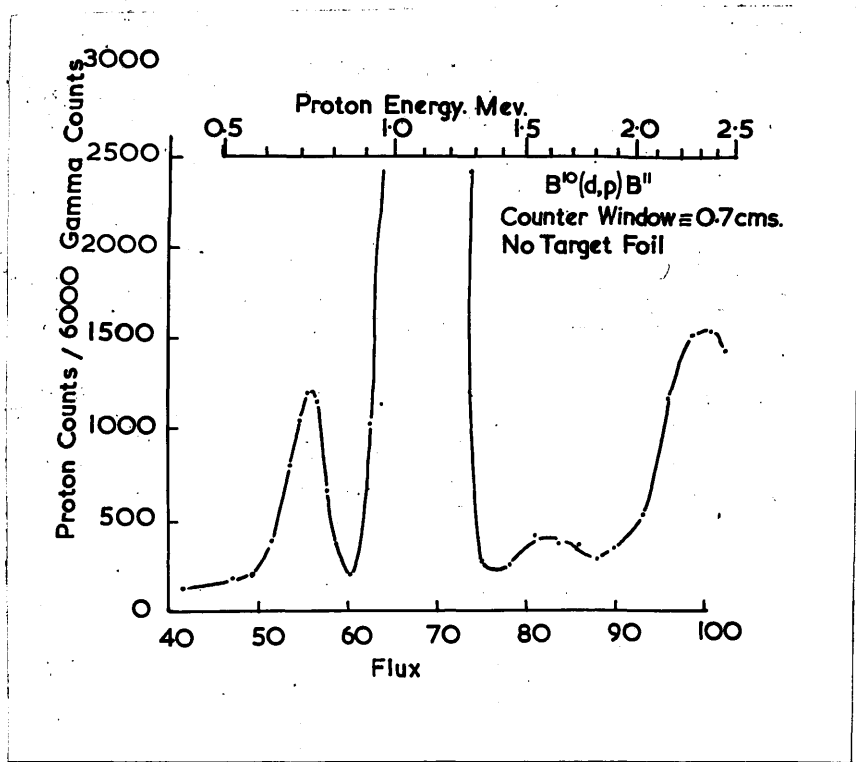


Figure 3.22. $B^{10}(d,p)B^{11}$ $E_d = 600$ KeV.

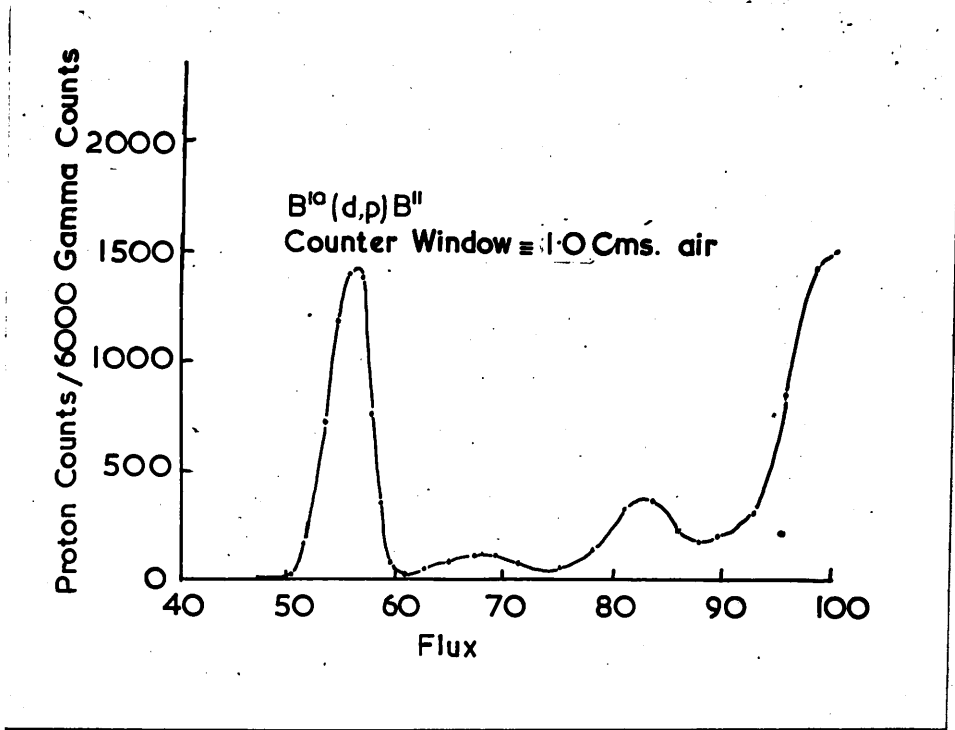


Figure 3.23. $B^{10}(d,p)B^{11}$ $E_d = 600$ KeV.

III. 3.2. The Reaction $B^{10}(d,p)B^{11}$.

Proton groups from this reaction were first detected by Cockroft and Lewis⁽⁹⁵⁾ in 1937; using 500 KeV. deuterons they found levels in B^{11} at 2.14 MeV. and 4.43 MeV. Since that date a number of investigations of this reaction have been made, all using deuterons of an energy of 1.5 MeV. or more. The latest measurements are those of Van Patter et al.⁽⁶⁹⁾ and were made with separated targets and a high precision spectrometer. The levels in B^{11} thus found are listed in Table 3.4.

In order to correlate the gamma-rays resulting from the deuteron bombardment of B^{10} (see Section III. 1.6.) with possible de-excitation of these levels in B^{11} , it was necessary to know the relative intensities of the relevant proton groups at a bombarding energy of 600 KeV. Owing to the effects of the Coulomb barrier it is likely that the lower energy proton groups will be relatively less intense than at the bombarding energy of 1.5 MeV. used by Van Patter et al.

A B^{10} target on a thick copper backing was, therefore, bombarded with 600 KeV. deuterons and a search made for protons with energies corresponding to transitions to the known levels in B^{11} . The detection of the two lowest energy groups was complicated by the scattered deuterons from the same H_p value as 1.2 MeV. protons, any proton groups of energies less than 1.2 MeV. are

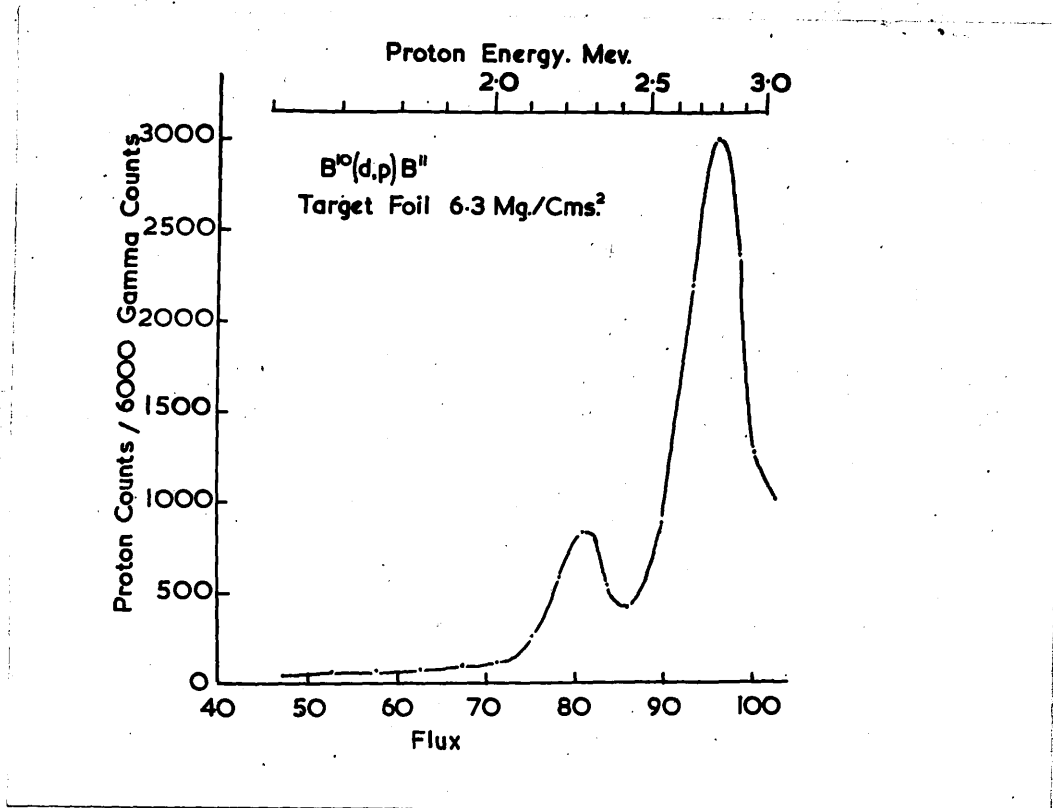


Figure 3.24. $B^{10}(d,p)B^{11}$ $E_d = 600$ KeV.

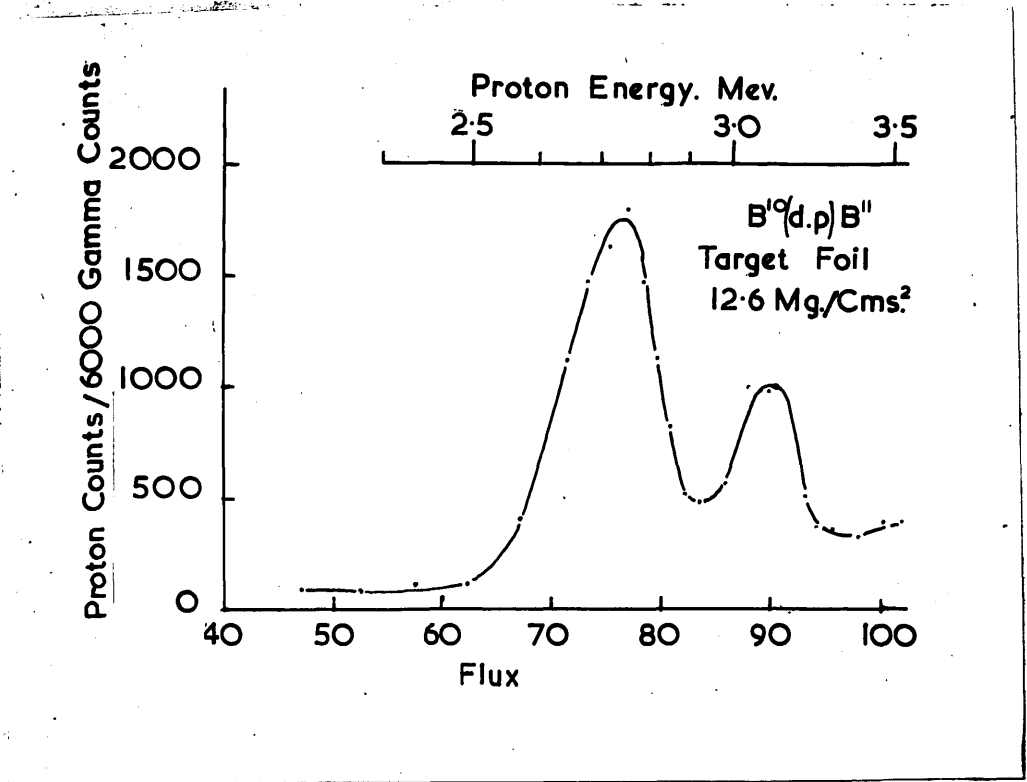


Figure 3.25. B¹⁰(d,p)B¹¹ Ed = 600 KeV.

liable to be obscured by the presence of large numbers of scattered deuterons. However, since 600 KeV. deuterons have the same range as 520 KeV. protons (see figure I.3.) it is possible to place foils in front of the counter to stop the deuterons while still allowing the proton group at an energy of 700 KeV. to reach the counter.

Figure 3.22. shows the spectrum obtained with no extra absorbing foil. In this case 600 KeV. deuterons are able to reach the counter and these give rise to the large peak at a flux of 70. The window, together with part of the counter gas that the particles had to traverse before reaching the sensitive volume of the counter, was sufficiently thick to stop deuterons of an energy less than about 450 KeV., so that the 700 KeV. proton group at a flux of 56 is not obscured. The effect of slightly increasing the stopping power of the window by placing a thin foil in front of it is shown in figure 3.23. The scattered deuteron group has now completely disappeared, and the second proton group at an energy of 1.1 MeV., which was previously obscured, is now clearly resolved.

In figure 3.22., proton groups of energies 1.6 MeV. and 2.3 MeV. are also resolved. Only the second of these is due to the $B^{10}(d,p)B^{11}$ reaction, the group at 1.6 MeV. originating from the $O^{16}(d,p)O^{17}$ reaction. As the magnetic field of the spectrometer cannot be increased beyond the value

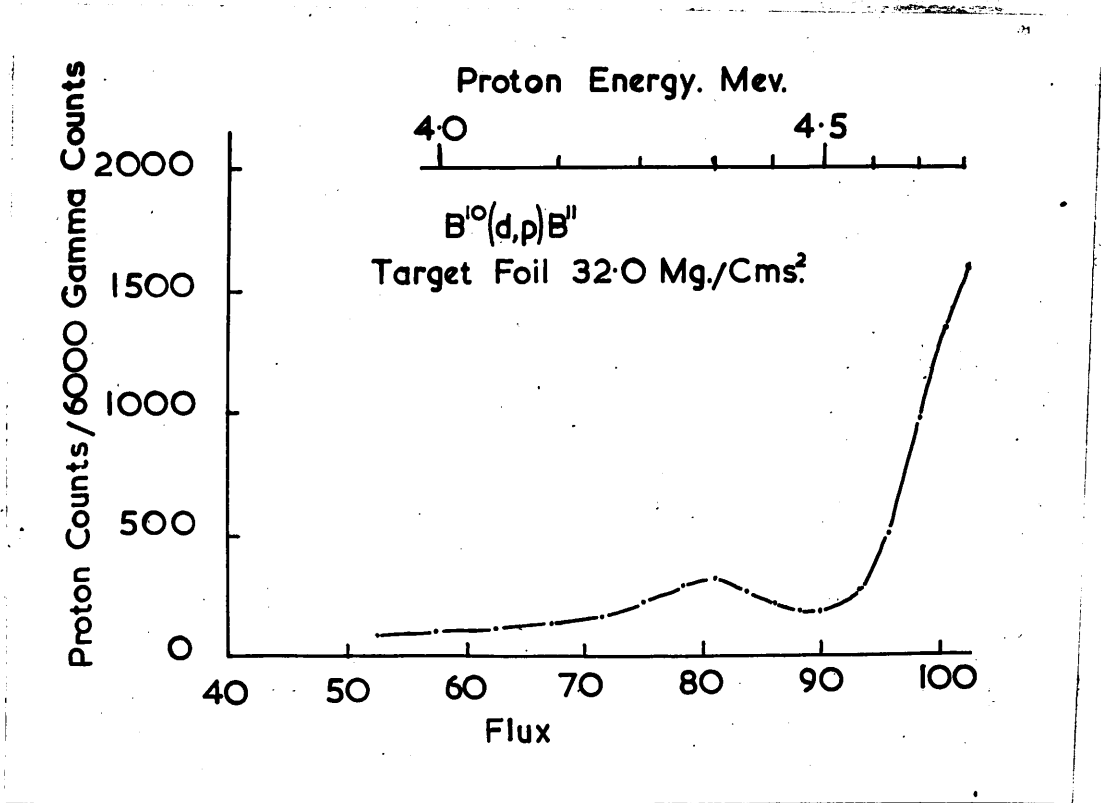


Figure 3.26. $B^{10}(d,p)B^{11}$ $E_d = 600$ KeV.

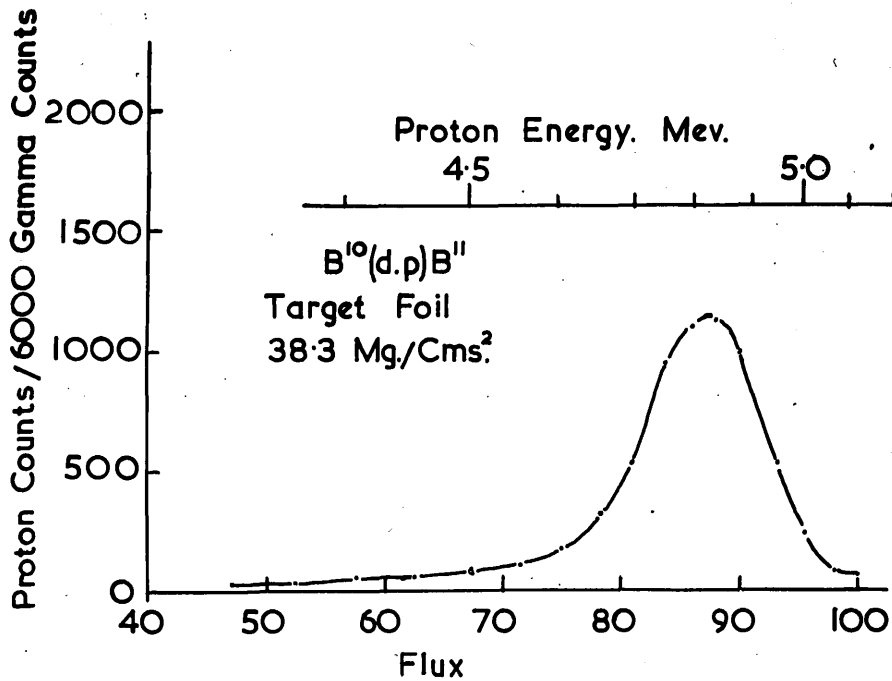


Figure 3.27. $B^{10}(d,p)B^{11}$ $E_d = 600$ KeV.

corresponding to 2.5 MeV. protons it is not possible to measure more energetic proton groups without slowing down the particles before they enter the analyser. This was done by mounting thin aluminium foils in front of the target so that the particles had to pass through the foil before entering the magnetic field. The foils were chosen so as to slow the proton groups down to energies between 700 KeV. and 2.2 MeV. The foil thicknesses were determined by weighing a known area of the foil. A check on the accuracy of these determinations were provided by those groups that were measured with more than one thickness of foil. The energy of the particles leaving the foil was found from the magnetic field and thus the energy of the incident proton determined by the use of published curves of the range energy relation for protons in aluminium⁽⁹⁶⁾. Figures 3.24., 3.25., 3.26. and 3.27. show the spectra obtained with successively thicker foils in front of the target. The effective window thickness (including the insensitive part of the counter) and the foil thickness used to slow the particles together with a scale giving the calculated energy of the protons before passing through the foil is shown on each figure. The energies and intensities of the proton groups deduced from these spectra are listed in Table 3.4. The group at 1.6 MeV., due to the reaction $O^{16}(d,p)O^{17}$ and that at 3.1 MeV., due to the reaction $H^2(d,p)H^3$ are excluded from this table.

Table 3.4. Proton Groups from $B^{10}(d,p)B^{11}$.

Energy (MeV.)	Relative Intensity	Q (MeV.)	Q (MeV.) (Buechner)	Level in B^{11} MeV.
0.729	1.0	0.302	0.311	8.924
1.09	0.1	0.720	0.667	8.568
2.26	0.5	1.97	1.935	7.300
2.75	2.2	2.51	2.480	6.755
4.32	0.3	4.22	4.199	5.036
4.79	1.9	4.73	4.775	4.446

The relative intensities of the various proton groups were deduced from the areas of the peaks in the spectra. (It is necessary to divide each area by the flux, as the spectrometer resolution varies with flux). The intensities thus recorded refer to the yields at 90° and as there is no reason to suppose all the groups to be isotropic⁽⁹⁷⁾, the relative intensities of the gamma-rays resulting from the subsequent de-excitations of the excited states of B¹¹ may differ from the relative intensities of the associated proton yields at 90° . Nevertheless, the error involved in the assumption that the yield is isotropic will not usually be large, and approximate agreement would be expected. In fact, the relative intensities of the proton groups do agree fairly closely with those of the gamma-rays (see Section III. 1.6.).

III. 3.3. The Reaction $\text{Al}^{27}(\text{p}, \alpha) \text{Mg}^{24}$.

The alpha-particles resulting from the proton bombardment of Al^{27} have been investigated by Freeman and Baxter⁽⁹⁸⁾ who found resonances at about 650 KeV. and 730 KeV., though the first of these was weak. Subsequently, the Q-value for the reaction was accurately re-determined by Freeman⁽⁹⁹⁾ who obtained a value of 1.585 ± 0.015 MeV. The Cambridge proton accelerator with which these measurements were made is not ideal for accurate measurement of excitation curves, as the ions have a

$\text{Al}^{27}(\text{p}, \alpha)\text{Mg}^{24}$ I $E_p = 503$ kev.

II $E_p = 630$ kev. III $E_p = 728$ kev.

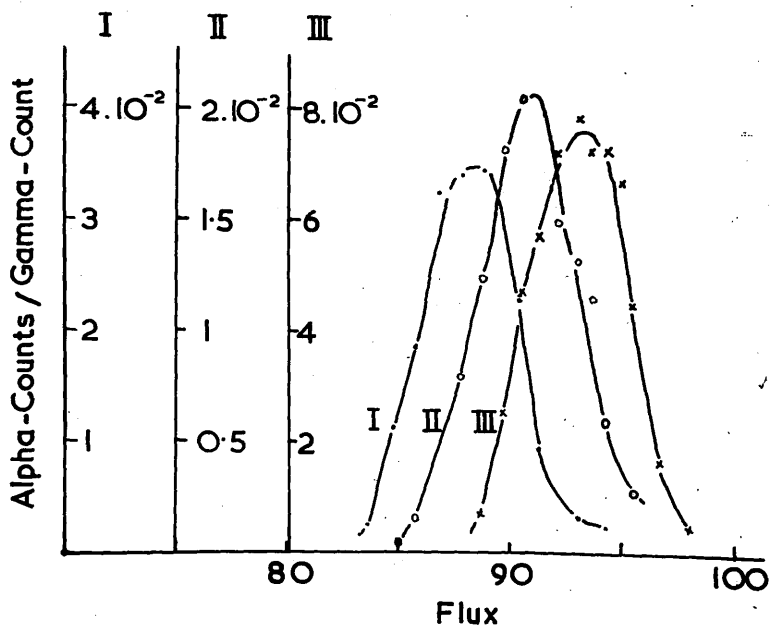


Figure 3.28. Alpha-particle spectra from $\text{Al}^{27}(\text{p}, \alpha)\text{Mg}^{24}$.

comparatively large spread in energy owing to the use of a high-voltage ion source. In view of the large number of sharp resonances that exist in the $\text{Al}^{27}(\text{p}, \gamma) \text{Si}^{28}$ reaction it was thought worth while to measure the excitation of the alpha-particles in greater detail; in order to determine whether or not any of the gamma resonances were associated with alpha-particle emission.

An aluminium target was, therefore, mounted in the spectrometer and bombarded with protons. The alpha-particles were detected with a proportional counter, biassed so as to discriminate against scattered protons as described in Section III.3.4.

The targets used, which had a stopping power for protons of about 10 KeV., were made by evaporating spectroscopically pure aluminium on to polished copper discs. Commercial aluminium sheet was found to be unsatisfactory as a target material, as impurities present gave rise to spurious alpha-particle groups (probably from the $\text{F}^{19}(\text{p}, \alpha) \text{O}^{16*}$ reaction). The gamma-radiation was detected with the thick-walled Geiger counter described in Section III. 1.3. The centre of the counter was 9.5 cm. from the target.

The alpha-particle spectra obtained at proton energies of 503 KeV., 630 KeV. and 728 KeV. are shown in figure 3.28. where the α/γ ratio is plotted as a function of the magnetic field. The shift of the peak with change of bombarding energy

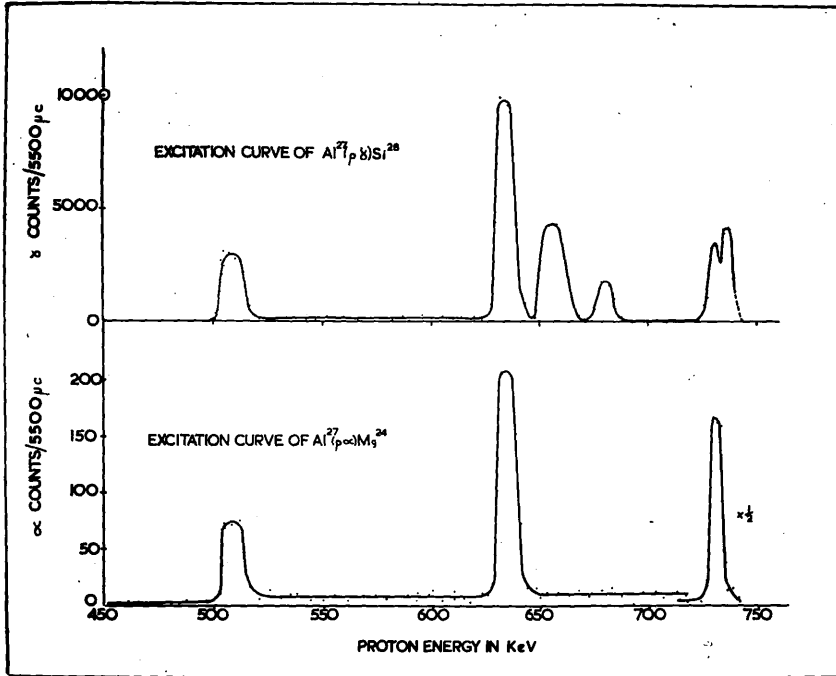


Figure 3.29. Excitation curve for gamma-radiation and for alpha-particles from $Al^{27} + p$.

is consistent with the assignment of the particles to the $Al^{27}(p, \alpha) Mg^{24}$ reaction. The energy of the alpha-particles was determined by comparison with the 1.837 MeV. alpha-particles from the 340 KeV. resonance of the $F^{19}(p, \alpha) O^{16}$ reaction (figure 3.21). The Q-value for the reaction thus obtained is 1.61 ± 0.01 MeV. in good agreement with the value obtained by Freeman and an indirect determination by Strait et al. ⁽⁸⁹⁾ which gave the value 1.600 ± 0.014 MeV.

The yield of alpha-particles and gamma-rays was measured over a range of proton bombarding energies from 340 KeV. to 740 KeV. The excitation curves above 500 KeV. are shown in figure 3.29. No alpha-particle resonances were detected below 500 KeV. The values obtained by Brostrom et al. ⁽⁵²⁾ for the position of the gamma-ray resonances, were used as calibration points for the proton bombarding energy. The ripple voltage on the H.T. was reduced to a minimum by careful adjustment of the cancellation circuit described in Section II. 2.6. The slope of the front edge of the peaks in the excitation curve is, however, still due to the energy spread of the incident protons. This spread, due mainly to voltage jumps caused by irregular striking of the rectifier valves, was about 1.5 KeV., and the actual width of the resonances must, therefore, be less. The peaks in the excitation are flat topped as the target thickness (10 KeV. below 700 KeV. and 5 KeV. above) was large compared with the energy spread of

Table 3.5.
 Experimental thick target yields of $Al^{27} + p$ and partial level widths calculated for $g = 0.5$.

Proton Energy Kev.	Yield per 10^{10} protons		Y_{α}	Partial Level Widths	
	Y_{α}	Y_{γ}		Γ_{α}	Γ_{γ}
503	1.2	0.95	1.27	.28	0.22
630	3.6	3.3	1.09	1.0	0.94
652	< 0.15	1.4	< 0.11	< .04	0.42
677	< 0.15	0.55	< 0.28	< .04	0.14
728	4.8	1.15	4.20	1.5	0.36
733	< 0.35	1.4	0.25	< .10	0.44

the beam. The heights of the peaks were, therefore, proportional to the "thick target yields" from the various resonances. (see Section I. 6.1.).

The yields of alpha-particles and gamma-rays were compared with those from the $F^{19}(p, \alpha, \gamma) O^{16}$ reaction. A calcium fluoride target was used and the value 0.15 alpha-particles per proton obtained by Chao et al.⁽¹⁰⁰⁾ used as standard. The yields from $Al^{27}(p, \alpha) Mg^{24}$ and $Al^{27}(p, \gamma) Si^{28}$ thus calculated for the resonances excited in the present work are given in Table 3.5. The gamma-ray yields differ appreciably from those given by Brostrom et al.⁽⁵²⁾ Part of this difference is due to the use of a different value for the yield of the $F^{19}(p, \alpha, \gamma) O^{16}$ reaction; part may be due to wrong assumptions about the relative efficiency of the Geiger counter for the gamma-rays involved; but some part of the discrepancy remains unaccounted for.

It will be seen from Table 3.5. that the resonance levels in the compound Si^{28} nucleus may be divided into two classes, those that emit only gamma-radiation and those that emit both alpha-particles and gamma-quanta in approximately equal numbers. The measurements on the gamma-ray spectrum (Section III. 3.3.) show that it is complex. It seems most likely that the energy of the radiation from the two types of level is different and that the ground-state transition occurs only from one type.

The most intense gamma-ray (10.5 MeV.) is

apparently due to a cascade transition through the known level at 1.80 MeV. in Si^{28} . Tentative values for the spin, i.e. total angular momentum and parity of this level, may be deduced from the beta-decay of Al^{28} which takes place entirely to this level, the ground-state transition being unobservable. The end-point of the beta-spectrum is 3.01 MeV. and the half-life is 2.3 minutes. From these values it appears that the transition to the 1.80 MeV. level is first forbidden and that the ground-state transition must, therefore, be at least second forbidden⁽¹⁰¹⁾. The ground-state of Si^{28} is known to have even parity and spin 0, while that of Al^{28} may be expected on the basis of the nuclear model, due to Mayer⁽⁹²⁾, to have a spin of 2 or 3 and even parity. The beta-decay of Al^{28} to the 1.80 MeV. level could then be explained if this state had a spin of 1 or 2 and even parity.

If the gamma-ray transition to the ground-state is electric quadrupole, then the transition to the 1.80 MeV. level could be electric dipole, thus explaining the comparatively low intensity of the gamma-ray corresponding to the ground-state transition.

The spin of the levels in Si^{28} excited by proton bombardment of Al^{27} depends on the orbital angular momentum contributed by the incident protons. The various possibilities are listed in Table 3.6. It is not necessary to consider d-wave

Table 3.6.
Levels in Si28 compound nucleus.

Incident Proton	Level in Si28 compound nucleus		Spin of alpha particle emitted to Mg24 ground state	Multipolarity of gamma-ray transition to Si28 ground state	Multipolarity of gamma-ray transition to 1.8 Mev. level in Si28	
	Spin	Parity			If level 1 -	If level 2 -
s-wave	2	+	2	E.Q.	ED or MQ	ED
	3	+	Forbidden	M.O.	MQ or EO	ED or MQ
p-wave	1	-	1	E.D.	MD or EQ	MD or EQ
	2	-	Forbidden	M.Q.	MD or EQ	MD or EQ
	3	-	3	E.O.	EQ or MO	MD or EQ
	4	-	Forbidden	M.4l.	E4 or MO	EQ or MD

protons or protons of higher orbital angular momentum owing to the increase of effective barrier height with angular momentum. For d-wave protons the penetration of the barrier is less than 1/100 that for s-wave protons. Also listed in Table 3.6. are the multipolarities of the gamma-ray transitions from the levels concerned and the orbital angular momentum of the emitted alpha-particles. If the parity of the level in Si^{28} is even, as the parity of the residual Mg^{24} nucleus is even, the emitted alpha-particle must carry away an even number of units of angular momentum. Thus alpha-emitting levels in Si^{28} if of even parity must have even spin and, similarly, if of odd parity must have odd spin.

It will be seen that the experimental facts could be qualitatively explained by assuming that the alpha-emitting levels are (2+), (i.e. have spin 2 and even parity) and associated with weak gamma-radiation to the ground-state of Si^{28} and that those levels that emit gamma-radiation only are (3-) (i.e. have spin 3 and odd parity), so that the ground-state transition is magnetic octupole and, therefore, of very low intensity.

If p-wave protons are considered, further possibilities arise. The alpha-emitting levels might be (3-), [(1-) is unlikely as it would allow an electric dipole transition to the ground state] and those levels emitting only gamma-radiation could be (2-) or (4-).

Further information could be obtained by measuring the angular distribution of the gamma-radiation. This should be isotropic from those levels resulting from s-wave capture, but not from those resulting from p-wave capture. It is also clear that a measurement of the gamma-ray spectrum from the individual levels would help in determining their spin values and such measurements are projected (Section III. 3.3.).

It was shown in Section I.4. that unless the partial widths for two competing reactions are nearly equal, the thick target yield of the reaction gives directly a value for one of the partial widths. If, for example, $\Gamma_p \gg \Gamma_\alpha$ and $\Gamma_p \gg \Gamma_\gamma$ then:

$$Y_{\infty\alpha} = Cg \Gamma_\alpha$$

$$Y_{\infty\gamma} = Cg \Gamma_\gamma$$

or if $\Gamma_p \ll \Gamma_\alpha$ and $\Gamma_\gamma \ll \Gamma_\alpha$

$$Y_{\infty\alpha} = Cg \Gamma_p$$

Γ_α = partial width for alpha-emission

Γ_γ = partial width for gamma-emission

Γ_p = partial width for re-emission of proton

g = statistical weight factor = $\frac{2J+1}{(2i+1)(2j+1)}$

C = constant = $\frac{h^2}{4E_r \xi}$ (see Section I.4.)

$Y_{\infty\alpha}$ = thick target alpha-yield

$Y_{\infty\gamma}$ = thick target gamma-yield.

In order to calculate the order of magnitude of Γ_p , it is convenient to write

$$\Gamma_p = P (E)^{\frac{1}{2}} \Gamma_0$$

where

P = Penetration probability for Coulomb barrier.

E = Energy of particle in MeV.

Γ_0 = "Width without barrier at 1 MeV."

An estimate for Γ_0 can be obtained from the average distance $\bar{D}(U)$ between similar energy levels of the same angular momentum and parity; for

$$\Gamma_0 = \frac{2k}{\pi K} \bar{D}(U)$$

where k/K is the ratio of the wave numbers of proton inside and outside nucleus⁽¹⁰²⁾.

$\bar{D}(U)$ may be estimated from a thermodynamical argument for a particular nuclear model⁽¹⁰³⁾, e.g. a degenerate Fermi gas of neutrons and protons, or may be deduced from experimental observations.

Alpha-emitting levels are found at proton energies of 0.5, 0.63 and 0.73 MeV. (present work) and 0.89, 0.92*, 0.94, 1.18*, 1.32, 1.39, 1.46* MeV.

(Shoemaker et al.⁽¹⁰⁴⁾). The stronger resonances in the latter work are marked *. It is not known whether any of these levels are, in fact, similar levels, nor are there sufficient levels to arrive at a true average spacing. However, it seems

Table 3.7.
Theoretical Proton Partial Level Width.

	Barrier Penetration Probability P.				Approximate Level Width Γ_p		
Proton Energy	503 KeV.	630 KeV.	730 KeV.		503 KeV.	630 KeV.	730 KeV.
s-wave	2.1×10^{-4}	1.1×10^{-3}	2.3×10^{-3}		11 eV.	65 eV.	150 eV.
p-wave	1.0×10^{-4}	2.8×10^{-4}	9.3×10^{-4}		5.3 eV.	17 eV.	60 eV.
d-wave	6.3×10^{-6}	2.8×10^{-5}	7.0×10^{-5}		0.3 eV.	1.7 eV.	45 eV.

unlikely that $D(U)$ is less than 150 KeV. or greater than 1 MeV. and a value of 500 KeV. is the best estimate that can be made at present. This value is of the same order as the theoretical value and experimental values for other similar nuclei. Thus, the value of Γ_0 is taken as 75 KeV.

The penetration probability P may be calculated from the Coulomb wave-functions. The values given in Table 3.7. are based on an extrapolation of the curves of Christy and Latter⁽¹⁰⁵⁾, and are accurate to within a factor of five.

The alpha-width may be calculated in a similar way to the proton width, though the dissociation of the alpha-particle within the nucleus makes it difficult to estimate the width without barrier. However, the Coulomb penetration factor for an alpha-particle of an energy of 1.8 MeV. is small, and any reasonable assumption for Γ_0 leads to level widths small compared with the proton widths listed in Table 3.7. The penetration factors and estimated partial level widths for 1.8 MeV. alpha-particles are given in Table 3.8.

The partial widths for gamma-radiation can be calculated in terms of the matrix element for electric radiation and the radiation magnetic moment for magnetic radiation. Using the notation of Fowler, Lauritsen and Lauritsen⁽¹⁰⁾, then for electric 2^l -pole radiation:

$$\Gamma_\gamma = \frac{4}{3} \alpha \left[\frac{r}{r_0} \right]^{2l} \left[\frac{\alpha h f}{mc^2} \right]^{2l+1} mc^2$$

Table 3.8. Theoretical Partial Widths for
1.8 MeV. Alpha-Particles.

l	P	Γ_{α} Approx.
0	8.5×10^{-6}	0.17 eV.
1	4×10^{-6}	0.08 eV.
2	8×10^{-7}	0.016 eV.

Table 3.9. Theoretical Partial Widths for
Gamma-Radiation.

E_{γ}	Electric Dipole	Electric Quadrupole	Magnetic Dipole	Electric Octupole
10.5 MeV.	23 eV.	3.3 eV.	0.8 eV.	0.02 eV.
12.1 MeV.	35 eV.	6.3 eV.	1.2 eV.	0.06 eV.

and for magnetic dipole radiation

$$= \frac{1}{3} \alpha \left[\frac{\mu}{\mu_n} \right]^2 \left[\frac{m}{M} \right]^2 \left[\frac{hf}{mc^2} \right]^3 mc^2$$

where

α = fine structure constant

m/M = ratio of electron and proton masses

r/r_0 = measure of the matrix element for electric radiation

μ/μ_n = measure of the radiation magnetic moment

hf = quantum energy

r/r_0 and μ/μ_n cannot, at present, be estimated theoretically to within a factor of ten, but from measurements on other light nuclei, where direct measurements of the level widths have been made, allow tentative values to be assigned. For electric dipole radiation r/r_0 was taken as 0.1, for electric quadrupole and octupole radiation r/r_0 was taken as 0.5, and for magnetic dipole radiation μ/μ_n was taken as 0.5. The radiation widths calculated in this way are shown in Table 3.9.

It will be seen that the radiation widths are in general smaller than the proton widths. The partial width for electric dipole radiation, however, appears to be of the same order as that for 503 KeV. s-wave protons though, owing to the uncertainties in r/r_0 and Γ_0 it is not possible to draw a definite conclusion on this point. Experimentally, the yield of the resonance at 503 KeV. is about a

third of that at 630 KeV. This ratio is greater than that of the theoretical widths for gamma-ray or alpha-particle emission and agrees with the supposition that the level width for the 503 KeV. resonance depends on the proton width. The yield at 728 KeV. is, however, not much greater than that at 630 KeV., although the theoretical proton width is twice as great. For these resonances, it seems certain that the proton width is the largest, so that the yields may be compared with the theoretical values for Γ_α and Γ_γ according to the relations:

$$Y_{\infty\alpha} = Cg\Gamma_\alpha$$

$$Y_{\infty\gamma} = Cg\Gamma_\gamma$$

From the measured thick target yields it is only possible to calculate $g\Gamma$, where 'g' is the statistical factor (see Section I.4.). For the various possible angular momenta of the compound nucleus, 'g' will vary from 0.25 to 0.75, while for those levels formed by s-wave protons it will be either 0.42 or 0.59. Thus it is sufficiently accurate to take 'g' as 0.5 and the experimental level widths thus calculated are shown in Table 3.5.

Comparison of these results with the theoretical widths show that they are at least of the same order of magnitude. The experimental alpha-widths are rather larger and the experimental gamma-widths rather smaller than the theoretical

values; but in view of the drastic assumptions made in the theoretical calculations closer agreement cannot be expected.

Since these experiments were completed similar excitation curves for the reactions $\text{Al}^{27}(\text{p}, \alpha) \text{Mg}^{24}$ and $\text{Al}^{27}(\text{p}, \gamma) \text{Si}^{28}$ have been measured by Shoemaker et al. at higher proton energies. Some of their results were referred to above in the discussion on average level spacing. The sensitivity of their apparatus was such that the alpha-particle resonances at 503 KeV., 630 KeV. and 728 KeV. were too weak to be detected. At the higher bombarding energies used, the penetration of the Coulomb barrier is so much greater that the capture of both p-wave and d-wave protons would be expected to be appreciable.

In the absence of detailed gamma-ray energy measurements and angular distributions at each resonance it is not possible to assign spins to the levels observed by Shoemaker et al.

III. 3.4. Constructional Details of Spectrometer.

At the time when the experiments described were made the largest electromagnet available was one with poles 10 cm. in diameter and capable of producing a field of 11,000 gauss in a 2 cm. gap. As it was desired to measure energies of alpha-particles up to 2 MeV, the radius of curvature of the particles in the magnet was limited to 15 cms.

and thus an analyser with a sector shaped field had to be used. In order to achieve the maximum possible solid angle subtended to the source by the analyser, Dr. J.G. Rutherglen designed a spectrometer which is virtually one half of the 90° deflection, slit to slit, focussing type of spectrometer described by Burcham and Freeman⁽¹¹⁾ and others.

From symmetry considerations it is evident that if a source of charged particles is placed at the point appropriate to point focussing after 90° deflection, after deflection through only 45° the particles will form a parallel beam. (Strictly, the projections of their paths on a plane perpendicular to the magnetic field will be parallel, as this type of spectrometer with a uniform field inside the sector, focusses in one plane only). Consequently, if the magnetic field is terminated at this point and the particles allowed to enter a detector sensitive only to particles travelling in a particular direction, the resolution of the spectrometer can be maintained. Furthermore, since the particles are diverging in a direction normal to the plane of deflection, the solid angle subtended by the spectrometer will be greater as the detector will be closer to the source than in the case of slit to slit focussing. The main disadvantages of this arrangement are that a

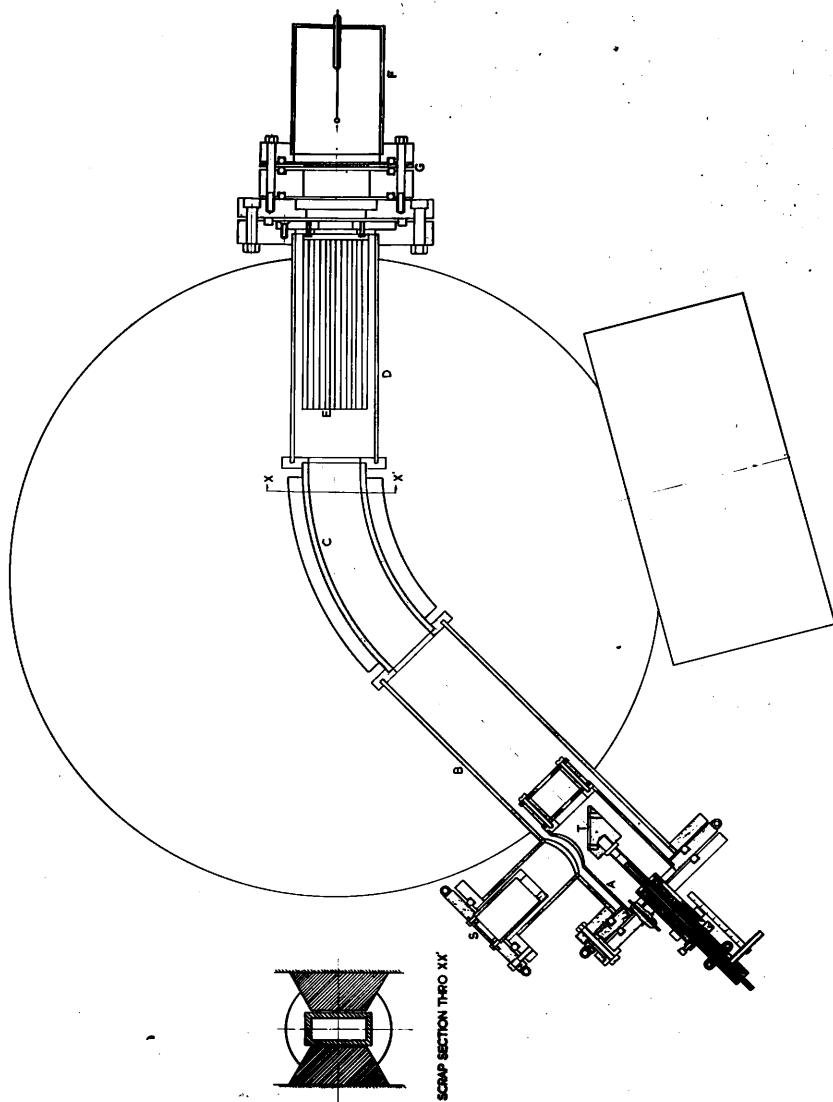


Figure 3.30. Particle Spectrometer.

detector sensitive over a large area is necessary and particles can more readily reach the detector from the target by scattering.

The constructional details of the spectrometer are shown in figure 3.30. The incident beam enters through the slit system S and strikes the target T at an angle of 45° . The target is surrounded with a cylinder A maintained at a negative potential to suppress secondary emission, and which supports a slit system collimating the particles entering the spectrometer. For the first part of their path they are screened from the magnetic field by the iron tube B. The particles are deflected through an angle of 45° in the section C which lies between specially shaped pole pieces. After deflection they enter the second iron tube D and pass through a system of parallel sheets of thin mica E. The sheets are 10 cms. long and are spaced by 0.36 cms., thus allowing particles having a direction within $\pm 2^\circ$ of the plane of the sheets to pass through to the proportional counter F. This counter has a thin collodion window supported on a perforated brass sheet having a transparency of 45%. The window thickness was equivalent to about 3 mm. of air. The choice of a proportional counter rather than a scintillation counter as a detector was due to the difficulties caused by the scattered protons from the incident

beam when (p, α) reactions were being investigated. These protons, of all energies up to that of the incident beam, reached the detector in large numbers, even when the field was set to deflect 1.5 MeV. alpha-particles. These protons cannot be prevented from reaching the detector by the use of absorbing foils as 600 KeV. protons have approximately the same range as 1.5 MeV. alpha-particles. (See figure 1.3.). When the proportional counter was filled to a pressure of about 4 cms.of mercury with methane, however, the alpha-particles gave pulses approximately three times as large as the protons and could easily be separated in an amplitude discriminator. With a scintillation counter using a zinc sulphide screen and a Type 931A photomultiplier, although a greater sensitivity was possible owing to the absence of the window grid, discrimination between alpha-particles and protons was not satisfactory.

Since the spectrometer occupies all the available space between the poles of the magnet, it was not possible to measure the magnetic field during the performance of an experiment. Instead, the magnetic field was determined as a function of magnet current using a search coil and a fluxmeter, and this calibration used for the conversion of current readings taken during the course of the experiments. In order to avoid errors due to hysteresis effects, the magnet current was always

raised to its maximum immediately before being reduced to the desired value.

In a spectrometer of this kind, absolute calibration is difficult, owing to the effects of fringing fields, and instead the alpha-particles from the 340 KeV. resonance of the reaction $F^{19}(p, \alpha, \gamma) O^{16}$ were used to calibrate the spectrometer. The Q-value of this reaction has been accurately measured by a number of workers and the best value for the energy of the strong alpha-particle group from this resonance is 1.837 MeV. The spectrum of these alpha-particles is shown in figure 3.20. By direct comparison the energy of other groups could be estimated to an accuracy of $\pm 1\%$. The maximum energy alpha-particle or proton group that could be measured directly was about 2 MeV. Higher energy groups were first slowed down by means of thin aluminium foils mounted on the exit slit on A (figure 3.30). The accuracy of measurement of the energy of these groups is diminished to some extent by the straggling in the fort.

III. 4. Summary of Experimental Results.

In the preceding Sections the results of measurements on the reactions $F^{19} + p$, $Al^{27} + p$, $Al^{27} + d$, $B^{10} + d$, and $B^{11} + d$ have been given. In each case, new information on the level schemes for the nuclei involved was obtained.

In general either the experimental data is inadequate or the nuclear theory is insufficiently precise to permit a close comparison between theory and experiment. In the case of the energy levels of Si^{28} , however, it was possible to assign tentative values to the spin and parity of some of the excited states. In addition, the experimental cross-sections were shown to be in accordance with approximate theoretical estimates.

The measurements on the reactions $\text{B}^{10} + \text{d}$ and $\text{B}^{11} + \text{d}$ have enabled the origin of the prominent gamma-ray lines to be established and revealed additional complexity in the gamma-ray spectrum from $\text{B}^{10} + \text{d}$.

The measurements of the gamma-ray energy in the reaction $\text{F}^{19}(\text{p}, \gamma) \text{Ne}^{20}$ established that the transition to the ground state is a cascade transition and, therefore, that the spin of the level at 13.4 MeV. in Ne^{20} must be such as to discourage the omission of the full energy gamma-ray.

The detection of the radiation from the 31 KeV. level in the Al^{28} nucleus confirms the existence of this unusually low-lying level. No other such levels are known in nuclei with $A < 30$ and the presence of such a level is contrary to the predictions of most nuclear models. The measurements on the X-radiation excited by proton bombardment have shown the present theory of this process to be inaccurate. This theory is a part of the general

theory of the loss of energy of charged particles in passing through matter. Although the energy required for the production of X-rays is a small fraction of the total, the inadequacy of the present theory for both the production of X-radiation and the rate of total energy loss at very low energies suggest that a revision of this part of the theory is desirable.

Appendix I.

The Calculation of the Energy Release in Nuclear Reactions

Let subscript 0 refer to the target nucleus, 1 to the incident particle, 2 to the observed particle, 3 to the residual particle. Let θ be the angle between the incident particle and the observed particle.

Thus M_0 = mass of initial particle.

E_1 = energy of incident particle.

Q = energy release in reaction considered.

Then in general

$$Q = \frac{M_2 + M_3}{M_3} E_2 - \frac{M_3 - M_1}{M_3} - \frac{2\sqrt{M_1 M_2} \sqrt{E_1 E_2}}{M_3} \cos \theta$$

$$\sqrt{E_2} = \frac{\sqrt{M_1 M_2}}{M_1 M_3} \sqrt{E_1} \cos \theta + \sqrt{\left[\frac{M_3 - M_1}{M_3 + M_1} + \frac{M_1 M_2}{(M_3 M_2)^2} \cos^2 \theta \right] \frac{E_1 + M_3 Q}{M_3 M_1}}$$

For observation in direction of beam ($\theta = 0$)

$$Q = \frac{M_2 + M_3}{M_3} E_2 - \frac{M_2 - M_1}{M_3} - \frac{2}{M_3} \sqrt{M_1 M_2 E_1 E_2}$$

$$E_2 = \frac{2 M_1 M_2 E_1}{(M_2 + M_3)^2} + \frac{M_3 Q + (M_3 - M_1) E_1}{M_2 + M_3}$$

$$\frac{2\sqrt{M_1 M_2 E_1}}{(M_2 + M_3)^2} \sqrt{M_1 M_2 E_1 + (M_1 + M_3) (Q + (M_3 - M_1) \cdot E_1)}$$

and for observation at 90° $\theta = 90^\circ$.

Appendix 2.

Details of Current Integrator

1. Action of Circuit.

The current to be measured is fed into the grid of a Miller valve (V_3 in figure 2.16). At the end of the Miller rundown the Miller condenser is recharged by unistable multivibrator. The pulses from this univibrator may be used to operate an external scalar or recorded on a built-in post office register.

Integration is started by closing switch S_1 . When the switch is opened the integrator will continue to operate until the next Miller rundown is completed, when it will turn itself off. Extra relay contacts are provided to allow external counting apparatus to operate only during the period of integration.

2. Circuit Details.

R_5 is adjusted so that the midpoint of the grid-swing of V_3 is at Earth potential. Errors due to the impedance of the input circuit (likely to be of the order of $5\text{ M}\Omega$ if the target is water cooled) are then minimised. With S_1 open, Relays A and B are both not energised and the grid of V_3 is held at a negative potential. R_9 is chosen so that the anode of V_3 is at the same potential as that to which it is returned by the action of the flip-flop. When S_1 is closed, relay B is actuated and holds itself on

via contacts B1 and A2. B3 is opened and allows other apparatus used in the experiment to operate for the period over which the current is integrated. The grid of V3 commences to run positive and the anode of V3 runs down negative. The rate of rundown is governed by the capacity of the input condenser (C_2 to C_6 selected by switch S_2) and the input current according to the normal Miller circuit relations.

At the start of V3 rundown, V6 is turned hard on and is taking grid current. V7 and V5 are cut off.

When the anode of V3 has run down to a point determined by the ratio of R7 and R8; V6 will start to cut off and V7 to conduct. As soon as this occurs the feedback of C_{10} will cause V6 to cut right off and V7 to turn hard on. The grid of V5 rises to 250V. where it is 'caught' by the diode V1, and V5 acting as a cathode-follower raises the anode potential of V3 at a rate determined by the available current in V5, the condenser $C_2 - C_6$ and the current in V3. The grid of V3 is prevented from going more than a few volts positive by the double diode V2. The grid of V5 is held positive until V7 starts to conduct (after a period determined by the time constant $C_{10}R_{16}$) and the univibrator reverses cutting off V5 and V7. R16 is adjusted to ensure that the voltage across $C_2 - C_6$ reaches a steady value. The circuit shown gives a discharge

time of about 200 microseconds and this is sufficient to recharge the $0.1 \mu\text{Fd}$ feed-back condenser C2. The time could, if required, be reduced for the other ranges by switching C10, but this complication was not thought to be worth while.

When the flip-flop cuts V4 off, the grid of V3 will adjust itself rapidly to its running potential and the normal Miller Section will follow. The anode of V3 is fed from a potential fixed by the neon V4 above the 250V. Line. The -250V. line and the -300V. line determine the limits of the anode rundown and must be stabilised as drifts in these voltages will affect the calibration of the integrator.

The meter in the anode circuit of V3 serves to check the action of the circuit. Any leak in the condensers C2 - C6 is shown as a change in current when the input is open circuited; and by feeding in a very small current the end-points of the Miller sweep can be measured. Though the integrator is normally only used for an integral number of cycles, fractions of a cycle can be read from the meter.

The discharge pulse appears at the anode of V7 and may be used to operate a sealing circuit. This negative pulse is fed to the grid of V9 and operates relay A in its anode circuit. Before a normal type relay can be made to operate it is necessary to widen the pulse. This is achieved by allowing the negative edge of the pulse to charge C11 via V8. At the end of the pulse V9 will run into grid current and will continue to pass anode

current until C_{10} discharges through R_{19} , the valve being conducting for about 1/20 second.

The circuit will continue to run, each complete cycle being recorded on a post office register activated by relay A_1 until S_1 is opened. This has no immediate effect as relay B will hold itself in via contacts B_1 and A_2 , but, as soon as relay A operates, i.e. at the end of the next Miller rundown, B will release, the external control contacts B_3 will close and the grid of V_3 will be fixed at the potential of the junction of R_9 and R_{10} .

3. Accuracy.

The circuit has been tested with input currents from 5 to 100 μ a, and is linear to better than 1%.

The lower limit of current that can accurately be integrated depends on leakage currents (including grid current in V_3) and the impedance of the source. By a careful choice of the integrating condenser and selection of V_3 for low grid current, the circuit should operate accurately on 1 μ a. input if the source impedance is greater than 100 M Ω . If the source impedance is lower than this, accuracy depends critically on the setting of R_5 as the voltage swing on the grid of V_3 (about 5 volts) will cause fluctuations in the input current. Operation on currents lower than 1 μ a. has not been tried.

The upper limit is set by the required ratio of Miller rundowns to discharge time. This ratio must be smaller than the ratios of the discharge current through V5 to the mean input current. The circuit was designed to work on currents up to 100 μ a. with a charge-discharge ratio of better than 500 to 1.

References.

- (1) W.F. Hornyak, T. Lauristen, P. Morrison and W.A. Fowler, Rev. Mod. Phys. 22, 291, (1950).
- (2) D.E. Alburger and E.M. Hafner, Rev. Mod. Phys. 22, 373, (1950).
- (3) E.C. Creutz, Phys. Rev. 55, 819, (1939).
- (4) A.P. French, P. Meyer and P.B. Tracy, Proc. Phys. Soc. A63, 666, (1950).
- (5) J.R. Oppenheimer and M. Phillips, Phys. Rev. 48, 500, (1935).
- (6) L.R. Hafsted and E. Teller, Phys. Rev. 54, 681, (1938).
- (7) K.M. Guggenheimer, Proc. Roy. Soc. A181, 169, (1942).
- (8) J.E. Mack, Rev. Mod. Phys. 22, 64, (1950)
- (9) E. Feenberg and K.C. Hammack, Phys. Rev. 75, 1877, (1949)
- (10) W.A. Fowler, C.C. Lauritsen and T. Lauristen, Rev. Mod. Phys. 20, 243, (1948).
- (11) W.E. Burcham and Joan M. Freeman, Phil. Mag. 60, 807, (1949).
- (12) W.E. Burcham and Joan M. Freeman, Phil. Mag. 61, 337, (1950).
- (13) W.A. Fowler, C.C. Lauritsen and T. Lauritsen, Rev. Mod. Phys. 20, 236, (1948).
- (14) R.L. Walker and B.D. McDaniel, Phys. Rev. 74, 315, (1948).
- (15) J.H. Carver and D.H. Wilkinson, Proc. Phys. Soc. 64A, 199, (1951).
- (16) H.I. West Jr., W.E. Meyerhof and R. Hofstadter, Phys. Rev. 81, 141, (1951).
- (17) R.D. Evans and R.O. Evans, Rev. Mod. Phys, 20, 305, (1948).

- (18) R. Hofstadter and J.A. McIntyre, *Phys. Rev.*
78, 619, (1950).
- (19) J.K. Bair, F.C. Maienschein and W.B. Baker,
Phys. Rev. 81, 283, (1951).
- (20) S.A.E. Johansson, *Nature*, 166, 794, (1950).
- (21) J.K. Bair and F.C. Maienschein, *Rev. Sci. Inst.*
22, 343, (1951).
- (22) W.H. Jordan and P.R. Bell, *Nucleonics*, V5, No.4.,
p.30, (1949).
- (23) H. Kallman and M. Furst, *Nucleonics*, V8, No.3.,
p.32, (1951).
- (24) G.H. Briggs, *Proc. Roy. Soc.* 157, 183, (1936).
- (25) S.K. Allison, S.P. Frankel, T.A. Hall, J.H.
Montague, A.H. Morrison and S.D. Warshaw,
Rev. Sci. Inst. 20, 735, (1949).
- (26) R.G. Herb, S.C. Snowden and O. Bala, *Phys. Rev.*
75, 246, (1949).
- (27) C.W. Snyder, S. Rubin, W.A. Fowler, C.C. Lauritsen,
Rev. Sci. Inst. 21, 852, (1950).
- (28) A.B. Brown, C.W. Snyder, W.A. Fowler and C.C.
Lauritsen, *Phys. Rev.* 82, 159, (1951).
- (29) W.E. Burcham, *Nature* 160, 316, (1947).
- (30) Heyn and Bouwers, *Philips Tech. Rev.* 6, 46, (1941).
- (31) V.K. Zworykin, G.A. Morton, E.G. Ramberg, J. Hillier,
A.W. Vance, "Electron Optics and the Electron
Microscope. John Wiley & Sons Ltd. New York (1945).
- (32) I.G. Maloff and D.W. Epstein, "Electron Optics in
Television". McGraw-Hill, New York (1938).
- (33) M.L.E. Oliphant and Lord Rutherford, *Proc. Roy. Soc.*
A141, 259, (1933).

- (34) D.W. Epstein, Proc. Inst. Radio Eng. 1095, 24, (1936).
- (35) B.v. Borries and J. Dosse, Archiv fur Electrotechnik, 32, 221, (1938).
- (36) L.P. Smith, W.E. Parkins and A.T. Forrester, Phys. Rev. 72, 989, (1947).
- (37) M. Hoyaux and I. Dujardin, Nucleonics, V4, No.5., p.7., No.6., p.12, V5., No.1., p.67, (1949).
- (38) J.D. Craggs, Proc. Phys. Soc. 54, p.245, (1942).
- (39) M.A. Tuve, O. Dahl and C.M. Van Atta, Phys. Rev. 46, 1027, (1934).
- (40) M.A. Tuve, O. Dahl and L.R. Hafsted, Phys. Rev. 48, 241, (1935).
- (41) P.C. Thonemann, Nature 158, 61, (1946).
- (42) J.G. Rutherglen and J.F.I. Cole, Nature 160, 545, (1947)
- (43) A.J. Baly and A.G. Ward, Can. Jour. Res. A26, 69, (1948)
- (44) M. Benedict and C. Williams, "Engineering Development in the Gaseous Diffusion Process", McGraw-Hill, (1949).
- (45) W. Heitler, "The Quantum Theory of Radiation", p.199, Oxford Univ. Press, (1939).
- (46) P.I. Dee, S.C. Curran and J.E. Strothers, Nature, 143, 759, (1939).
- (47) S. Devons and H.G. Hereward, Proc. Camb. Phil. Soc. 36, 252, (1940).
- (48) J.V. Jelley, Proc. Phys. Soc. A63, 538, (1950).
- (49) C.F. Powell, Proc. Roy. Soc. A181, 344, (1943).
- (50) C.F. Powell, A.N. May and J. Chadwick and T.G. Pickavance, Nature, 145, 893, (1940).

- (51) E.R. Rae, J.G. Rutherglen and R.D. Smith,
Proc. Phys. Soc. A63, 775, (1950).
- (52) G.P. Plain, R.G. Herb, C.M. Hudson and R.E. Warren,
Phys. Rev. 57, 187, (1940).
- (53) K.J. Brostrom, T. Huus and R. Tangen, Phys. Rev.
71, 661, (1947).
- (54) R. Tangen, K. Norske, Vidensk. Selsk. Skr. No.1,
(1946).
- (55) E.C. Pollard, V.L. Sailor and L.D. Wyly.
Phys. Rev. 75, 725, (1949).
- (56) J. Benes, A. Hodgran and N. Hole, Ark. Mat. Astr.
Phys. 35A, No.12., (1948).
- (57) R.A. Peck, Phys. Rev. 76, 1279, (1949).
- (58) D.E. Alburger, Phys. Rev. 75, 51, (1949).
- (59) J.G. Rutherglen, E.R. Rae and R.D. Smith.
Proc. Phys. Soc. A64, 906, (1951).
- (60) E.R. Gaerttner, W.A. Fowler and C.C. Lauritsen,
Phys. Rev. 55, 27, (1939).
- (61) J. Halpern and H.R. Crane, Phys. Rev. 55, 415, (1939).
- (62) C.L. Smith and E.B.M. Murrel, Proc. Camb. Phil. Soc.
35, 298, (1939).
- (63) W.M. Gibson, Proc. Phys. Soc. A62, 586, (1949).
- (64) C.P. Swann and E.L. Hudspeth, Phys. Rev. 76, 168,
(1949).
- (65) C.D. Curling and J.O. Newton, Nature, 166, 339, (1950).
- (66) J. Thirion, C.R. Acad. Sci. Paris, 229, 1007, (1949).
- (67) D.M. Van Patter, W.W. Buechner and A. Sperduto,
Phys. Rev. 82, 248, (1951).

- (68) R. Malm and W.W. Buechner, Phys. Rev. 81, 519, (1951).
- (69) D.M. Van Patter, A. Sperduto, K. Huang, E.N. Strait and W.W. Buechner, Phys. Rev. 81, 233, (1951).
- (70) J. Terrell and G.C. Phillips, Phys. Rev. 83, 703, (1951).
- (71) E.R. Rae, Jour. Sci. Instrum. 27, 143, (1950).
- (72) G. Gamow and C.L. Critchfield, "Atomic Nucleus and Nuclear Energy Sources", p.239 ff Clarendon Press, Oxford (1940).
- (73) W. Heitler, "The Quantum Theory of Radiation", p.102, Oxford University Press, (1944).
- (74) I.S. Lowen, Phys. Rev. 59, 835, (1941).
- (75) H.A. Bethe, Rev. Mod. Phys. 9, 220 ff. (1937).
- (76) K.M. Guggenheimer, Proc. Roy. Soc. A181, 169, (1942).
- (77) P. Preiswerk, Helv. Phys. Acta. 23, 7, (1950).
- (78) Sir E. Rutherford, J. Chadwick and C.D. Ellis, "Radiations from Radioactive Substances", p.147, Camb. Univ. Press, (1930).
- (79) J. Chadwick, Phil. Mag. 25, 193, (1913).
- (80) W. Bethe and H. Franz, Zeits. fur Physik. 52, 466, (1928).
- (81) C. Gerthsen and W. Reusse, Phys. Zeitz. 34, 478, (1933).
- (82) O. Peter, Ann. Phys. Lpz. 27, 299, (1936).
- (83) W. Henneberg, Zeits. Phys. 86, 592, (1933).
- (84) S.D. Warshaw, Phys. Rev. 76, 1759, (1949).

- (85) E.H.S. Burhop, Proc. Roy. Soc. A148, 272, (1935).
- (86) L.H. Martin and F.H. Egglestone, Proc. Roy. Soc.
A158, 46, (1937).
- (87) M.S. Livingston, F. Genevese and E.J. Konopinski,
Phys. Rev. 51, 835, (1937).
- (88) H. Enge, D.M. Van Patter, W.W. Buechner and A.
Sperduto, Phys. Rev. 81, 317, (1951).
also Phys. Rev. 83, 31, (1951).
- (89) E.N. Strait, D.M. Van Patter, W.W. Buechner and
A. Sperduto, Phys. Rev. 81, 747, (1951).
- (90) S.C. Curran, J. Angus and A.L. Cockroft,
Phil. Mag. 40, 36, (1949).
- (91) A.L. Cockroft and S.C. Curran, Rev. Sci. Inst.
22, 37, (1951).
- (92) M.G. Mayer, Phys. Rev. 78, 16, (1950).
- (93) L.H. Martin, J.C. Bower and T.H. Laby,
Proc. Roy. Soc. A148, 40, (1935).
- (94) R.D. Smith and R.A. Anderson, Nature 168, 429, (1951).
- (95) J.D. Cockroft and W.B. Lewis, Proc. Roy. Soc.
A154, 246, (1936).
- (96) J.H. Smith, Phys. Rev. 71, 32, (1947).
- (97) W.C. Redman, Phys. Rev. 79, 6, (1950).
- (98) J.M. Freeman and A.S. Baxter, Nature, 162, 696, (1948).
- (99) J.M. Freeman, Proc. Roy. Soc. A63, 668, (1950).
- (100) C.V. Chao, A.V. Tollestrup, W.A. Fowler and
C.C. Lauritsen, Phys. Rev. 79, 108, (1950).
- (101) P.B. Moon, Artificial Radioactivity, p.44, ff.
Camb. Univ. Press, (1949).

- (102) G. Gamow and C.L. Critchfield, Atomic Nucleus and Nuclear Energy Sources, p.241 ff. Oxford. Clarendon Press. (1949).
- (103) H.A. Bethe, Rev. Mod. Phys. 9, 79,(1937).
- (104) F.C. Shoemaker, J.E. Falkner, G.M.B. Bouricus, S.G. Kaufmann and F.P. Mooring, Phys. Rev. 83, 1011,(1951).
- (105) R.F. Christy and R. Latter, Rev. Mod. Phys. 20, 185,(1948).
- (106) W.E. Burcham, Nature, 160, 136,(1947).
- (107) F.P. Slater, Phil. Mag. 42, 904,(1921).
- (108) S.J. Bame and L.M. Baggett, Phys. Rev. 84, 891,(1951).